IOWA STATE UNIVERSITY
Digital Repository

Retrospective Theses and Dissertations

Iowa State University Capstones, Theses and Dissertations

1983

Intercalation of interstitial derivatives of yttrium monochloride

Jeffrey Earl Ford
Iowa State University

Follow this and additional works at: https://lib.dr.iastate.edu/rtd

 Part of the Inorganic Chemistry Commons

Recommended Citation
Ford, Jeffrey Earl, "Intercalation of interstitial derivatives of yttrium monochloride " (1983). *Retrospective Theses and Dissertations*. 8471.
https://lib.dr.iastate.edu/rtd/8471

This Dissertation is brought to you for free and open access by the Iowa State University Capstones, Theses and Dissertations at Iowa State University Digital Repository. It has been accepted for inclusion in Retrospective Theses and Dissertations by an authorized administrator of Iowa State University Digital Repository. For more information, please contact digirep@iastate.edu.

www.manaraa.com

INFORMATION TO USERS

This reproduction was made from a copy of a document sent to us for microfilming. While the most advanced technology has been used to photograph and reproduce this document, the quality of the reproduction is heavily dependent upon the quality of the material submitted.

The following explanation of techniques is provided to help clarify markings or notations which may appear on this reproduction.

1. The sign or "target" for pages apparently lacking from the document photographed is "Missing Page(s)". If it was possible to obtain the missing page(s) or section, they are spliced into the film along with adjacent pages. This may have necessitated cutting through an image and duplicating adjacent pages to assure complete continuity.

2. When an image on the film is obliterated with a round black mark, it is an indication of either blurred copy because of movement during exposure, duplicate copy, or copyrighted materials that should not have been filmed. For blurred pages, a good image of the page can be found in the adjacent frame. If copyrighted materials were deleted, a target note will appear listing the pages in the adjacent frame.

3. When a map, drawing or chart, etc., is part of the material being photographed, a definite method of "sectioning" the material has been followed. It is customary to begin filming at the upper left hand corner of a large sheet and to continue from left to right in equal sections with small overlaps. If necessary, sectioning is continued again—beginning below the first row and continuing on until complete.

4. For illustrations that cannot be satisfactorily reproduced by xerographic means, photographic prints can be purchased at additional cost and inserted into your xerographic copy. These prints are available upon request from the Dissertations Customer Services Department.

5. Some pages in any document may have indistinct print. In all cases the best available copy has been filmed.

University Microfilms International
300 N. Zeeb Road
Ann Arbor, MI 48106

8407070

Ford, Jeffrey Earl

INTERCALATION AND INTERSTITIAL DERIVATIVES OF YTTRIUM MONOCHLORIDE

Iowa State University PH.D. 1983

University
Microfilms
International 300 N. Zeeb Road, Ann Arbor, MI 48106

PLEASE NOTE:

In all cases this material has been filmed in the best possible way from the available copy. Problems encountered with this document have been identified here with a check mark __√__.

1. Glossy photographs or pages _____
2. Colored illustrations, paper or print _____
3. Photographs with dark background _____
4. Illustrations are poor copy _____
5. Pages with black marks, not original copy _____
6. Print shows through as there is text on both sides of page _____
7. Indistinct, broken or small print on several pages __√__
8. Print exceeds margin requirements _____
9. Tightly bound copy with print lost in spine _____
10. Computer printout pages with indistinct print _____
11. Page(s) _____ lacking when material received, and not available from school or author.
12. Page(s) _____ seem to be missing in numbering only as text follows.
13. Two pages numbered _____. Text follows.
14. Curling and wrinkled pages _____
15. Other _____

University
Microfilms
International

Intercalation of interstitial derivatives of yttrium monochloride

by

Jeffrey Earl Ford

A Dissertation Submitted to the

Graduate Faculty in Partial Fulfillment of the

Requirements for the Degree of

DOCTOR OF PHILOSOPHY

Department: Chemistry
Major: Inorganic Chemistry

Approved:

Signature was redacted for privacy.

In Charge of Major Work

Signature was redacted for privacy.

For the Major Department

Signature was redacted for privacy.

For the Graduate College

Iowa State University
Ames, Iowa

1983

TABLE OF CONTENTS

INTRODUCTION

The binary Y-YCl_3 system has been the source for two independent investigations in recent years.[1,2] Two reduced phases, YCl and Y_2Cl_3, have been characterized in each.[1,2,3] Although the number of reduced phases in this system has not matched the Sc-$ScCl_3$ system[4] it has nonetheless been a system with interesting synthetic problems and results.

The early work in the Y-YCl_3 system was limited to the proposed phase diagrams by Polyachenok and Novikov[5] and Corbett et al.[6] Both investigations reported a YCl_3 melting point of 721°C, a eutectic at 715-716°C, and an approximate 2 mole percent metal solubility at that point. In the phase diagram by Polyachenok and Novikov[5] there was an effect at 740°C which was attributed to a monotectic transformation of an unidentified YCl_3-rich solid. This effect was dismissed as one seen in other rare earth metal-trichloride systems.[7] Neither investigation reported any evidence for reduced phases.

The reduced halides of yttrium, Y_2Cl_3, YCl, Y_2Br_3, and YBr, were subsequently reported by Mattausch et al.[3] Reactions of YCl_3 with excess Y strips at 797°C in sealed Ta tubes produced black fur-like aggregates of Y_2Cl_3 needles with lattice parameters $\underline{a}$ = 15.144(3) Å, $\underline{b}$ = 3.825(1) Å, $\underline{c}$ = 10.077(2) Å and β = 118.24°. Y_2Cl_3 crystallizes in the C2/m space group and is isotypic with Gd_2Cl_3. The structure consists of parallel infinite chains of composition $Y_{4/2}Y_2Cl_4Cl_2$ formed by condensing M_6X_8-type clusters via trans edges. The packing of infinite chains leaves voids of approximate trigonal antiprismatic symmetry in the chlorine

layers. Attempts at filling these voids in Y_2Cl_3 and Gd_2Cl_3 with Li^+, thereby adding an electron to the metal-metal bonding in the infinite chains, have been unsuccessful.[8] The best explanation of why these voids cannot be filled is that band calculations, photoemission spectra, and temperature-dependent conductivity studies show that Gd_2Cl_3 is a filled band semiconductor (band gap $\sim$0.7 eV).[9,10]

Thin, highly reflective black plates of YCl were prepared by reacting a large excess of Y powder with YCl_3 at 790°C for 30 days.[1,3] In these reactions, the yield of YCl was generally quite small, <15%. There has been some disagreement over the lattice parameters of YCl obtained with Guinier techniques. Mattausch et al.[3] report hexagonal lattice constants of $\underline{a}$ = 3.748(1) Å and $\underline{c}$ = 27.318(9) Å while N. Holzer[2] reports $\underline{a}$ = 3.7478(9) Å and $\underline{c}$ = 27.525(5) Å. YCl has been determined by powder patterns to be isotypic with ZrBr.[3] The crystal structure of YCl will be discussed in detail in later sections of this dissertation.

The monohalides, MX, where M = Sc-La, Pr, Gd, Tb, Ho, Er, Zr, Hf and X = Cl or Br, have structures which consist of close packed metal and halogen atoms in alternate double layers in the form of a slab, X-M-M-X.[11] The slabs stack along $\underline{c}$ and two stacking variations are known. The ZrCl structure-type has an ABCA slab stacking while the ZrBr-type has ACBA stacking.[12,13] The structures are characterized by strong intralayer and interlayer metal-metal bonding and weak van der Waals interactions between halogen layers.

The monohalides are somewhat similar to the transition metal dichalcogenides, MCh_2, in that both have layered structures which consist of

slabs that are bound by weak van der Waals interactions. The dichalcogenides, about 60 in number including the various polymorphs and polytypes, have hexagonal or trigonal structures with fairly strong covalent bonding.[14] This class of materials readily undergoes intercalation reactions. Intercalation is the reversible insertion of guest species into a host lattice. Examples of guest species in MCh_2 compounds include organic bases, solvated cations, and various metal cations of alkali metals, alkaline earth metals, transition metals (Ti-Zn), and post transition metals (Al-Tl; Si-Pb; Bi).[15,16]

One of the most widely studied classes of intercalation reactions is the intercalation of alkali metals (M^I) into MCh_2.[15,16] The four most common methods of preparing M^IMCh_2 are: a) reaction of alkali metal solutions in liquid ammonia, b) in the case of lithium derivatives, use of n-butyllithium in hexane, c) high temperature synthesis from the host material and alkali metal or from the elements, d) electrochemical methods.[15] The compounds can be best represented by $M_x^{I+}(MCh_2)^{x-}$, where the valence electrons of the alkali metal have been transferred to the MCh_2 slab to fill the lowest unoccupied d-band levels and the alkali metal cation resides in the van der Waals gap between the chalcogen layers. The reason these reactions have been so extensively studied, in particular the lithium intercalation of TiS_2, is that they have been proposed as cathode materials for lithium batteries.[15] The net cell reactions for Li batteries:

$$\text{anode:} \quad Li \rightleftarrows Li^+ + e^-$$

$$\text{cathode:} \quad Li^+ + e^- + TiS_2 \rightleftharpoons LiTiS_2$$

The only examples of the intercalation of any normal-valent halide occurs among the oxyhalides of FeOCl, VOCl, and CrOCl.[15] The orthorhombic FeOCl structure consists of distorted sheets of edge-shared octahedra of the nonmetal atoms centered about iron, the coordination polyhedra consisting of four-coordinate oxygen and two-coordinate chlorine, with the chlorine atoms defining the outside of the layers. Reaction of n-butyllithium at 60°C with FeOCl, or the isostructural VOCl and CrOCl, gives the lithium intercalates of the FeOCl structure-type.[15] As in the previously described intercalates, the Li^+ and in many cases solvent are inserted in the van der Waals gap between the halide layers.

Attempts at intercalation of ZrCl and ZrBr by n-butyllithium, alkali metals in liquid ammonia, and high temperature reactions with Zr, ZrX_4, and alkali metal halides have been unsuccessful[13,17] even though band structure calculations have shown an empty metal d-band just above the Fermi level.[18] It has been suggested that the instability of the ZrX intercalates may be due to the already high electron density in the intermetal region.[17]

ZrCl and ZrBr have yielded some very interesting light atom interstitial derivatives. Marek et al. have reported the structures of $ZrBrH_{0.5}$, ZrBrH, and ZrClH obtained from Guinier powder pattern data.[19] Although these compounds have different stacking orders within the slabs than the monohalides the hydrogen atom resides in the tetrahedral holes between the double metal layers. Recently, Seaverson and Corbett reported the formation of $ZrClO_x$ and $ZrBrO_x$, where $0<x\leq0.43$ for $ZrClO_x$ and $0<x\leq0.35$ for $ZrBrO_x$, by reaction of ZrX with ZrO_2 at temperatures greater

than 800°C.[17] The structures show that the oxygen atoms are disordered in the tetrahedral-like holes between the metal layers in the expanded ZrX framework.

The present work investigates the intercalation of YCl and of the oxide and carbide interstitial derivatives of YCl. This will include the synthesis, identification of the phases by single crystal studies and powder patterns, and the properties of the compounds.

EXPERIMENTAL

Synthesis Techniques

General

The air and moisture sensitivity of the reactants and products required transfers and manipulations to be performed with dry box and vacuum line techniques. The dry boxes were constantly purged with dry nitrogen which was recirculated through a Molecular Sieve column. This and a tray of P_2O_5 in the dry boxes typically reduced the water content to 1-3 ppm. Recently, the dry box atmosphere has been recirculated through a second column containing Ridox to remove oxygen. The amount of oxygen in the box was not determined quantitatively but a 60 Watt light bulb burned for 30-60 minutes. Vacuum lines with Hg diffusion pumps were used for evacuation of sample tubes, sublimations, distillations, hydrogenation, dehydrogenation, solvent transfer, and dehydration reactions.

Niobium containers (0.95 cm o.d., 0.055 cm wall thickness) sealed in fused silica jackets were used for the reactions.[20] The fused silica jackets and the sealed container were washed with a 10% HF solution, then rinsed with distilled water and dried. The jacket was then attached to the vacuum line, flamed with a hot gas-oxygen flame, and sealed off. The cleaning and flaming of the jacket was instituted to hinder fused silica failure and oxygen contamination of the products. Chromel-alumel thermocouples were attached on the outside of the jacket to monitor reaction temperatures.

Reactants

The Y strips were prepared by B. Beaudry and P. Palmer from Ames Lab yttrium, with typical major impurity levels (atomic ppm) of 15 Fe, 2 Ni, 20 W, <5 individual rare earths, 3 Cl, 4 Cu, 400-850 O, 150 C, 20 N, and 700 H. To form strips the Y was jacketed in stainless steel, hot rolled to 50% reduction in thickness (0.32 to 0.15 cm), cold rolled to 0.79 mm, heat treated and cold rolled to approximately 0.15 mm. The strips were electropolished to remove any hydrocarbon greases and other surface impurities picked up during the cold rolling process and were stored under vacuum.

The Y turnings were prepared from bulk metal on a lathe in an inert gas-filled dry box. The turnings were used in the preparations of YCl_3 and Y powder.

Yttrium powder was prepared by first hydrogenating Y turnings in a Mo boat at 400°C for 2-3 hours. The brittle YH_2 was ground with an agate mortar and pestle to a particle size less than 149 microns in the dry box. The powdered dihydride was dehydrogenated in a dynamic vacuum by heating from 250-750°C and maintaining that temperature for 3-4 days until the system was below discharge ($<10^{-5}$ torr). If the metal sintered during heating it was reground to a particle size less than 149 microns. Published Y-H equilibrium data indicate a residual H/Y ratio of 0.01.[21]

The YCl_3 was prepared by reaction of Y strips or turnings with electronic grade HCl gas at 750-800°C.[22] The crude YCl_3 was then distilled four times in a Ta sublimation apparatus at 850°C under high vacuum ($<10^{-5}$ torr). After the final distillation, the YCl_3 was sealed

off in small quantities in Pyrex ampoules to prevent excessive exposure of the YCl_3 to the dry box atmosphere during subsequent use.

The sources of the alkali metal chlorides, M^ICl where M^I=Li-Cs, were the Fisher Scientific Co. or the J. T. Baker Chemical Co. The purity of LiCl was 98.7% with H_2O (0.1%), Li_2CO_3 (0.01%), and Na (0.15%) as the most abundant impurities. The rest of the alkali metal chlorides were 99.7 - 99.9% pure with the alkali metal impurities less than 0.003%. The salts were dried by slow heating under high vacuum until near the melting point where they sublimed. In the case of LiCl, a great deal of care was taken to heat very slowly to avoid the hydrolysis to LiOH. The sublimed salts were sealed and stored under vacuum in Pyrex ampoules.

The Y_2O_3 was obtained from the Ames Laboratory and is the oxide used in the preparation of high purity Y. The typical major impurity levels (atomic ppm) were 2Fe, 4Cl, 3Ca, and less than 2 for the individual rare earth metals. The YOCl was prepared from $YCl_3 \cdot 6H_2O$ which is made by adding concentrated HCl to Y_2O_3 and boiling to dryness. The $YCl_3 \cdot 6H_2O$ was then heated to 550-600°C in a stream of oxygen to produce YOCl with the PbFCl structure.[14,23]

Spectroscopic grade powdered graphite was obtained from Ed DeKalb. The powdered graphite was outgassed by heating to 550°C under vacuum for 12-24 hours. The sample was stored in evacuated Pyrex ampoules.

A 1.6 M solution (in n-hexane, Foote Mineral Co.) of n-butyllithium, C_4H_9Li, and a second 2.2 M solution (in n-hexane, Alfa Products) of C_4H_9Li were handled in the Ar-filled solvent box because of the pyrophoric nature of n-butyllithium. Dry acetonitrile, CH_3CN, was obtained from Bill

Beers. The acetonitrile had been dried by refluxing over CaH_2 and storing under vacuum over molecular sieve. The CH_3CN-I_2 solution was prepared by vacuum distilling CH_3CN into a Pyrex 2-arm apparatus which contained excess I_2.

Reactions

The $M^ICl-YCl_3-Y$ "ternary" reactions were prepared by loading the desired amounts of the salts with a three-fold excess of Y strips or powder in a Nb tube. The reactions were heated at 900-950°C for 3-5 weeks and quenched in air by removal from the furnace.

Two different types of reactions were used in the oxygen-containing system. In the first type a desired mixture of $YCl_3/Y_2O_3/M^ICl/Y$ powder was loaded in a Nb tube. In the second a desired ratio of $YOCl/M^ICl/Y$ powder was used. Both types were heated to 900-975°C for ∿2 weeks and typically air quenched.

Reactions in the quaternary system containing carbon were prepared by loading the desired mixture of Y powder/$YCl_3/M^ICl/C$ in a Nb tube. The reactions were heated at ∿950°C for 5-8 days and air quenched.

The reactions of $M^I_xYClO_z$ with CH_3CN-I_2 were carried out in a 2-arm apparatus. The $M^I_xYClO_z$, 50-60 mg, was loaded in one arm and the CH_3CN-I_2 solution was vacuum distilled into the second arm and then the two were combined and let stand at room temperature for 1-2 days. The solvent was then removed by vacuum distillation and the sample was pumped down until below discharge.

In the dehydration reactions the sample was placed in a capped 3/8" diameter Ta tube, both were weighed in the dry box and placed in an

evacuable fused silica container. This was then evacuated and heated to 270°C for one hour. A liquid nitrogen-cooled trap was used to collect the water. The sample was air quenched and transferred to the dry box where it was weighed and a powder pattern was prepared.

Reactions with n-butyllithium were all loaded in the solvent box. In a typical reaction, four to five milliliters of n-butyllithium was added with a syringe to 50-60 mg of sample. The room temperature reactions were placed in capped vials in the solvent box. For the reactions at 60°C, the sample and solution were poured into a sample tube and sealed under vacuum. The sample was suspended in a mineral oil bath at 60±2°C for 5-7 days. When the reactions were deemed complete, the n-butyllithium solution was decanted off and the remaining solvent was removed under vacuum.

Characterization Techniques

General

Electron microprobe studies were conducted by Fran Laabs using an ARL-model EMX instrument with a focused 20 Kv beam and a specimen current of 2 namps. The transfer of the sample to the spectrometer was accomplished in a N_2-filled glove bag attached directly to the port of the spectrometer.

The Guinier powder pattern technique was used extensively during this investigation. Details of its uses and advantages have been described elsewhere.[24,25] Most samples were prepared by grinding the product directly on the cellophane tape and adding Si as an internal standard. The reflection positions were measured in millimeters (±0.01 mm) using a

Nonius Guinier viewer. The 2θ and d values for each reflection were calculated using a program, GUIN, developed by Hideo Imoto and described by Araujo.[26] The patterns were indexed either manually or by comparison with the calculated powder pattern. The calculated powder patterns were obtained using the Penn State program developed by Clark et al.[27] The lattice constants were calculated using LATT.[28]

Single crystal work

Single crystals were found on opening the Nb reaction tube in a dry box equipped with a microscope. The crystals were picked up with a vaseline-tipped glass wand and mounted in 0.2 or 0.3 mm Lindeman glass capillaries, which were temporarily sealed with silicon grease. Once outside the dry box the capillaries were sealed with a microtorch and the ends covered with Apiezon W. Oscillation photos were used to determine if each crystal was single. If the crystal was single, Weissenberg photographs, usually both 0-level and 1st level, were taken (Charles Supper Co. camera) to obtain cell constants, symmetry information, and check for possible superlattice reflections.

All data sets were collected on the Ames Laboratory diffractometer[29,30] which is interfaced with a PDP-15 computer and has monochromatized Mo $K\alpha_1$ (λ=0.71034 Å) radiation. Three standard reflections were selected ($2\theta>25^{\circ}$ and total counts >1500) and rechecked every 75 reflections to ensure instrument and crystal stability. No significant decay was observed in any of the data sets. Four octants of data were collected with the maximum $2\theta=50^{\circ}$ or 60°. An HPR plot, tuned PHI-scan

($\chi=90^{o}\pm5^{o}$), and LATT[28] (which used tuned Friedel-related peaks ($25^{o}<2\theta<40^{o}$)) were run after data collection. An empirical absorption correction using the diffractometer PHI-scan data and the program ABSN[31] was applied to all data sets. The absorption coefficient (μ) of yttrium compounds for Mo Kα is large, $\mu\sim248$ cm^{-1}. The data were reduced using DATRD[32] with the appropriate extinction conditions applied where necessary, and the observed reflections ($I>3\sigma(I)$) were corrected for Lorentz-polarization[32] effects and their standard deviations[33] were calculated as usual. The data sets were averaged using FDATA[34] with a 6σ cutoff. Structure factor calculations and least squares refinement using only neutral atom scatterers were done using the full matrix program ALLS.[35] Fourier series calculations were accomplished with FOUR.[36] Except for YCl all structure calculations were carried out on a VAX 11/780 computer. The structure of YCl was solved and all of the ORTEP[37] drawings were run at the ISU computation center. All ORTEP[37] drawings have thermal ellipsoids drawn at 95% probability.

The data collection details for all crystal structures are presented in Table 1.

Table 1. Data collection details for all crystal structures

Phase	YCl	$3R\text{-}Li_{0.09}YCl$	$2H\text{-}K_{0.08}YClO_{0.82}$	$3R\text{-}Na_{0.08}YClO_{1.0}$	$1T\text{-}K_{0.52}Y_2Cl_2C_{0.80}$
Size (mm)	0.2x0.2x0.01	0.2x0.2x0.01	0.3x0.3x0.01	0.3x0.03x0.01	0.4x0.4x0.03
Octants	4	4	4	4	4
2θ-maximum (deg)	50	60	50	50	50
Phi-scan reflection	$4\bar{3}\bar{1}$	$\bar{3}1\bar{4}$ $5\bar{2}7$	$1\bar{3}3$	$\bar{4}1\bar{5}$	$\bar{2}\bar{1}0$
(h,k,ℓ, 2θ (deg))	46.50	34.21 58.02	33.85	46.49	34.32
Reflections					
Checked	546	2604	1336	1794	644
Observed	523	808	934	501	550
Independent	101	156	141	101	106
R (ave)	0.038	0.038	0.065	0.074	0.040

RESULTS

Yttrium Monochloride

YCl has been observed in varying amounts throughout this investigation. The most general method for the preparation of YCl is the reaction of an excess of Y powder with YCl_3 at temperatures ranging from 675°C - 900°C and air quenching.[1] The black plate-like YCl is generally found in a 50/50 mixture with Y_2Cl_3 at temperatures less than ≈825°C. YCl can be physically separated from Y_2Cl_3 but only small amounts are recovered, 5-30 mg. Using a larger excess of Y powder at a higher temperature (>825°C) yields only YCl. The physical separation of the monohalide from the yttrium powder is very difficult.

YCl has also been produced in "low" temperature reactions using LiCl as a flux. The phase diagram for $LiCl/YCl_3$ is presented in Figure 1.[38] Reactions using 10 mole % LiCl at 650°C, 32 mole % at 550°C and 40 mole % at 500°C produced a 10-50% yield of YCl with the remainder Y_2Cl_3. There still remains the problem with separating the YCl from Y_2Cl_3, Y and LiCl. When Y strips are used in LiCl-fluxed reactions at 500-600°C, the only product is Y_2Cl_3 in a greater than 95% yield. This has proved to be a useful preparative method for relatively pure Y_2Cl_3.

The use of a LiCl flux at higher temperatures (>800°C) also produces a mixture of both YCl and Y_2Cl_3 in an 80% total yield. If 22 mole % KCl (78% YCl_3) is reacted with Y at 950°C then YCl is produced in a 70% yield with the remainder KY_2Cl_7.

A small plate crystal from a reaction of Y powder with YCl_3 at 850°C was selected for data collection. One hemisphere of data were collected

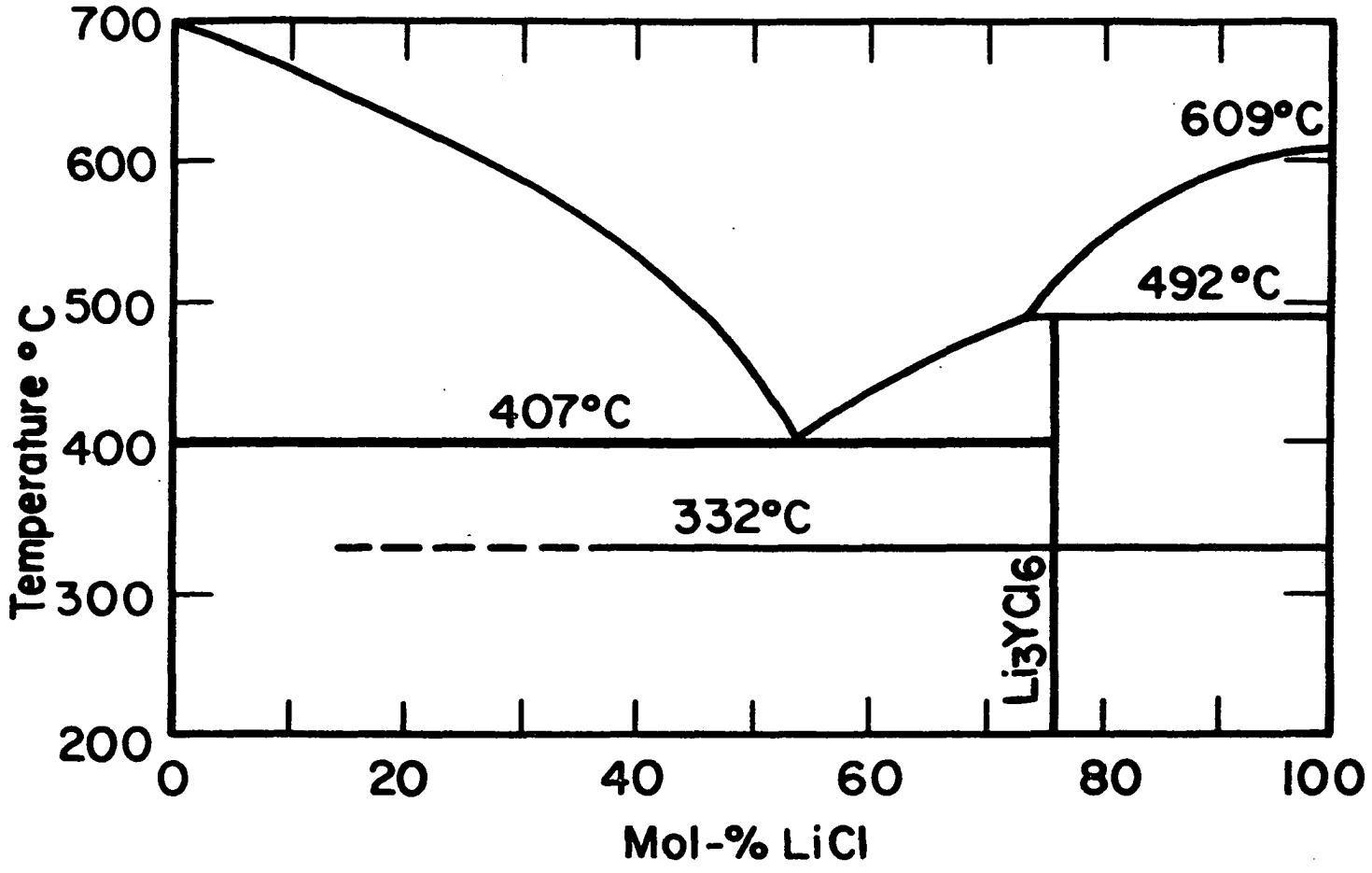

Figure 1. The phase diagram for $LiCl/YCl_3$ [38]

with the triclinic cell: $\underline{a}$ = 3.750 Å, $\underline{b}$ = 9.439 Å, $\underline{c}$ = 3.750 Å, $\alpha = 90.01^{o}$, $\beta = 119.95^{o}$, and $\gamma = 101.48^{o}$. Later it was observed that the indicies could be transformed to R-hexagonal by $h_R=h_T$, $k_R=\ell_T$, and $\ell_R=-2h_T-3k_T-\ell_T$. (This transformation is not given by the system manual.) The lattice constants for the R-hexagonal cell are: $\underline{a} = \underline{b}$ = 3.7523(2) Å, $\underline{c}$ = 27.525(5) Å and $\gamma = 120.0^{o}$. The absorption corrected data were then reduced and averaged in $\bar{3}m$ Laue symmetry.

The trial Y and Cl atom positions were obtained by examination of the atom positions for the isostructural ScCl[39] and ZrBr.[13] Full matrix least squares refinement using isotropic thermal parameters gave an unweighted residual of $R = \Sigma||F_o|-|F_c||/\Sigma|F_o| = 0.045$ and $R_w = (\Sigma w(|F_o|-|F_c|)^2/\Sigma w|F_o|^2)^{1/2} = 0.059$. Conversion to anisotropic thermal parameters yielded R = 0.039 and R_w = 0.054. The difference electron density map was flat to $<1e^-/Å^3$.

The final atom parameters together with important bond distances and angles are given in Table 2. The $(1\bar{1}0)$ projection and (110) section of the structure are shown in Figures 2 and 3, respectively. Observed and calculated structure factors are reported in Appendix A.

The four-layer sheet structure found for YCl is polytypic with ZrCl (allowing for the change in metal atom) and isomorphous with ZrBr.[12,13] The basic unit is a slab composed of four cubic-closed-packed and tightly bound layers Cl-Y-Y-Cl with the usual description of the layering geometry•••|AbcA|CabC|BcaB|••• or alternately, in terms of slabs•••ACB••• where the upper case letters represent the chlorine atoms orientations. The slabs are weakly bound by van der Waals interactions between the

Table 2. Final atom parameters, interatomic distances, and angles in YCl

Cell: Trigonal, $R\bar{3}m$

Lattice Constants: a = 3.7523(2) Å, c = 27.525(5) Å

Refinement: R = 0.039, R_w = 0.054

Atom Parameters:	x	y	z	$B^a_{11}=B_{22}$	B_{33}
Y	0.0	0.0	0.21683(5)	1.08(6)	1.31(9)
Cl	0.0	0.0	0.3883(1)	1.5(1)	1.2(1)

Distances (Å):

Intralayer		Interlayer	
Y-Y	3.7523(2)	Y-Y	3.511(2)
Cl-Cl	3.7523(2)	Cl-Cl	3.722(5)
		Y-Cl	2.750(2)

Interlayer Angles (deg):

Angles defining the antiprismatic coordination of Y		Angles defining the primatic coordination of Cl	
Y-Y-Y	64.62(4)	Cl-Cl-Cl	60.56(9)
Cl-Y-Y	103.96(4)	Cl-Cl-Y	92.39(3)
Cl-Y-Cl	86.05(7)	Y-Cl-Y	86.05(7)

[a]The thermal parameter expression used is $\exp-(1/4(B_{11}a^{*2}(h^2+hk+k^2) + B_{33}\ell^2c^{*2}))$, $B_{12}=1/2B_{11}$, $B_{13}=-B_{23}=0$.

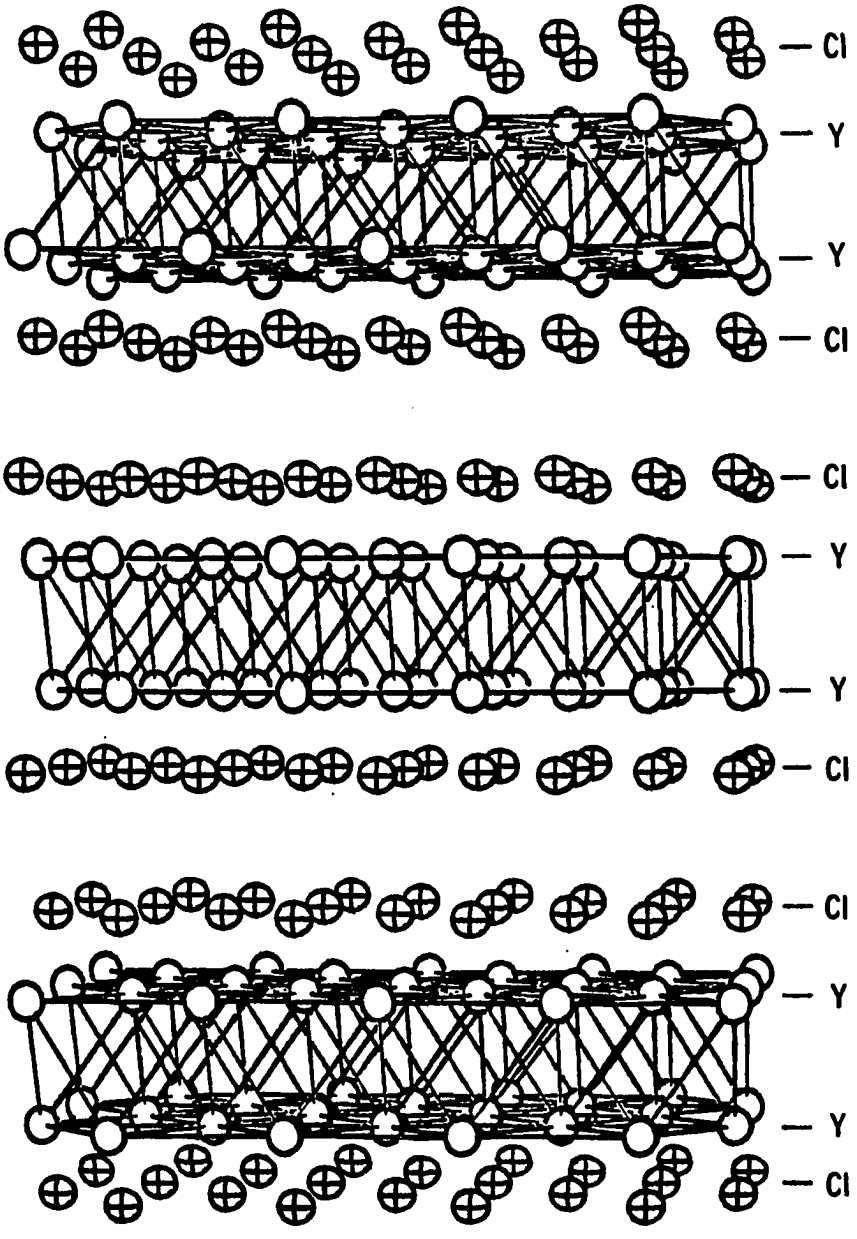

Figure 2. Three slabs in the ($\bar{1}10$) projection of YCl with the neighboring yttrium atoms interconnected; c-axis vertical

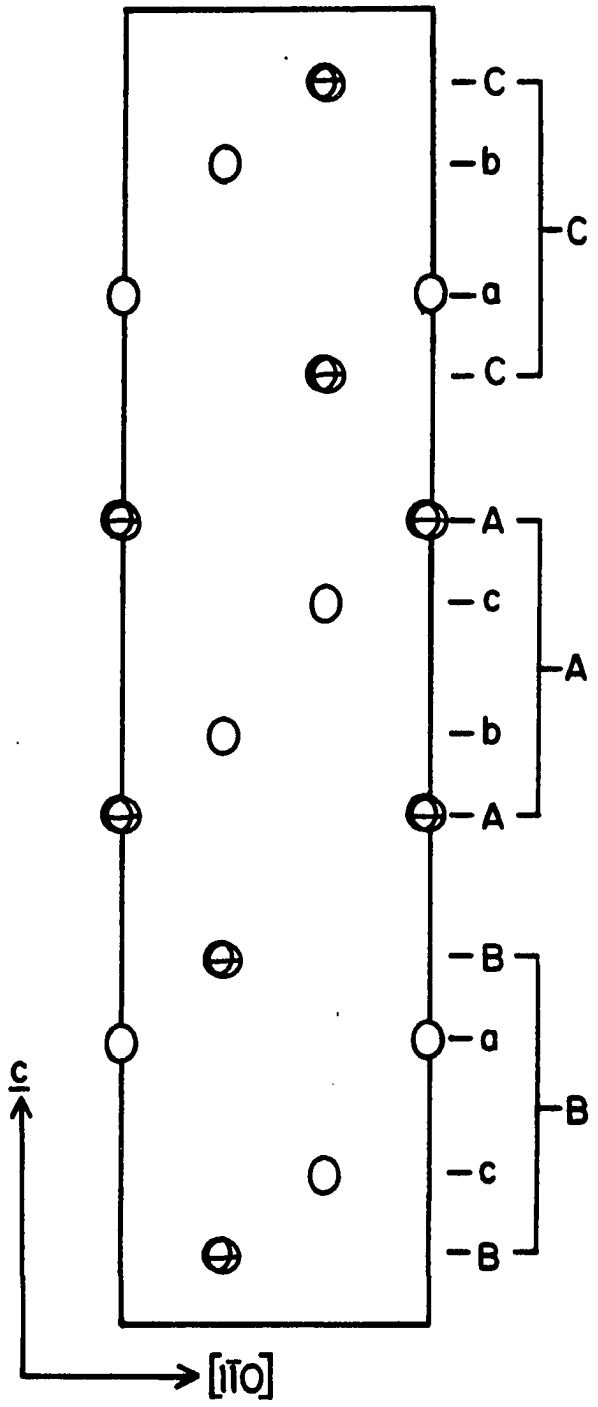

Figure 3. The (110) section of YCl with the layer packing sequence labelled inside the bracket and the slab packing sequence on the outside of the brackets. The upper case letters correspond to the Cl layers and the lower case the Y layers

chlorine layers. The result is the antiprismatic coordination of the Y atoms and prismatic coordination of the chlorine atoms.

The two yttrium-yttrium distances, 3.511 and 3.7523 Å, indicate strong metal-metal bonding between the metal layers and a somewhat lower bond order for the metal-metal bonds between atoms in a layer. In hcp yttrium metal the distances are 3.56 Å and 3.629 Å for inter- and intra-layer distances, respectively, the difference arising because of a small distortion from the ideal c/a ratio for close-packed structures.[40] The distortion in YCl is even greater but chemically reasonable since each metal layer is now adjacent to and commensurate with a chlorine layer. The yttrium-chlorine distance, 2.750 Å, compares closely with the sum of the crystal radii (Shannon[41]) for six coordinate yttrium and chlorine, 2.71 Å. The Cl-Cl interlayer distance of 3.722 Å compares favorably with 3.70 Å in ScCl and 3.61 Å in ZrCl.[39,12] This represents a very reasonable distance for weak Cl-Cl van der Waals interactions. This weak interlayer binding is also responsible for the graphitic properties of YCl along with, in part, the intercalation reactions which will be discussed in later sections.

Intercalation of Yttrium Monochloride

These reactions were complicated by the presence of impurity phases, $M^I_xYClO_z$ and $M^I_xY_2Cl_2C_z$. Reactions with M^ICl, YCl_3, and Y have yielded $M^I_xYClO_z$ in up to 50% yields while $M^I_xY_2Cl_2C_z$ is typically produced in 10 - 15% yields. The presence of these phases makes it very difficult to separate a possible M^I_xYCl phase because all three phases have black plate-like morphologies. In order to have a reasonable chance of finding M^I_xYCl the impurities should be removed. This should include careful cleaning and handling of the Nb tube, flaming the quartz jacket, and the use of freshly distilled YCl_3 and M^ICl. Powdered yttrium has the advantage of providing better contact with the melt but it also has the disadvantage of a higher oxygen content. On the other hand, yttrium strips contain less oxygen but contact with the melt is limited. One possible method for increasing the contact between the metal and the melt and reducing the oxygen content is to use a large excess of yttrium strips in pressed tube reactions.

Two reactions with powdered Y, YCl_3, and LiCl at 875°C produced 3R-Li_xYCl in 5-15% yields. These reactions also produced 30-40% yields of 3R-Li_xYClO_z. The black hexagonal-shaped platelets of 3R-Li_xYCl were found growing from sintered clumps of yttrium. Powder patterns of the plate crystals showed an expanded YCl-type structure with lattice constants, $\underline{a}$ = 3.7481(3) Å and $\underline{c}$ = 27.796(7) Å and γ = 120.0°. Oscillation and Weissenberg photographs of a nearly single crystal showed R-centering and $\underline{a} = \underline{b}$ = 3.75 Å and $\underline{c}$ = 27.81 Å. This crystal was not

chosen for data collection but a small plate crystal from a second reaction was used in data collection.

A full hemisphere of data, 2604 reflections, were collected out to $2\theta<60^{o}$. The hexagonal lattice constants are: $\underline{a}$ = 3.7513(2) Å and $\underline{c}$ = 27.803(2) Å. The data set was absorption corrected using two ϕ-scans. The R-centering condition, which was evident from the data collection and Weissenberg photographs, was applied during data reduction. There were 28 violations of the R-centering condition that were not observed every time with F_{obs} values that ranged from 5 to 14.2. The elimination of these reflections can be justified on the basis that in every case there was some overlap of strong adjacent peaks. Averaging the data in $R\bar{3}m$ yielded 156 independent reflections with an R = 0.038.

Using the Y and Cl positions from YCl and anisotropic thermal parameters yielded an R = 0.055 and R_w = 0.073. The resulting electron density map showed two possible positions for Li^+. The first position was a trigonal antiprismatic hole between the chlorine layers which had a peak height of 2 relative to a yttrium peak height of 241. The second was a tetrahedral position with a peak height of 3. Attempts to refine the structure with lithium in the tetrahedral hole caused the position to "blow up". On the other hand, the lithium refined without any problems in the trigonal antiprismatic hole. The multiplier and B for Li were allowed to vary simultaneously to give final R and R_w values of 0.056 and 0.072, respectively. The resulting difference electron density map was flat to $<1e^{-}/Å^3$. The final atom parameters are reported in Table 3.

The conclusion that lithium is present based only on the structure

refinement is tenuous at best. The lattice constants and interlayer distances reported in Table 4 help to support the conclusion that lithium is present. The formulation $Li^{+}_{0.09}(YCl)^{0.09}$ leads to a prediction that the intralayer and interlayer yttrium-yttrium distances should be shortened (relative to YCl) by the reduction of the YCl host lattice. The interlayer yttrium-yttrium distance does indeed show an 8σ decrease from that in YCl. The intralayer distances from the single crystal lattice constants do not show a significant decrease but intralayer distances (a-axis) according to Guinier powder data show an 11σ decrease. The insertion of lithium is also reflected in the lengthening of the c-axis from 27.525 Å to 27.803 Å and the Cl-Cl interlayer distance from 3.722(5) Å to 3.747(5) Å. The Li-Cl distance, 2.651 Å, is slightly longer than the sum of the six coordinate crystal radii (Shannon[41]), 2.57 Å.

The (110) section for $Li_{0.09}YCl$ is shown in Figure 4. The structure is that of the YCl host lattice with the trigonal antiprismatic site between the chlorine layers randomly occupied approximately 36% by lithium. This structure results in the trigonal antiprismatic coordination of all atoms in this structure.

Table 3. Crystallographic data for 3R-$Li_{0.09}YCl$

Composition: $Li_{0.09(8)}YCl$

Cell: Trigonal, $R\bar{3}m$

Lattice Constants: a = 3.7513(2) Å, c = 27.803(2) Å

Refinement: R = 0.056 R_w = 0.072.

Atom Parameters:[a]

	z	$B_{11}=B_{22}$[b]	B_{33}
Y	0.21583(4)	1.12(5)	1.15(6)
Cl	0.3883(1)	1.40(8)	1.1(1)
Li[c,d]	0.0	1.1(46)	

---

[a] x = 0.0, y = 0.0.

[b] The thermal parameter expression used is $\exp-(1/4(B_{11}a^{*2}(h^2+hk+k^2) + B_{33}\ell^2c^{*2}))$, $B_{12}=1/2B_{11}$, $B_{13}=-B_{23}=0.0$.

[c] Occupancy = 0.09(8).

[d] Isotropic B.

Table 4. Comparison of interlayer distances in YCl and 3R-$Li_{0.09}YCl$ and the angles for 3R-$Li_{0.09}YCl$

Interlayer Distances, (Å)

	YCl	$Li_{0.09}YCl$
Y-3Y	3.511(2)	3.488(2)
Y-3Cl	2.750(2)	2.777(2)
Cl-3Cl	3.722(5)	3.747(5)
Li-6Cl		2.651(2)

Interlayer Angles, (deg)

Angles defining the antiprismatic coordination of Y

Y-Y-Y	57.47(2)
Cl-Y-Y	104.38(4)
Cl-Y-Cl	84.98(8)

Angles defining the antiprismatic coordination of Cl

Y-Cl-Y	84.98(8)
Li-Cl-Li	90.06(8)
Y-Cl-Li	92.43(1)

Angles defining the antiprismatic coordination of Li^+

Cl-Li-Cl	90.06(8)
Cl-Li-Cl	89.94(8)

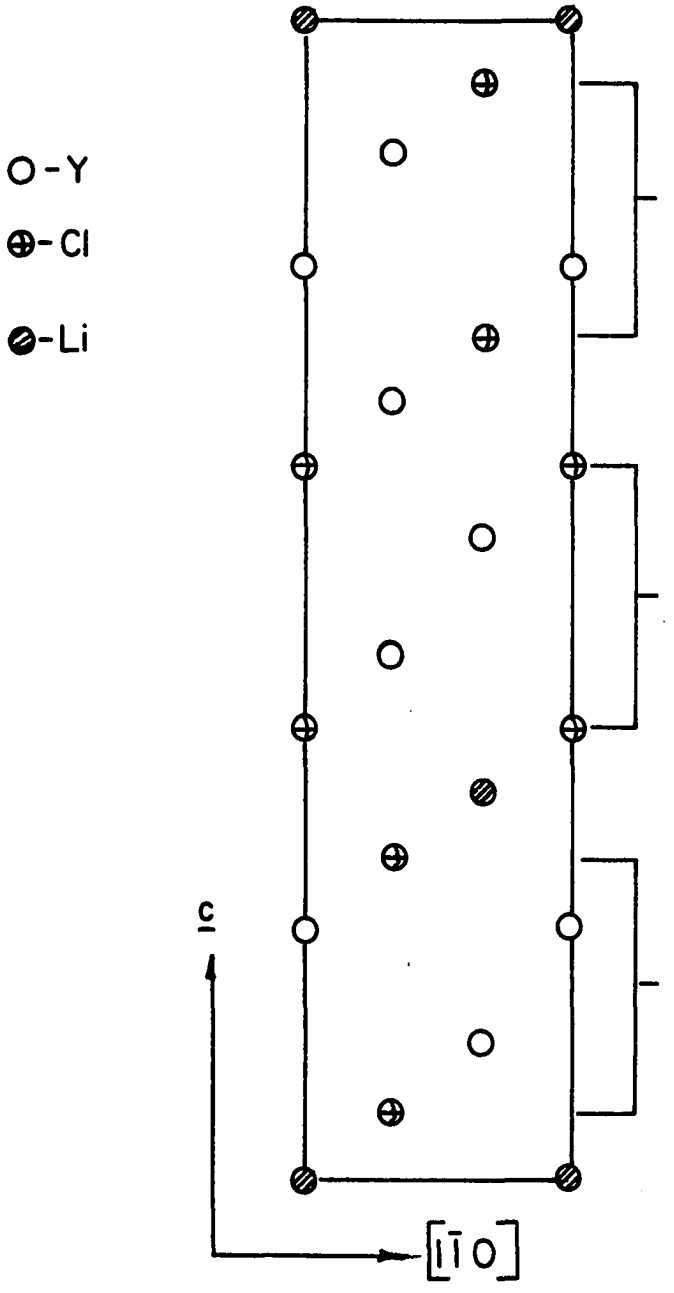

Figure 4. The (110) section of 3R-$Li_{0.09}YCl$ with the brackets used to identify each slab

Intercalation of Oxide Interstitial Derivatives of YCl

Compounds of the general formula type $M^I_xYClO_z$ with M^I=Li-Cs were first prepared accidentally by reactions of powdered Y, YCl_3, and M^ICl at temperatures greater than 875°C for 2-4 weeks. The resulting products are irregularly shaped black plate crystals which grow from the melt. The yields ranged from 5-60%. All powder patterns could be indexed with a hexagonal/trigonal cell with a small increase along a (vs. YCl) and a c-axis value which corresponded to the insertion of the alkali metal. A plot of the one slab thickness (=c/n) vs. M^I crystal radii for the $M^I_xYClO_z$ phases is shown in Figure 5. At first it was assumed that these compounds were the ternary M^I_xYCl phases.

It was not until the crystal structure of $2H\text{-}K_{0.08}YClO_{0.82}$ was solved that the true identity of these compounds was discovered. The refinement of this structure is discussed in a following section. The structure showed that there was something in the tetrahedral-like interstices between the yttrium layers. The most likely source of the oxygen impurity is a poor batch of powdered yttrium but the YCl_3 and M^ICl salts are also possibilities. Subsequent reactions using Y_2O_3 or YOCl as oxygen sources gave high yields of the same phase as the "ternary" reactions with the oxygen impurity. The presence of oxygen has also been confirmed qualitatively by microprobe.

The best preparative methods for producing $M^I_xYClO_z$ are from the compositions (1) or (2) with $0.3<d\lesssim 1.0$. The amount of oxygen from impurity

(1) $dY \text{ powder} + dM^ICl + YCl_3 + Y_2O_3 \xrightarrow{>925^oC} M^I_dY_{3+d}Cl_{3+d}O_{3+e}$

(2) $dY \text{ powder} + dM^ICl + 3YOCl \xrightarrow{>925^oC} M^I_dY_{3+d}Cl_{3+d}O_{3+e}$

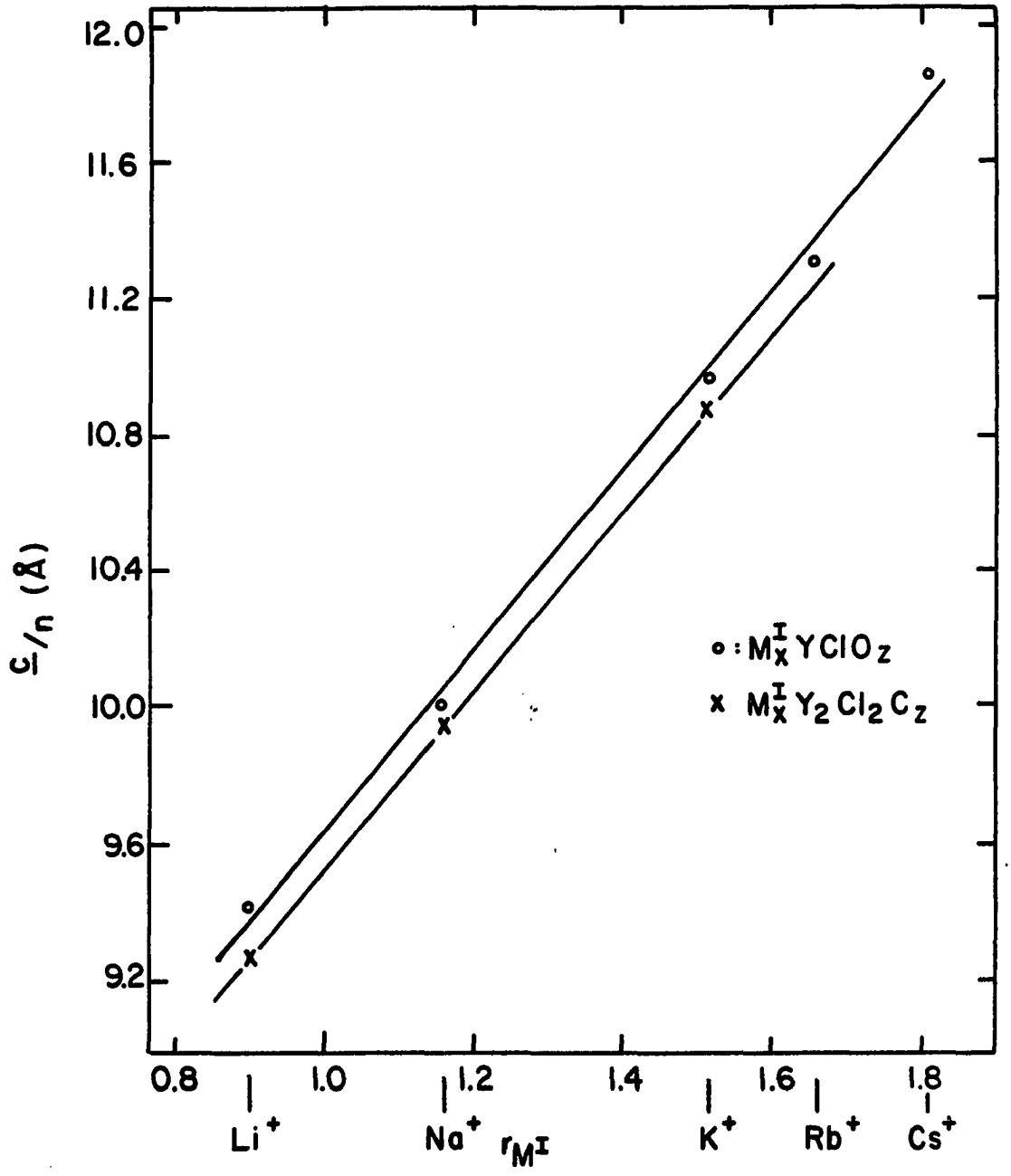

Figure 5. A plot of c/n, where n=number of slabs/unit length, versus the alkali metal radius (M^I) for $M^I_xYClO_z$ and $M^I_xY_2Cl_2C_z$

sources is not known and labeled e in these reactions. The phase obtained depends on the stoichiometry of the reactants but the yields are nearly 100% with these conditions.

Many of these compounds have polymorphs so the following nomenclature has been adopted. The number of slabs (the repeat unit $\cdots M^{I}ClYOOYCl\cdots$ which stack along c) in the unit cell along with the symmetry of the cell will preceed the formula for that phase. For example, there are two Na_xYClO_z phases, 2H-Na_xYClO_z and 3R-Na_xYClO_z where the first phase has two slabs per unit cell ($c \approx 20$ Å) and hexagonal symmetry while the second has three slabs per unit cell ($c \sim 30$ Å) and rhombohedral symmetry.

K_xYClO_z system

This has been the most extensively studied system of the reactions involving alkali metal chlorides and oxygen. There are two structural varieties in this system, 2H- and 3R-K_xYClO_z. The structural determination and features of these structures will be discussed in the following sections.

In Table 5, the molar ratios and lattice constants of the products from the "ternary" reactions are given. Reactions in the "ternary" Y, YCl_3, and KCl system yield exclusively the 2H-K_xYClO_z phase in yields up to 50%. In many cases, there is also a 10-15% yield of 1T-$K_xY_2Cl_2C_z$. The irregularly shaped black plate crystals of the 2H phase are usually found on the walls of the Nb reaction tube and are most often coated with K_3YCl_6. The observed powder patterns match very well with both the calculated pattern of 2H-K_xYClO_z based on the structure of $K_{0.08}YClO_{0.82}$ and the powder patterns of the 2H phase obtained from reactions using Y_2O_3.

Table 5. The stoichiometries, products, and lattice constants for reactions in the K_xYClO_z system

$dY + dKCl + Y_2O_3 + YCl_3$

d(moles)	Product(s)	Lattice Constants,(Å)	
		a	c
0.68	2H-K_xYClO_z	3.7894(2)	21.939(4)
	3R-K_xYClO_z	3.7897(2)	32.893(7)
2.4	3R-K_xYClO_z,KCl,Y	3.7910(2)	32.887(8)

$dY + dKCl + 3YOCl$

d(moles)	Product(s)	Lattice Constants,(Å)	
		a	c
1.6	3R-K_xYClO_z,KCl,Y	3.7898(5)	32.87(2)
1.3	3R-K_xYClO_z,KCl,Y	3.7908(3)	32.881(9)
1.0	3R-K_xYClO_z	3.7921(3)	32.852(8)
0.52	3R-K_xYClO_z	3.7894(2)	32.76(1)
0.36	3R-K_xYClO_z,YOCl	3.7899(3)	32.72(1)
0.18	3R-K_xYClO_z	3.7956(4)	32.87(1)
	(?)3/2-K_xYClO_z	3.769(1)	31.6(2)

$4Y + dKCl + YCl_3$ $+ K_3YCl_6$

d(moles)	Product(s)[a]	Lattice Constants,(Å)	
		a	c
0.66	2H-K_xYClO_z	3.7843(3)	21.96(1)
0.68	2H-K_xYClO_z	3.7858(1)	21.903(4)
0.76	2H-K_xYClO_z	3.7877(4)	22.08(4)

[a]Oxygen is from an impurity source.

Quaternary reactions similar to reaction (1) produced both the 2H- and 3R-K_xYClO_z. In these reactions, the product is usually black microcrystalline plates which aggregate into chunks or clumps. The yields for reaction (1) are nearly 100%. In Table 5, the molar stoichiometries, products, and lattice constants for reaction (1) are given. There have been other reactions, which are not listed in Table 5 where the molar ratios of all components have been varied and these have produced the 2H- or 3R- or both phases. The consistent trend that these reactions have shown is that as the KCl concentration is decreased then only the 2H phase is obtained. When the KCl concentration is large only the 3R phase is obtained. At intermediate ratios, e.g., d = 0.68, both phases are obtained.

The results from the variation in composition, d in reaction (1), show that there are minimum and maximum values of d which produce only 3R-K_xYClO_z. The composition limits for 3R-K_xYClO_z on this basis are $0.18 < x < 0.3$ and $0.70 \lesssim z \lesssim 0.94$, assuming a single phase product.

A second type of quaternary reactions, reaction (2) with YOCl, has produced 3R-K_xYClO_z and <u>no</u> 2H-K_xYClO_z. The 3R product is again black microcrystalline plates which aggregate into chunks. Reaction (2) was run with d = 1.6, 1.3, 1.0, 0.66, 0.52, 0.36, and 0.18 moles at 945°C for 2-3 weeks. When d = 1.6 and 1.3 moles the product is the 3R phase and unreacted KCl and Y. When d = 1.0, 0.66, and 0.52 there was nearly a quantitative yield of the 3R phase. The implied compositions, based on the stoichiometries of reaction (2), are $K_{0.25}YClO_{0.75}$, $K_{0.18}YClO_{0.82}$, and $K_{0.14}YClO_{0.85}$, respectively. For d = 0.36 there was a 70% yield of

3R and a 30% yield of YOCl (PbFCl structure). The product from this reaction was black chunks which when cleaved showed a yellow center of YOCl. For d = 0.18 there was 60% unreacted YOCl (PbFCl structure) and an ∿40% yield of gray material, the powder patterns showed the 3R phase with a slightly expanded a-axis and extra lines which paralleled the 3R lines with higher θ values. The extra lines are broad and give hexagonal lattice constants of a smaller cell with large standard deviations. This phase does not appear to be a staged K_xYClO_z because the c-axis is not a multiple of that of K_xYClO_z. It may be an intercalated form of YOCl in a 3R distortion of the PbFCl or FeOCl structure. The stoichiometries, products, and lattice constants for reaction (2) are summarized in Table 5.

A plot of the c-axis for 3R-K_xYClO_z vs. d, the number of moles KCl in reaction (2), is presented in Figure 6. The value for d = 0.18 was omitted since the yield of 3R-K_xYClO_z was so low. The number of data points is limited but the plot clearly shows that as the concentration of KCl (d) is increased the c-axis also increases until d ∿ 1.1 where the curve appears to flatten out. The explanation is that at d ∿ 1.1 saturation is reached and the saturation composition, i.e., maximum composition, based on the d value from the plot and reaction (2) is $K_{0.27}YClO_{\sim 0.73}$. The d value at saturation agrees with the observations that at d = 1.0 there was no KCl remaining after reaction and at d = 1.3 KCl was present. The saturation value is also supported by the results discussed in the next section with M^I=Li in reaction (2) where at d = 1.0 moles there was no LiCl present after the reaction while at d = 1.1 there was a small amount of LiCl and Y present. Both results support $M^I_{0.27}YClO_{\sim 0.73}$ as the

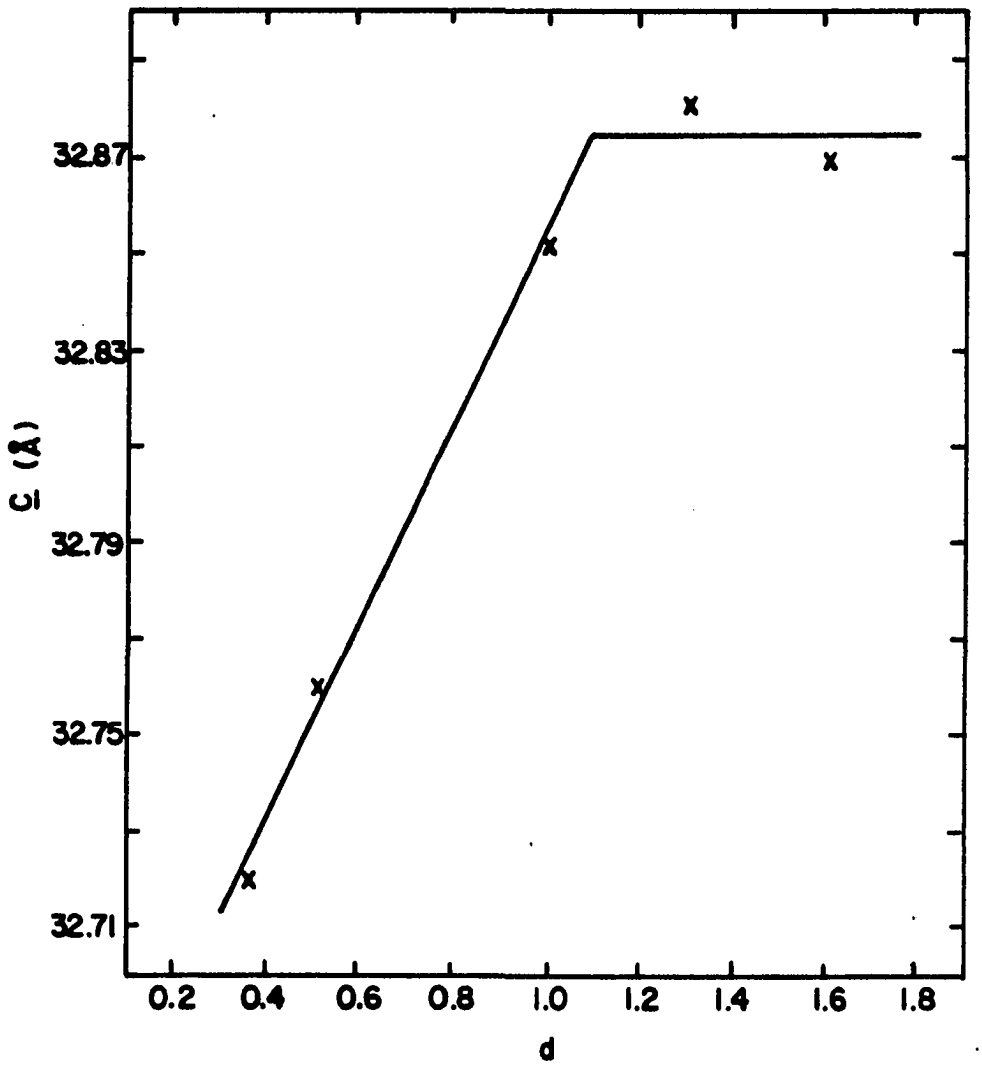

Figure 6. A plot of c versus d in the reaction: $dY + dKCl + 3YOCl \xrightarrow{\sim 950^{\circ}C} K_{d/3+d}YClO_{\sim 3/3+d}$

maximum alkali metal composition for the 3R phase. No information was gained from a plot of the a-axis vs. composition (d).

For the quaternary reactions, the 2H phase was identified by comparison of the observed powder patterns with that based on the $2H\text{-}K_{0.08}YClO_{0.82}$ structure. The 3R phase was likewise identified by comparison of the observed and calculated patterns based on the $3R\text{-}Na_xYClO_z$ structure.

A plate crystal from a "ternary" reaction was chosen for data collection. A full hemisphere of data, 1336 reflections, were collected on a primitive hexagonal cell: a = 3.7873(6) Å, c = 21.860(8) Å and $\gamma = 120.0^{\circ}$. Weissenberg photographs showed that 0,0,ℓ; ℓ = 2n+1 and h-k=3n; ℓ = 2n+1 extinction conditions were present. Examination of the diffractometer data showed there were 43 violations of the second extinction condition for which F_{obs} ranged from 7 to 71. Closer examination of these reflections showed that most were not observed every time, there was overlap with strong adjacent peaks, and the observed peak profiles had no maximum. The data set was absorption corrected and reduced with the extinction conditions applied. The data were averaged first in $P6_3/m$ and later in $P6_3/mmc$ when it was observed that $P6_3/mmc$ was equivalent and had higher symmetry.

The structure was solved using a Patterson map which indicated a Y atom at 1/3, 2/3, 4.5/64. Putting the Y position into ALLS yielded an R = 0.34. The chlorine position was obtained from the resulting electron density map. Refinement of the Y and Cl positions while varying the isotropic B's yielded R = 0.17. Letting the thermal parameters on Y and

Cl vary anisotropically dropped the R to 0.147. The resulting electron density map showed two extra peaks, one at 2/3, 1/3, 1/4 (between Cl layers) at 10% of Y and a second at 2/3, 1/3, 3/64 at 15% of Y. The peak at 2/3, 1/3, 1/4 was refined as a potassium atom. Varying the positions and anisotropic thermal parameters for Y and Cl and the multiplier and isotropic B for K yielded an R = 0.14 and a composition of $K_{0.06}YCl$.

At first, it was believed that this was the final solution of the structure and the extra peak in the e.d. map and the large R values were the result of poor crystal quality. The long Y-Y interlayer distances, 3.57 Å in the supposedly more reduced phase vs. 3.511 Å in YCl, could not be explained and this led to reassessment of the structure. Closer examination of the extra peak revealed it was in the tetrahedral-like interstice between the yttrium layers. The tetrahedral-like position and distances to yttrium of approximately 2.25 Å were all reasonable for an oxygen atom. Insertion of an oxygen atom and variation of the position dropped the R to 0.062. The structure refined to a final R = 0.057 and R_w = 0.075 on varying the positions and anisotropic thermal parameters on Y and Cl and the multipliers and isotropic B's on K and O.

The final atom parameters and a comparison of bond distances with YCl are given in Tables 6 and 7, respectively. The (110) section is shown in Figure 7.

The basic unit in the structure is a Cl-Y-O-O-Y-Cl slab which consists of four cubic-closed-packed layers of Cl-Y-Y-Cl with the oxygen atoms randomly disordered over the tetrahedral-like interstices between the metal layers. The layering geometry using only the chlorine (upper

Table 6. Crystallographic data for 2H-$K_{0.08}YClO_{0.82}$

Composition: $K_{0.08(2)}YClO_{0.82(6)}$

Cell: Hexagonal, $P6_3/mmc$

Lattice Constants: a = 3.7873(6) Å, c = 21.860(8) Å

Refinement: R = 0.057 R_w = 0.075

Atom Parameters:

	x	y	z	$B_{11}=B_{22}$[a]	B_{33}
Y	1/3	2/3	0.06447(9)	1.16(9)	2.7(1)
Cl	0.0	0.0	0.1469(3)	1.6(2)	2.8(2)
O[b,c]	2/3	1/3	0.0400(7)	0.78(47)	
K[c,d]	2/3	1/3	1/4	3.0(16)	

[a]The thermal parameter expression used is $\exp-(1/4(B_{11}a^{*2}(h^2+hk+k^2) + B_{33}\ell^2c^{*2}))$, $B_{12}=1/2B_{11}$, $B_{13}=-B_{23}=0$.

[b]Occupancy = 0.82(6).

[c]Isotropic B.

[d]Occupancy = 0.08(2).

Table 7. A comparison of distances in YCl and 2H-$K_{0.08}YClO_{0.82}$ and the bond angles for 2H-$K_{0.08}YClO_{0.82}$

Intralayer Distances, (Å)		
	YCl	$K_{0.08}YClO_{0.82}$
	3.7523(2)	3.7873(6)
Interlayer Distances, (Å)		
	YCl	$K_{0.08}YClO_{0.82}$
Y-3Y	3.511(2)	3.567(3)
Y-3Cl	2.750(2)	2.833(4)
Cl-3Cl	3.722(5)	4.51
K-6Cl		3.140(4)
Y-1O		2.284(15)
Y-3O		2.251(4)
O-3O		2.80(2)

Interlayer Angles,(deg)

Angles defining the tap[a] coordination about Y		Angles defining the tap[a] coordination about Cl	
Cl-Y-Cl	88.88(4)	Y-Cl-Y	83.88(4)
O-Y-O	114.55(2)	K-Cl-K	74.18(11)
O-Y-Cl	77.07(27)	K-Cl-Y	100.82(3)
Angles defining the tp[b] coordination about K		**Angles defining the tet[c] coordination about O**	
Cl-K-Cl	74.18(11) (base)	Y-O-Y	114.55(28) (base)
Cl-K-Cl	91.73(14)	Y-O-Y	103.74

[a] tap = trigonal antiprismatic.
[b] tp = trigonal prismatic.
[c] tet = tetrahedral.

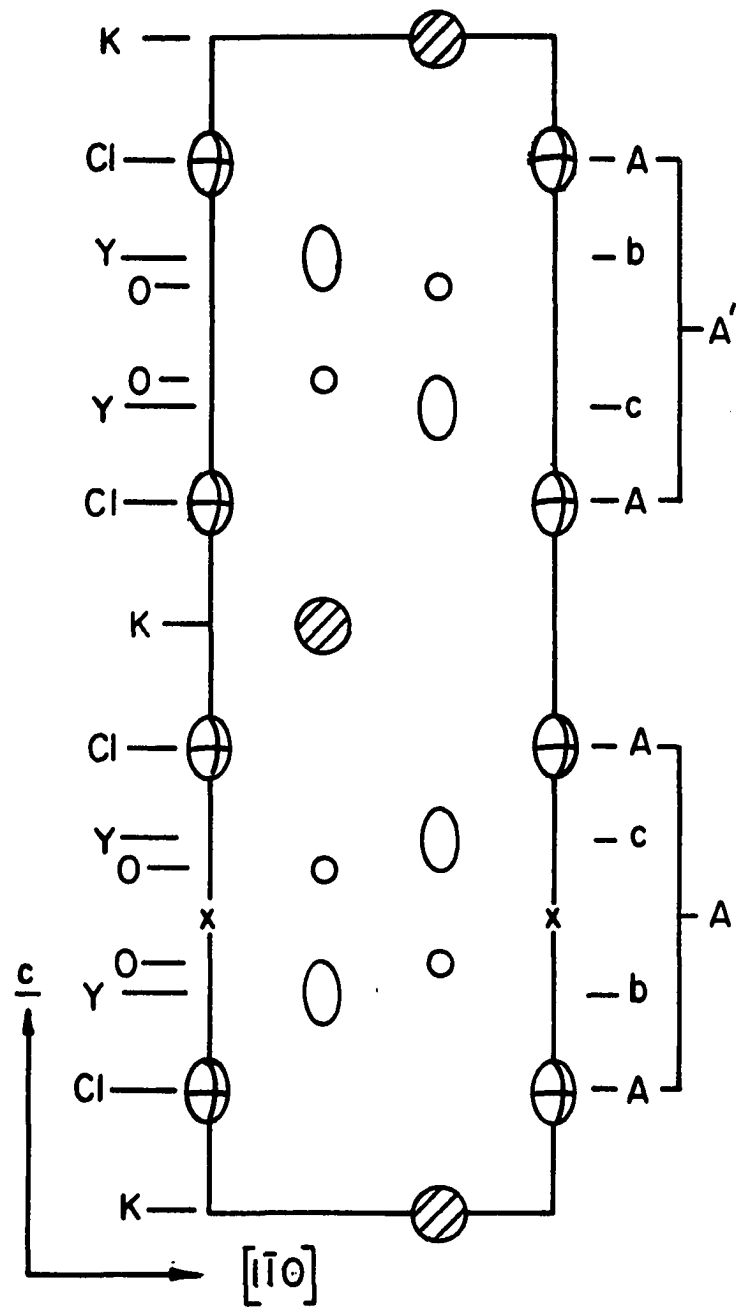

Figure 7. The (110) section of $2H\text{-}K_{0.08}YClO_{0.82}$, the correct origin is at x

case letters) and yttrium layers is •••|AbcA|AcbA|••• or alternately in terms of slabs •••AA'••• where the A' slab involves a reversal of the metal atom positions from the A slab. The A slab is the same as the slabs in YCl, ZrCl, ZrBr, etc. (ignoring the oxygen atoms) and taking into account the oxygen atoms is isostructural with the slabs in $ZrClO_x$ and $ZrBrO_x$.[12,13,17] The A' slab is different from any slab sequence in the monohalides and thus in order to obtain this 2-slab structure from the 3-slab monohalides there would have to be a "sliding" within the slabs, that is, a structural rearrangement of the metal atoms within every other slab.

The placing of all chlorine atoms at 0,0,z positions results in trigonal prismatic holes between the chlorine layers. There are two possible trigonal prismatic holes and the potassium occupies that with oxygen atoms as second nearest neighbors.

The oxygen atoms lie above and below the trigonal prism of chlorine atoms. It is the advantage of having two oxygen atoms as second nearest neighbors for potassium that may create the •••AA'••• slab stacking. If the slabs stacked •••AA•••, as they do in 1T-Cs_xYClO_z (a derivative of the 3R-$M^I_xYClO_z$ structure which is described in a following section), there would be a yttrium atom as a second nearest neighbor for potassium. Thus, the 2H structure provides a very rational way of incorporating oxygen atoms in the tetrahedral-like interstices and providing trigonal prismatic coordination of the alkali metal.

The distances in the structure are all very reasonable. The Y-Y inter- and intralayer distances have increased slightly relative to YCl

to accommodate the oxygen in the tetrahedral-like interstices. The Cl-Cl interlayer distance has increased dramatically to accommodate the potassium. This is also reflected in the lengthening of the c-axis. The K-Cl distance of 3.140 Å is only slightly shorter than the sum of the six coordinate crystal radii for K^+ and Cl^-, 3.19 Å. The Y-O distances of 2.25 - 2.28 Å are very reasonable when compared to Y-O distances of 2.28 Å in both Y_2O_3[42] and YOCl (PbFCl structure).[14]

Li_xYClO_z system

Only one phase has been observed in this system, 3R-Li_xYClO_z. The stoichiometries and lattice constants for the reactions that produced 3R-Li_xYClO_z are listed in Table 8.

Reactions in the "ternary" Y, YCl_3, and LiCl system yielded 3R-Li_xYClO_z as the major product along with small amounts of 1T-$Li_xY_2Cl_2C_z$ and 3R-Li_xYCl. This contrasts with other systems which generally yield 2H-$M^I_xYClO_z$ and 1T-$M^I_xY_2Cl_2C_z$. The 3R-phase is characterized as black irregularly shaped plates which are found on the walls of the Nb reaction tube. The observed powder patterns of the black plates match very well with the calculated pattern of 3R-Li_xYClO_z based on the 3R-Na_xYClO_z structure and the powder patterns of the 3R-Li_xYClO_z phase prepared in reactions using Y_2O_3 or YOCl.

Reactions (1) and (2) have both produced 3R-Li_xYClO_z in nearly quantitative yields. The 3R phase forms as black microcrystalline plates which aggregate into chunks or clumps. When d is 0.65 - 0.69 for reaction (1) and d = 1.0 for reaction (2) only the 3R phase is formed with no Y and

Table 8. The stoichiometries, products, and lattice constants for reactions in the Li_xYClO_z system

$dY\ powder + dLiCl + Y_2O_3 + YCl_3 \xrightarrow{\sim 950^oC}$

		Lattice Constants, (Å)	
d(moles)	Products	a	c
0.68	$3R\text{-}Li_xYClO_z$	3.7873(1)	28.259(4)
0.64	$3R\text{-}Li_xYClO_z$	3.7851(3)	28.271(7)
0.69	$3R\text{-}Li_xYClO_z$	3.7855(1)	28.197(4)

$dY\ powder + dLiCl + 3YOCl \xrightarrow{\sim 950^oC}$

		Lattice Constants, (Å)	
d(moles)	Products	a	c
1.0	$3R\text{-}Li_xYClO_z$	3.7872(2)	28.262(5)
1.0	$3R\text{-}Li_xYClO_z$	3.7867(3)	28.22(1)
1.1	$3R\text{-}Li_xYClO_z$,LiCl,Y	3.7864(2)	28.249(6)
1.1	$3R\text{-}Li_xYClO_z$,LiCl,Y	3.7870(2)	28.250(4)
1.1	$3R\text{-}Li_xYClO_z$,LiCl,Y	3.7868(2)	28.242(5)
1.1	$3R\text{-}Li_xYClO_z$,LiCl,Y	3.7867(2)	28.228(5)

$x.s.\ Y + dLiCl + 1YCl_3 \xrightarrow{\sim 875^oC}$

		Lattice Constants, (Å)	
d(moles)	Products[a]	a	c
3.0	$3R\text{-}Li_xYClO_z$,$3R\text{-}Li_xYCl$	3.7800(7)	28.11(4)
2.1	$3R\text{-}Li_xYClO_z$,$1T\text{-}Li_xYClC_z$	3.791(1)	28.19(5)

[a]Oxygen is from an impurity.

LiCl observed in the powder patterns. Based on the stoichiometries of the reactions the compositions are $Li_{0.18}YClO_{0.82}$ and $Li_{0.25}YClO_{0.75}$, respectively. When d = 1.1 for reaction (2), the products contained unreacted Y and LiCl along with the 3R phase. This places a maximum of x = 0.27 and z = 0.73 for 3R-Li_xYClO_z which is in agreement with the previous section.

The products with composition $Li_{0.18}YClO_{0.82}$ and $Li_{0.25}YClO_{0.75}$ were used for ^7Li NMR studies. The samples were ground in the dry box (with a mortar and pestle) and sealed off under vacuum in a 10 mm o.d. fused silica tube. In each case, there was enough sample to fill the tube 1.1 - 1.2 cm. high. Both samples show a wide line at room temperature.

The details and (110) section of the 3R structure can be found in the section on the crystal structure of 3R-Na_xYClO_z.

Na_xYClO_z system

There are two phases which have been characterized in this system, 2H-Na_xYClO_z and 3R-Na_xYClO_z. The stoichiometries, products, and lattice constants for the reactions that produced these phases are listed in Table 9.

Reactions in the "ternary" Y, YCl_3, and NaCl produced almost exclusively the 2H-Na_xYClO_z in yields up to 50%. The 2H phase forms as irregularly shaped black plate crystals on the walls of the Nb reaction tube. The observed powder pattern of these plates match moderately well (considering the broad lines in the observed pattern) with the calculated

Table 9. The stoichiometries, products, and lattice constants for reactions in the Na_xYClO_z system

g Y powder + dNaCl + Y_2O_3 + YCl_3 $\xrightarrow{>900^oC}$

g(moles)	d(moles)	Products	Lattice Constants,(Å) a	c
0.67	0.66	2H-Na_xYClO_z	3.7863(5)	20.13(1)
0.82	0.63	2H-Na_xYClO_z	3.7861(2)	20.039(7)
0.63	1.4	2H-Na_xYClO_z		
		3R-Na_xYClO_z	3.7883(5)	29.947(8)
1.1	3.1	2H-Na_xYClO_z		
		3R-Na_xYClO_z	3.7854(5)	29.96(2)

x.s. Y powder + dNaCl + YCl_3 $\xrightarrow{>875\ C}$ Na_3YCl_6+

d(moles)	Products[a]	Lattice Constants,(Å) a	c
3.0	2H-Na_xYClO_z	3.7847(8)	20.0(1)
2.5	2H-Na_xYClO_z, 1T-$Na_xY_2Cl_2C_z$	3.7836(4)	20.00(1)
3.0	2H-Na_xYClO_z	3.7835(2)	20.25(6)
7.6	2H-Na_xYClO_z		
	3R-Na_xYClO_z	3.7881(3)	29.445(5)

[a]Oxygen is from an impurity.

powder pattern based on the $K_{0.08}YClO_{0.82}$ structure and are identical with the patterns of the 2H phase prepared in reactions using Y_2O_3.

In a "ternary" reaction using a large amount of NaCl, (see Table 9) the major product was the 2H phase along with a small yield of 3R-Na_xYClO_z. The 3R phase was identified by the Weissenberg photographs of two crystals which showed the R symmetry. The crystal used in the structure determination of 3R-$Na_{0.08}YClO_{1.0}$ was obtained from this reaction. This is the only "ternary" reaction for M^I= Na-Cs which produced a 3R-$M^I_xYClO_z$ phase. The formation of the 3R phase can probably be attributed to the large concentration of NaCl.

Quaternary reactions using Y powder, NaCl, YCl_3, and Y_2O_3 have produced both the 2H- and 3R-Na_xYClO_z phases. The products in these reactions are black microcrystalline plates which aggregate into chunks. Reactions with less NaCl produce only the 2H phase while reactions with more NaCl produce both the 2H and 3R phases. No reactions in this system have produced exclusively the 3R phase but this probably is the result of the incorrect reaction conditions. Reactions similar to reactions (1) and (2) in the K_xYClO_z system with d>1.0 should yield only the 3R phase.

In contrast to the behavior of all other phases, the Guinier powder patterns of the Na-2H phase produced in both "ternary" and quaternary reactions show many broad lines. The inaccuracy in reading the broad reflections has led to larger standard deviations of the lattice parameters. It is interesting that Weissenberg photographs (0-4th level in k) of 2H-Na_xYClO_z show streaking along all festoons where $h-k\neq 3n$ while all festoons with h-k=3n show only single spots. The streaking in the

Weissenberg photos can be correlated with the broad lines in the powder patterns by the same h-k≠3n condition. In the powder pattern, all lines with h-k≠3n are sharp while all lines with h-k≠3n are broad. The cause of the broad lines and streaked festoons is believed to be disorder along the c-axis. In the 3R-Na_xYClO_z powder patterns, all lines are sharp and there is very good agreement with the calculated powder pattern based on the 3R-$Na_{0.08}YClO_{1.0}$ structure.

A black plate crystal obtained from a "ternary" reaction was used for data collection. A full hemisphere of data, 1794 reflections, were collected on the hexagonal cell: a = 3.7881(3) Å and c = 29.445(5) Å. Weissenberg photographs and the crystal data showed that the R-centering condition extinction condition was present, -h+k+ℓ≠3n. The data were absorption corrected, reduced with the R-centering condition applied, and averaged in $R\bar{3}m$(R=0.074).

The yttrium and chlorine positions were obtained from the YCl structure. The isotropic refinement of the Y and Cl positions resulted in an R = 0.215 and R_w = 0.258. The oxygen and sodium positions were determined from the resulting electron density map. Varying the positions and anisotropic thermal parameters on Y and Cl and the position, multiplier and isotropic B on O yielded an R = 0.112 and R_w = 0.125. The sodium was added to the refinement and its isotropic B went negative when both the multiplier and B were varied together. The multiplier and B were then alternately varied on successive cycles and the structure refined to a R = 0.109 and R_w = 0.122.

The difference electron density map showed an extra peak at 0,0,0.454 of ∿2.3 electrons. The extra peak is not in any type of an interstitial position in the structure and can only be considered as electron density which is slightly displaced from the metal layers towards the oxygen layers. The distances from the extra peak to neighboring atoms are very unreasonable for bonding distances, e.g., the distance from the peak to Cl, Y, and O are 1.83 Å, 2.19 Å, and 2.21 Å, respectively. This implies the peak is not the result of an atom and is caused by some type of crystal imperfection. The extra peak and poor refinement are probably caused by poor crystal quality which is evident in the averaging of the data and Weissenberg photos that show streaking along all festoons. The streaking along the festoons was also observed in Weissenberg photos of the 2H phase but in this case they only have 10% of the intensity of the large peaks. The streaking implies some type of disorder along the c-axis.

The final atom parameters along with the distances in this structure, YCl, and $K_{0.08}YClO_{0.82}$ are given in Tables 10 and 11, respectively. A schematic representation of the (110) section is shown in Figure 8.

The basic YCl slab unit of Cl-Y-Y-Cl and the YCl slab stacking described by the layering geometry •••|AbcA|CabC|BcaB|••• or •••ACB••• is retained with all the tetrahedral-like interstices between the yttrium layers filled with oxygen and the trigonal antiprismatic holes between the chlorine layers randomly occupied with sodium. The structure, ignoring the sodium atoms, is isostructural with $ZrBrO_x$ and YOF.[17]

Table 10. Crystallographic data for 3R-$Na_{0.08}YClO_{1.0}$

Composition: $Na_{0.08(3)}YClO_{1.0(1)}$

Cell: Trigonal, $R\bar{3}m$

Lattice Constants: a = 3.7881(3) Å, c = 29.445(5) Å

Refinement: R = 0.109 R_w = 0.122

Atom Parameters:[a]

	z	$B_{11}^b=B_{22}$	B_{33}
Y	0.2148(1)	0.53(15)	2.87(22)
Cl	0.3915(3)	1.33(27)	1.63(38)
O[c,d]	0.1306(8)	0.68(80)	
Na[e,d]	0.0	1.25	

---

[a] x = 0.0 and y = 0.0.

[b] The thermal parameter expression used is $\exp-(1/4(B_{11}a^{*2}(h^2+hk^2+k^2) + B_{33}\ell^2c^{*2}))$, $B_{12}=1/2B_{33}$, $B_{13}=-B_{23}=0$.

[c] Occupancy = 1.0(1).

[d] Isotropic B.

[e] Occupancy = 0.08(3).

Table 11. Comparison of distances in YCl, 2H-$K_{0.08}YClO_{0.82}$, and 3R-$Na_{0.08}YClO_{1.0}$

Intralayer Distances (Å):

YCl	2H-$K_{0.08}YClO_{0.82}$	3R-$Na_{0.08}YClO_{1.0}$
3.7523(2)	3.7873(6)	3.7881(3)

Interlayer Distances (Å):

	YCl	2H-$K_{0.08}YClO_{0.82}$	3R-$Na_{0.08}YClO_{1.0}$
Y-Y	3.511(2)	3.567(3)	3.581(7)
Y-Cl	2.750(2)	2.833(4)	2.820(7)
Y-(1)O		2.284(15)	2.472(25)
Y-(3)O		2.251(4)	2.217(4)
O-(3)O		2.80(2)	3.038(33)
M^I-(6)Cl		3.140(4)	2.776(6)
ΣM^I-Cl[a]		3.19	2.83

[a]Sum of six coordinate crystal radii.

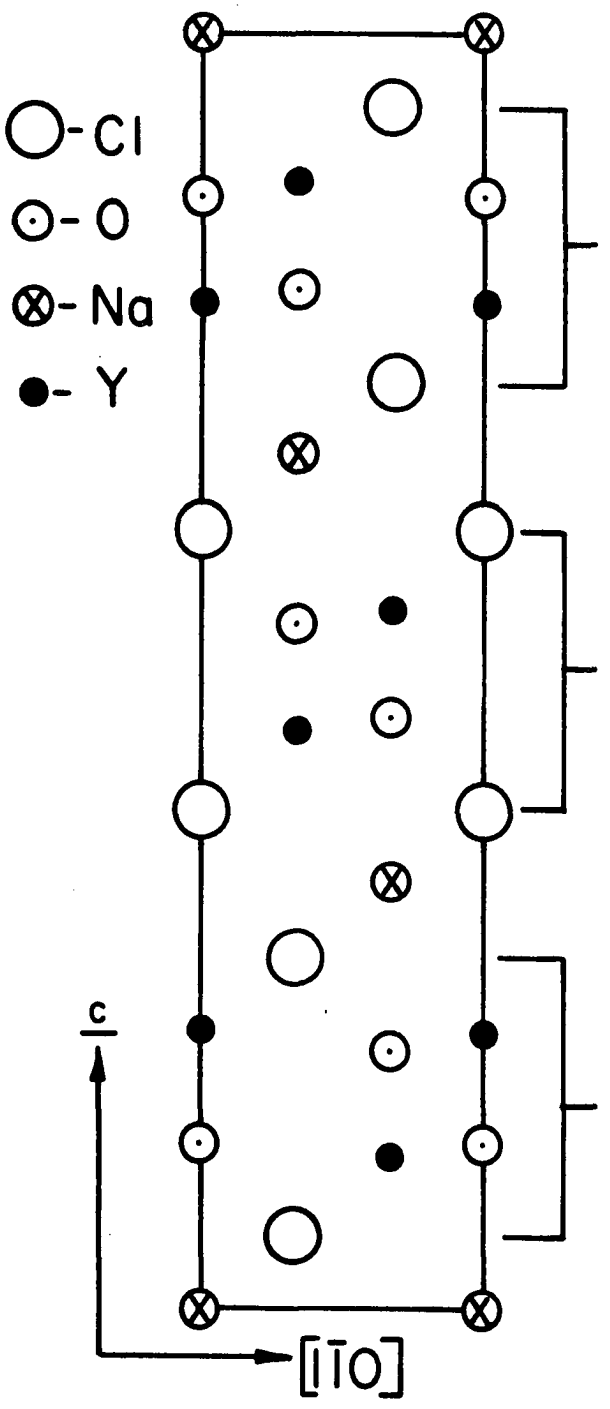

Figure 8. A schematic (110) section of 3R-$Na_{0.08}YClO_{1.0}$ with each slab identified by a bracket

A comparison of the 3R-$Na_{0.08}YClO_{1.0}$, 2H-$K_{0.08}YClO_{0.82}$, and YCl distances is given in Table 11. The intra- and interlayer Y-Y distances of 3.7881 Å (a-axis) and 3.58 Å are reasonable and compare favorably with those in 2H-$K_{0.08}YClO_{0.82}$. The Na-Cl distance, 2.78 Å, agrees well with the sum of the six coordinate crystal radii, 2.83 Å. The apical Y-O distance of 2.48 Å is much longer than the Y-O distance in 2H-$K_{0.08}YClO_{0.82}$ or the distances in Y_2O_3[42] and YOCl.[14] The electron density map indicated the oxygen in the center (±0.02 Å) of the tetrahedral-like interstice but during least squares refinement the atom moved towards the basal yttrium atoms. This type of behavior was also observed in $ZrBrO_{0.29}$ where the oxygen atoms actually refined outside the tetrahedral-like interstice.[17]

Rb_xYClO_z system

Only a limited number of reactions have been run in this system but the results are similar to those in systems discussed previously. Two phases, 2H- and 3R-Rb_xYClO_z, have been observed and powder patterns show that they are isostructural with 2H-$K_{0.08}YClO_{0.82}$ and 3R-$Na_{0.08}YClO_{1.0}$, respectively. The stoichiometries, products and lattice constants for reactions in this system are given in Table 12.

The 2H phase was first formed in small yields in the "ternary" reactions using powdered Y, YCl_3, and RbCl. Subsequent reactions in the quaternary system using powdered Y, RbCl, YCl_3, and Y_2O_3 have produced both the 2H and 3R phases in nearly quantitative yields. Increasing the concentration of Y and RbCl has yielded only the 3R phase and some unreacted Y and RbCl.

Table 12. The stoichiometries, products, and lattice constants for reactions in the Rb_xYClO_z and Cs_xYClO_z systems

d Y powder + dM^ICl + Y_2O_3 + YCl_3 $\xrightarrow{\sim 950^oC}$

M^I	d(moles)	Products	Lattice Constants, (Å) a	c
Rb	0.68	2H-Rb_xYClO_z	3.7888(3)	22.737(6)
		3R-Rb_xYClO_z	3.7890(4)	34.13(1)
Rb	1.5	3R-Rb_xYClO_z	3.7909(4)	34.10(1)
Cs	0.49	1T-Cs_xYClO_z	3.7919(2)	11.932(9)
		2H-Cs_xYClO_z	3.7920(2)	23.818(3)
		3R-Cs_xYClO_z	3.7901(5)	35.60(2)
Cs	0.68	1T-Cs_xYClO_z	3.7949(9)	11.92(3)
		3R-Cs_xYClO_z	3.7941(9)	35.62(2)

d Y powder + dCsCl + 3YOCl $\xrightarrow{\sim 950^oC}$

d(moles)	Products	Lattice Constants, (Å) a	c
0.50	1T-Cs_xYClO_z	3.7914(2)	11.878(4)
0.83	1T-Cs_xYClO_z	3.7933(5)	11.84(1)
	3R-Cs_xYClO_z	3.7933(4)	35.47(2)
1.00	1T-Cs_xYClO_z	3.7931(4)	11.88(1)
	3R-Cs_xYClO_z	3.7936(4)	35.54(1)
1.03	1T-Cs_xYClO_z	3.7938(5)	11.92(2)
	3R-Cs_xYClO_z	3.7939(5)	35.58(2)
1.2	1T-Cs_xYClO_z	3.7915(4)	12.06(1)

x.s. Y powder + dM^ICl + YCl_3 $\xrightarrow{\sim 950^oC}$

M^I	d(moles)	Products[a]	Lattice Constants, (Å) a	c
Rb	4.1	2H-Rb_xYClO_z	3.7848(5)	22.82(5)
Cs	1.9	2H-Cs_xYClO_z, 1T-Cs_xYClO_z	3.7881(2)	23.84(1)
Cs	1.9	2H-Cs_xYClO_z, 1T-Cs_xYClO_z	3.7878(2)	23.841(9)

[a]Oxygen is from an impurity.

Cs_xYClO_z system

This system is not as simple or as well understood as the previously discussed systems. It is complicated by the existence of a third polytype, 1T-Cs_xYClO_z, and the possibility of superstructures for 1T-, 2H-, and 3R-Cs_xYClO_z. The synthesis of these phases will be discussed first followed by structural considerations. The stoichiometries, products, and lattice constants for reactions in this system are given in Table 12.

Reactions in the "ternary" CsCl, YCl_3, and powdered Y system produced 30-50% yields of black irregularly shaped plate crystals which were found mainly on the walls of the Nb reaction tube. In many cases, thin foil-like pieces as large as 1-2 cm across could be removed from the walls of the tube. Examination under the microscope showed many growth steps on the surface of the foil. Powder patterns of these plates could be indexed as mixture of the 1T and 2H phases with a few weak lines at low angles not indexed.

Electron microprobe results using plate crystals from the "ternary" reactions yielded an average composition of $Cs_{0.10}YCl$. There was no significant deviation from unity for the Y/Cl ratio. This indicates that the surface of the crystals were salt free. At the time these samples were run, the electron microprobe was not able to detect oxygen.

Quaternary reactions, given by reaction (1), have produced a mixture of 1T- , 2H- , and 3R-Cs_xYClO_z totalling a nearly stoichiometric yield. At d = 0.49 all three phases are present in the powder patterns in yields of 50% 1T, 30% 2H, and 20% 3R. At a slightly larger concentration of Y and CsCl, d = 0.68, only 1T and 3R were observed in 60% and 40% yields

respectively. The disappearance of the 2H phase at larger Y and $M^{I}Cl$ concentrations has been observed in other $M^{I}_{x}YClO_{z}$ systems.

A second type of quaternary reactions, reaction (2), has produced only a mixture of 1T- and 3R-$Cs_{x}YClO_{z}$ in nearly quantitative yields. The proportion of the 1T and 3R phases is not related to the concentration of CsCl and Y because reactions with d = 0.5 and d = 1.2 both gave the 1T phases in 90-100% yields. Reactions with intermediate concentrations, d = 0.83, 1.0, and 1.03, have produced both the 1T and 3R phases in a ∿50/50 mixture. The rate at which the reaction was cooled also had little effect on the phases formed. The 1T phase was produced in nearly 100% yields by either cooling at 10°C/hr or air quenching. In another case, two reactions with the same stoichiometries, d = 0.84, were run at 950°C for 12 days and one was slow cooled at ∿4°C/hr while the other was air quenched. The slowly cooled reaction did produce a slightly higher yield of the 1T phase than the air quenched reaction. It should be noted that the crystallinity of the products did improve with slow cooling but the crystals were still not large enough to mount for single crystal studies.

Two 75-100 mg samples which contained ∿50/50 mixture of the 1T and 3R phases were loaded in Nb tubes, annealed at 935-950°C for several days and then air quenched. The samples which were initially a black powder were white or clear after annealing. Powder patterns of the annealed product show only 1T-$Cs_{x}YClO_{z}$ lines.

Comparison of the calculated versus observed powder patterns clearly show that 2H- and 3R-$Cs_{x}YClO_{z}$ are isostructural with 2H-$K_{0.08}YClO_{0.82}$ and 3R-$Na_{0.08}YClO_{1.0}$, respectively. This leaves the Cs in trigonal

prismatic coordination for the 2H phase and trigonal antiprismatic coordination in the 3R phase. There are two possible stacking variations in a one-slab structure and these are described in more detail in the section on the hydrates of $M_x^I YClO_z$ compounds. It has been found by comparison of calculated versus observed powder patterns that 1T-Cs_xYClO_z stacks AbcA along the c-axis, where the upper case letters are Cl and the lower case Y, with the oxygen atoms assumed to be in the tetrahedral-like interstices between the Y layers. There are two equivalent trigonal prismatic holes between the Cl layers and it is not clear which site is occupied by cesium. These sites are different from those in the 2H and 3R structures in that the second nearest neighbors in the 1T structure (out the top or bottom of the trigonal prism) are oxygen and yttrium while in the 2H and 3R structures both have only oxygens as second nearest neighbors.

Powder patterns of only the 1T phase show two weak lines (intensities of 1-2 on a scale of 10) which cannot be accounted for by known phases. These same lines, and sometimes one or two others, are also present in powder patterns which contain both the 1T and 3R or 2H phases and are assumed to be from the 1T phase. All extra lines in the 1T pattern can be indexed with 2 x a(b) and are best indexed with 3 x a(b). This suggests a superlattice where the cesium atoms may order in a more complex way in the trigonal prismatic sites but more evidence is needed to locate the positions. Thus, the 1T structure indicated is based more on the Y and Cl positions than on the Cs positions.

The powder patterns and lattice constants of 1T-Cs_xYClO_z are nearly identical with those of the K_xYClO_z and Rb_xYClO_z hydrates and consideration has to be given to the possibility that 1T-Cs_xYClO_z is actually a hydrate (1T-$Cs_x(H_2O)_yYClO_z$). The unlikely sources of H_2O would have been the dry box (<2 ppm H_2O) or the transfer of the Guinier sample to the camera. Considering the Cs has a relatively small hydration energy and the dry box and sample transfer conditions were not unusual it seems unlikely that a hydrate could have always been formed. Further proof was provided when a 233 mg sample which contained a 50/50 mixture of the 1T and 3R phase was weighed in the dry box and heated to 275°C under vacuum. There was no change in the weight of the sample and the powder pattern was identical to the initial pattern. If the 1T phase was hydrated there should have been a weight loss and the amount of 3R-Cs_xYClO_z would have increased. Thus, it does not appear that 1T is a hydrate. It is isostructural with the 1-slab hydrates, neglecting the H_2O, and because the size of Cs^+ is nearly identical to a hydrated K or Rb ion the lattice constants only resemble those from the hydrates.

The 3-slab structure of 3R-Cs_xYClO_z can be converted to 1T-Cs_xYClO_z by "sliding" the slabs. The same "sliding" of slabs to get from the 3R structure to the 1-slab hydrates has been observed in the hydration reactions. It is presumed that the change from the 3R to the 1T structure, which involves the change in coordination of the Cs from trigonal antiprismatic to trigonal prismatic, involves a small energy change that reflects the fact that the large cesium atom is equally well-coordinated in the trigonal prismatic hole.

Deintercalation

The oxidation of 2H- and 3R-$M^I_xYClO_z$ to $YClO_z$ was achieved with I_2 according to reaction (3). The solvent in all these reactions was dried acetonitrile. In a typical reaction 50-100 mg of sample was reacted with an excess of I_2 in acetonitrile for 1-2 days at room temperature. The lattice constants obtained after the reaction (3) are given in Table 13.

(3) $M^I_xYClO_z + 1/2I_2(\text{solution}) \longrightarrow YClO_z + \alpha M^I I$, where M^I=Li,K

The powder patterns of the black powder and chunks after the reaction showed sharp lines which could be indexed as a 3-slab structure. The striking feature of the 3R-K_xYClO_z samples is the shift of the 0,0,3 line from d = 11.476 Å to d = 9.342 Å in 3R-$YClO_z$. A calculated powder pattern of 3R-$YClO_z$ based on the YOF[43] structure-type or the isostructural $ZrBrO_x$[17] was in excellent agreement with the observed patterns.

A K_xYClO_z sample which contained a mixture of the 2H and 3R phases showed sharp lines from 3R-$YClO_z$ after reaction (3) and very broad lines from 2H. A calculated powder pattern for 2H-$YClO_z$, based on the 2H-$K_{0.08}YClO_{0.82}$ structure without the potassium atoms, matched the positions of the broad lines. The removal of the alkali metal from the M^I2H structure would result in a nonclosed-packed arrangement of slabs. The disorder caused by the movement of the slabs toward a close-packed arrangement would explain the broad lines. The 2H-$YClO_z$ "structure" would then be a modified version of the 2H-K_xYClO_z structure.

Table 13. The lattice constants for 3R-$YClO_z$ (Å)

Sample	a	Δa^a	c	Δc^a
2H- and 3R-K_xYClO_z	3.7950(2)	+0.0053	27.938(8)	-4.955
3R-K_xYClO_z	3.7968(3)	+0.0058	27.960(8)	-4.927
3R-Li_xYClO_z	3.7899(3)	+0.0026	28.021(6)	-0.238
3R-Li_xYClO_z	3.7884(3)	+0.0011	28.045(9)	-0.214

[a]Δ = lattice constant of 3R-$YClO_z$ - average lattice constant of $M^I_xYClO_z$.

Unsuccessful reactions

Reintercalation of 3R-$YClO_z$, which was produced via the oxidation of $M^I_xYClO_z$ with CH_3CN-I_2 solutions, has been unsuccessful. One of the most common preparative methods for forming Li intercalation compounds is through the use of n-butyllithium, C_4H_9Li. When 3R-$YClO_z$ was added to 1.6M or 2.4M solutions of C_4H_9Li in hexane at room temperature or 60°C there was no reaction. 3R-$YClO_z$ was also dispersed in alkaline solutions, pH=8-10, of sodium dithionite, $Na_2S_2O_4$, with no reaction.

During this investigation there were several attempts at intercalating MOCl phases which normally occur in the PbFCl structure.[14] The first method that was tried involved reacting NdOCl (PbFCl) with LiCl, Nd, and sometimes $NdCl_3$ at 700-800°C. Nd was chosen because of the relative ease

of reduction to the +2 state. These reactions yielded black polycrystalline chunks and powder which powder patterns identified as NdOCl. The lattice constants were within 3σ of the reported values for NdOCl. Why the products are black cannot be explained but similar results have also been observed with YOCl and GdOCl.

The second method involved reacting MOCl with intercalating agents (reducing agents). Reactions involving NdOCl and 1.6M C_4H_9Li at room temperature and 60°C were unsuccessful. The NdOCl remained light blue and powder patterns showed no change in the lattice constants. When alkaline solutions (pH=8-10) of sodium dithionite, $Na_2S_2O_4$, and NaCl were reacted with SmOCl at room temperatures and 60°C there was no change in the powder patterns or lattice constants of SmOCl.

Hydrates

The effect of water on $M^I_xYClO_z$ samples was first noticed with a sample of 3R-K_xYClO_z. A drop of water was added to a chunk of the 3R phase and the following was observed with a microscope. First, the chunk broke into small plate-like pieces with some H_2 evolution. The black plates slowly turned brown and exfoliated into accordian-shaped pieces. The increase in the thin plate direction was generally greater than 100-fold. With time, the "crystals" transform from a translucent brown appearance to translucent green. It was then possible to remove the exfoliated "crystal" from the water after which the microscope light created enough heat to evaporate the remaining water and to shrink the "crystal" to a thin plate. This process is reversible, although the effect is somewhat diminished with each repetition. The plate after

evaporation is usually dark green around the edges and light green or transparent in the middle. The longer the crystals remained in the water the clearer and more translucent they became. Even after four hours in water the exfoliated, clear "crystals" could be dehydrated to form clear plates.

This effect has also been observed with other 3R-$M^{I}_{x}YClO_{z}$ phases, where M^{I}=Li-Cs. For 3R-$Cs_{x}YClO_{z}$, the rate of formation of the exfoliated plates is noticeably slower. This can probably be associated with the smaller hydration energy of Cs^{+}. Samples of 2H-$M^{I}_{x}YClO_{z}$ and 3R-$YClO_{z}$ do not show any appreciable exfoliation with the addition of water. The $Li_{x}YCl$ and $M^{I}_{x}Y_{2}Cl_{2}C_{z}$ samples react quite rapidly with $H_{2}O$ and evolve H_{2}.

It was also observed that powder patterns of 3R-$K_{x}YClO_{z}$ samples which had been exposed to air (1 hr-8 days) gave a different powder pattern which could be indexed as an expanded 1-slab structure. The best explanation for these changes was that the sample had hydrated with very little or no oxidation.

To prove the existence of a hydrated $K_{x}YClO_{z}$, a sample of the 3R phase was left in air for several days to give the expanded 1-slab structure. The sample was then heated under vacuum as described in the experimental section. The sample, which originally weighed 0.218 g, showed a weight loss of 0.005 g. If it is assumed that the complete sample has a composition of $K_{0.20}YClO_{0.80}$ (there was some $Y_{2}O_{3}$ in the sample and the coefficients for K and O are only estimates) then the dehydration equation is $(H_{2}O)_{0.2}K_{0.20}YClO_{0.80} \xrightarrow[\text{vacuum}]{\Delta=270^{\circ}C} K_{0.20}YClO_{0.80} + 0.18H_{2}O$. The $\sim$ 1:1

ratio of H_2O/K agrees well with the hydration reactions of $M^I_xMS_2$ as reported by Röder et al.[44]

The powder pattern of the sample after heating under vacuum was that of the original 3R-K_xYClO_z phase. It is remarkable how the quality of powder patterns (indicative of structural order) has been maintained throughout these reactions. Lattice constants of the original 3R-K_xYClO_z, the hydrate 1T-$(H_2O)_aK_xYClO_z$, and the 3R-K_xYClO_z after dehydration are given in Table 14. The differences between the 3R-K_xYClO_z lattice parameters before and after hydration are less than 1σ. The weight loss and powder patterns confirm the hydration and show that the hydration is reversible.

A structural model for 1T-$(H_2O)_aM^I_xYClO_z$ has been obtained by considering the two possible packing arrangements in a 1-slab structure. One possibility is stacking the chlorines (upper case letters) and yttrium in a hcp fashion along $\underline{c}$, AbaB, where the oxygens are assumed to be in the tetrahedral like interstices. This results in a trigonal antiprismatic coordination about M^I and H_2O. The other way is a ccp stacking, AbcA, where the M^I and H_2O have trigonal prismatic coordination. The first is unreasonable for two reasons: (i) the oxygen and chlorine atoms would be nearest neighbors and (ii) intraslab bonds would have to be broken to get from the 3-slab structure to the 1-slab structure. Calculated powder patterns based on the ccp packing match very well with the observed powder patterns for the hydrates. In the one slab structure it is assumed that the alkali metal and water molecules are disordered

Table 14. The lattice constants for 3R-$YClO_z$, $M^I_xYClO_z$, and $M^I_x(H_2O)_aYClO_z$ (Å)

	a	c	c/n^a	$\Delta c/n^b$
3R-$YClO_z$	3.7925	27.99	9.33	-
3R-K_xYClO_z	3.7910(2)	32.887(8)	10.96	
1T-$K_x(H_2O)_aYClO_z$	3.7857(4)	11.864(5)	11.864	2.53
3R-K_xYClO_z [c]	3.7900(6)	32.87(1)	10.96	
1T-$K_x(H_2O)_aYClO_z$	3.7849(2)	11.970(7)	11.970	2.64
3R-Rb_xYClO_z	3.7890(4)	34.13(1)	11.38	
1T-$Rb_x(H_2O)_aYClO_z$	3.7881(2)	11.92(1)	11.92	2.59
3R-Rb_xYClO_z	3.7909(4)	34.10(1)	11.37	
1T-$Rb_x(H_2O)_aYClO_z$	3.7873(4)	11.88(1)	11.88	2.55
2H-Rb_xYClO_z	3.7888(3)	22.737(6)	11.37	
2H-$Rb_x(H_2O)_aYClO_z$	3.7881(2)	23.834(7)	11.92	2.59

[a] c/n = c-axis divided by the number of slabs per unit cell.

[b] $\Delta c/n$ = difference in c/n between 3R-$YClO_z$ and 1-$M^I_x(H_2O)_aYClO_z$.

[c] After dehydration.

over both trigonal prismatic sites. The reversible structural change can be easily achieved by "sliding" the slabs as shown in Figure 9.

The hydrates of both 2H- and 3R-Rb_xYClO_z have also been observed with lattice constants reported in Table 14. The 3R phase forms a 1-slab hydrate, 1T-$(H_2O)_aRb_xYClO_z$, which is isostructural with 1T-$(H_2O)_aK_xYClO_z$. When the 2H phase is hydrated, by exposure to air, the powder pattern shifts to lower 2θ values which can be indexed as a 2-slab structure. Since there were no changes in the line intensities or no extra lines in the powder pattern after dehydration it is assumed that the original 2H-Rb_xYClO_z structure (space group $P6_3/mmc$) is retained. The water would account for the c lattice expansion and be accommodated in the empty trigonal prismatic holes between the chlorine layers. The occupation of the trigonal prismatic holes with water (and alkali metal) in the 2H structure is also consistent with the 1T structure where the water is also in a trigonal prismatic site.

Ground samples of 3R-Li_xYClO_z left in air for several days showed no evidence of hydration. It should be noted that all hydration studies were carried out during the winter months, i.e., lower relative humidities. Studies which involve changes in the relative humidity, i.e., increasing the humidity, may show that 3R-Li_xYClO_z can be hydrated and should be tried. Samples of Na_xYClO_z and Cs_xYClO_z were not examined for hydration products.

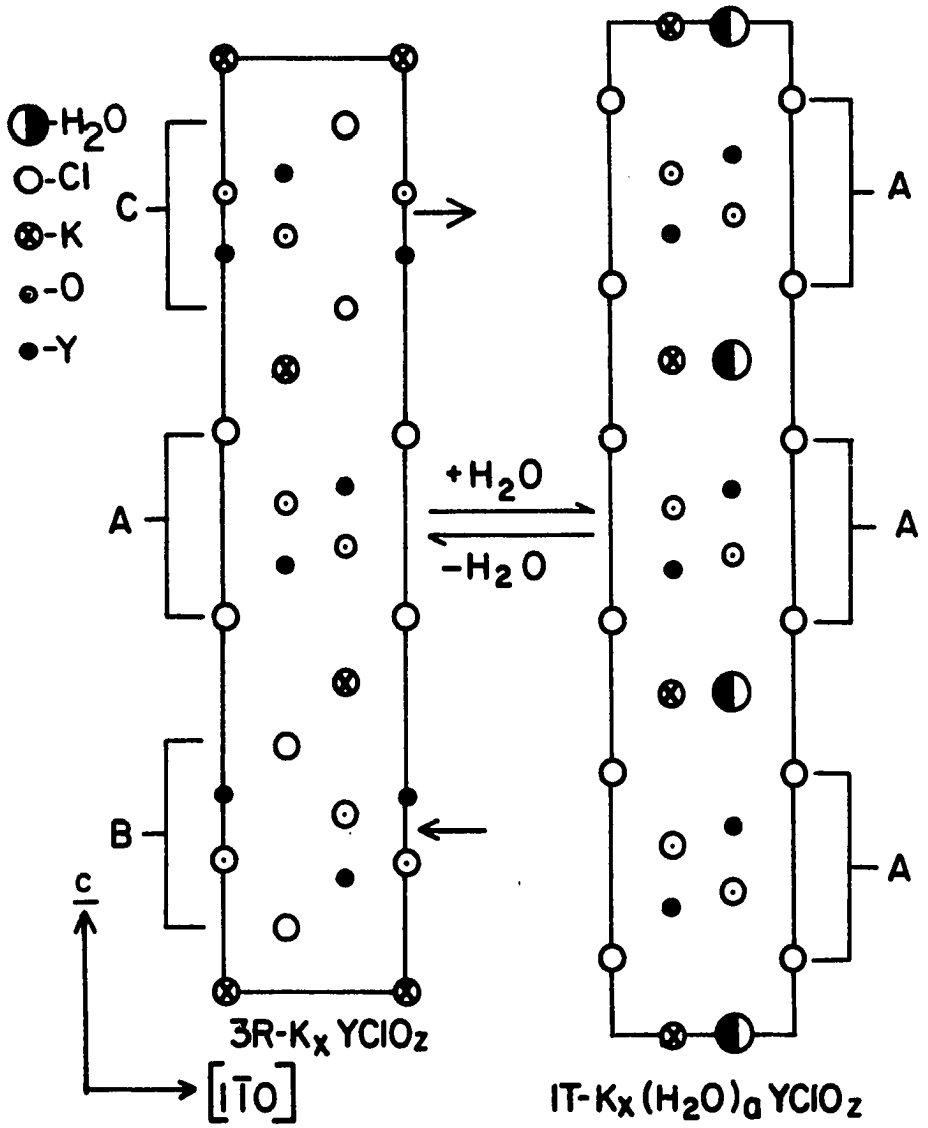

Figure 9. The proposed slab sliding mechanism for the hydration of $3R\text{-}K_xYClO_z$ by moist air is illustrated by the schematic (110) sections of $3R\text{-}K_xYClO_z$ and $1T\text{-}K_x(H_2O)_aYClO_z$

Carbide Interstitial Derivative of YCl

The ternary interstitial carbide has only been synthesized in reactions that contained powdered graphite. The full carbide, Y_2Cl_2C, is produced in greater than 95% yields by reaction (4). The product is

$$(4)\quad 4\ Y\ \text{powder} + 2YCl_3 + 3C \xrightarrow[5\ \text{days}]{950^oC} 3\ 1T\text{-}Y_2Cl_2C$$

a brown-black powder with a bronze reflectance that grinds with a graphitic feel.

All lines in the powder pattern of the ground product were indexed as a 1-slab structure. The lattice parameters obtained from the powder patterns are given in Table 15. The Y, Cl, and C positions from what is concluded to be the $1T\text{-}K_{0.52}Y_2Cl_2C_{0.80}$ structure generated a calculated powder pattern which gave excellent agreement with the observed powder pattern. The (110) section of $1T\text{-}Y_2Cl_2C$, Figure 10, shows that the Cl (upper case letters) and Y layers pack $\cdots|AbaB|\cdots$ along the c-axis with the carbons occupying the trigonal antiprismatic holes between the Y layers. This phase is also isostructural with $1T\text{-}Ta_2S_2C$[45] and the recently found $1T\text{-}Sc_2Cl_2C$.[46]

A second reaction using one-third of the powdered graphite necessary for the stoichiometric reaction, (4) produced $1T\text{-}Y_2Cl_2C_z$ along with unreacted Y powder and YCl_3. If the reaction had gone to completion the product would have had the composition $1T\text{-}Y_2Cl_2C_{0.33}$. The lattice parameters (Table 15) show a 7σ decrease in a and a typical c-axis. The decrease in a and a greater than 50% yield suggest that the product is

Table 15. The stoichiometries, products, and lattice constants for reactions in the $Y_2Cl_2C_z$ and $M^I_xY_2Cl_2C_z$ systems

4 Y powder + $2YCl_3$ + aC

a(moles)	Products	Lattice Constants, (Å) a	c
3.0	$1T\text{-}Y_2Cl_2C$	3.7051(5)	9.183(2)
1.0	$1T\text{-}Y_2Cl_2C_z$+Y+YCl_3	3.7008(4)	9.19(3)

b Y powder + d M^ICl + $2YCl_3$ + 1C ⟶ 1T $M^I_xY_2Cl_2C_z$ + $M^I_3YCl_6$ + Y

M^I	b(moles)	d(moles)		
Na	5.68	1.62	3.6750(4)	9.965(4)
Na	5.10	0.50	3.6795(3)	9.922(2)
K	5.22	3.80	3.6794(2)	10.886(1)
K	5.32	1.22	3.6771(2)	10.886(2)
K	5.34	1.12	3.6765(4)	10.883(4)

x.s. Y powder + d M^ICl + $1YCl_3$ ⟶ $1T\text{-}M^I_xYClC_z$ [a]

M^I	d(moles)		
Li	0.84	3.6703(5)	9.25(1)
Li	0.91	3.6712(3)	9.266(9)
Li	1.0	3.6636(2)	9.264(9)
Na	1.9	3.6648(7)	9.95(3)
Na	2.9	3.6686(5)	9.94(2)
K	1.3	3.6710(2)	10.888(8)
K	1.9	3.6710(8)	10.86(4)
K	2.0	3.6741(2)	10.889(9)
K	2.3	3.6713(2)	10.862(7)

[a] Reactions which involved an impurity as a source of carbon.

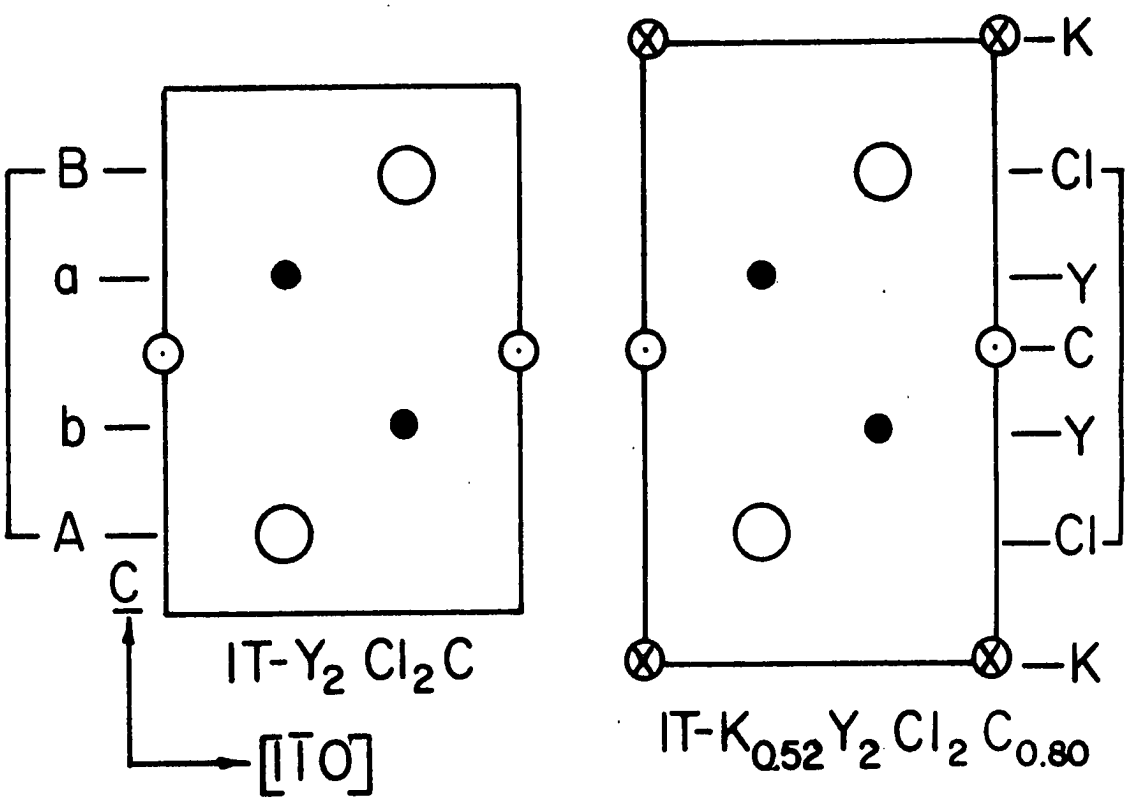

Figure 10. Schematic (110) sections of $1T\text{-}Y_2Cl_2C$ and $1T\text{-}K_{0.52}Y_2Cl_2C_{0.80}$

somewhat nonstoichiometric with respect to carbon. The exact composition cannot be determined but the limits on z in 1T-$Y_2Cl_2C_z$ are $0.5<z<1.0$.

Intercalation of Carbide Interstitial Derivatives of YCl

Compounds of the general formula type $M^I_xYClC_z$, where M^I=Li, Na, K, and Cs and $z \sim 1$, were first prepared accidentally by reaction of Y powder or strips, YCl, and M^ICl at temperatures greater than 900°C. The black, often hexagonally shaped plate crystals were usually found in 5-15% yields in the crimped end of the reaction tube. The crystals grow from the melt and are generally coated with or embedded in a $M^I_3YCl_6$ salt matrix.

The above reactions also produced $M^I_xYClO_z$ (if M^I=Na-Cs then 2H-$M^I_xYClO_z$ or if M^I=Li then 3R-Li_xYClO_z) in yields ranging from 5-50%. Since both products form as black plates this made separating them very difficult. The most distinguishing features of $M^I_xY_2Cl_2C_z$ was the location in the crimped end and the hexagonal shape of the crystals.

All powder patterns can be indexed in a 1-slab hexagonal cell. When compared with YCl the a-axis shows a significant decrease while the c-axis shows an increase with the corresponding size of the alkali metal. A plot of the c-axis versus M^I crystal radii for the $M^I_xY_2Cl_2C_z$ phases are shown in Figure 5. At first it was assumed that these compounds were the ternary M^I_xYCl phases and the decrease in the a-axis was due to the reduction of the YCl host lattice, $M^{I+}_x(YCl)^{x-}$.

It was not until $K_{0.52}Y_2Cl_2C_{0.80}$ was purposely synthesized and its crystal structure solved that the compounds were correctly identified as containing interstitial carbon. The details of the structure refinemet for 1T-$K_{0.52}Y_2Cl_2C_{0.80}$ are discussed in a following section. The structure contained electron density in the octahedral-like interstices between the yttrium layers and Y-Y bond lengths less than expected for a small reduction. A carbide was the most likely light atom interstitial based on the location and bond lengths. Subsequent reactions with powdered graphite have produced the same phases in greater than 60% yields.

The source of carbon in the "ternary" Y, YCl_3, and M^ICl reactions has led to much speculation. In order to produce 1T-$M^I_xY_2Cl_2C_z$ in 10% yields only a small amount of carbon is necessary. Since 1T-$M^I_xY_2Cl_2C_z$ was not formed in all "ternary" reactions it can probably be assumed that the Y, YCl_3 and M^ICl are not responsible. Furthermore, the metal contained less than 0.04 mg C per reaction and the YCl and M^ICl were both distilled. The leading candidate for carbon contamination is a white precipitate which has been found in the crimped end of many Ta and Nb reaction containers. Jerome Smith has determined the precipitate is formed on the addition of acetone to tubes from which the Ta cleaning solution has not been completely rinsed with distilled water.[47] The composition of the precipitate is unknown but microprobe analysis showed varying amounts of fluorine and oxygen in different regions of the precipitate. The presence of carbon cannot be detected with the electron microprobe. The white precipitate has also been suspected of being an agent in the formation of "Nb_6I_{10}"[47] and a source of oxygen.

The recommended method for the preparation of 1T-$M^{I}_{x}Y_2Cl_2C_z$

(5) $4+dY$ powder + $dM^{I}Cl + 2YCl_3 + 3C \xrightarrow{>925^{o}C} 3(1T\text{-}M^{I}_{d/3}Y_{2+d/3}Cl_{2+d/3}C)$

is reaction (5). The product is a brown-black powder which can be produced in yields of greater than 80%.

$Na_xY_2Cl_2C_z$ system

1T-$Na_xY_2Cl_2C_z$ was first produced in 10-15% yields in the "ternary" reactions using Y powder, YCl_3, and NaCl. The product was usually found as black plates in the crimped end of the reaction tube. Powder patterns from these reactions matched very well with those from reactions discussed below where powdered graphite was included in the reaction. In Table 15, the lattice constants from these reactions are compared with the lattice constants from the quaternary reactions. The "ternary" reactions are the only reactions to produce sizeable crystals of 1T-$Na_xY_2Cl_2C_z$. A Weissenberg photo of a nearly single crystal with double spots confirmed the 1-slab cell and showed no extinction conditions. The space group is assumed to be $P\bar{3}m1$.

Reactions in the quaternary system with Y powder, NaCl, YCl_3, and C system produced 1T-$Na_xY_2Cl_2C_z$ in >60% yields. The equation and molar ratios for the first reactions in this system are reported in Table 15. These reactions are carbon deficient and produced 1T-$Na_xY_2Cl_2C_z$ along with Na_3YCl_6 and unreacted Y. A second type of reaction designed to produce 1T-NaY_2Cl_2C by the stoichiometric reaction (6) was unsuccessful.

(6) $5Y$ powder + $3NaCl + YCl_3 + 3C \xrightarrow{950^{o}C} 3(1T\text{-}NaY_2Cl_2C)$

Powder patterns of the ground product showed an ~70% yield of 1T-$Na_xY_2Cl_2C_z$ along with NaCl and a number of lines which could not be identified. The reaction appears to be YCl_3 limited (see reaction (5)) which would mean there must also be an excess of Y and C. This leaves the possibility that the extra lines are from a YC_x species. Binary yttrium carbides can be formed at temperatures greater than 900°C but none of the reported YC_x patterns matches the extra lines.[48] It is also possible the lines could be another $Y_xCl_yC_z$ or $NaY_xCl_yC_z$ phase. Further work on the identification of this phase was not pursued.

Based on the experience gained from the above reactions the best way to prepare 100% yields of 1T-$Na_xY_2Cl_2C_z$ (and in general any 1T-$M^I_xY_2Cl_2C_z$) is reaction (5). Note that reaction (5) is similar to reaction (1) in the $M^I_xYClO_z$ system which produces nearly quantitative yields of $M^I_xYClO_z$.

Lattice constants obtained from the quaternary reactions are summarized in Table 15. The 1T-$Na_xY_2Cl_2C_z$ was confirmed to be isostructural with 1T-$K_xY_2Cl_2C_z$ by comparison of the observed vs. calculated powder patterns based on the $K_{0.52}Y_2Cl_2C_{0.80}$ structure. The reduction which occurs in the formation of $Na^+_x(Y_2Cl_2C_z)^{x-}$ can be observed in the >0.0200 Å decrease in a from $Y_2Cl_2C_z$ to $Na_xY_2Cl_2C_z$, see Table 15.

$K_xY_2Cl_2C_z$ system

1T-$K_xY_2Cl_2C_z$ was first produced in "ternary" reactions using Y strips or powder, YCl_3, and KCl. The black plate crystals grew from the melt and were usually covered or imbedded in a salt matrix. The crystals were

usually found in the crimped end of the tube in 10-15% yields plus 2H-K_xYClO_z in 20-40% yields. The powder patterns of the carbide from these reactions were indexed as a 1-slab cell and the lattice constants are reported in Table 15. These powder patterns have since been compared with the powder patterns of 1T-$K_xY_2Cl_2C_z$ produced from reactions which contained powdered graphite (discussed below) and found to be identical. The "ternary" reactions are the only reactions to produce sizeable crystals of 1T-$Cs_xY_2Cl_2C_z$, presumably aided by the slow growth from the melt. A single crystal of $K_xY_2Cl_2C_z$ was found in these reactions and its structure determination is discussed below.

Quaternary reactions using Y powder, KCl, YCl_3, and powdered graphite have produced 1T-$K_xY_2Cl_2C_z$ in greater than 60% yields, plus K_3YCl_6, and Y. The molar compositions for these reactions along with the lattice constants for 1T-$K_xY_2Cl_2C_z$ are given in Table 15. These reactions are carbon deficient which is the reason they are incomplete. As proposed in the preceding section, if the carbon content was tripled then 1T-$K_xY_2Cl_2C_z$ could be produced almost quantitatively.

1T-$K_xY_2Cl_2C_z$ is found as a brown-black microcrystalline powder which grinds with a graphitic feel. Observed powder patterns of this phase give excellent agreement with the calculated powder pattern based on the $K_{0.52}Y_2Cl_2C_{0.80}$.

Data collection was started with a standard ω-scan but the early reflections showed background counts that were 1/2 - 2/3 of the total counts. The scan width was increased from 0.5° to 0.9° and one hemisphere of data (664 reflections) was collected. The background counts remained

large, typically one-half of the total counts, and the peak profiles were broad. ALICE predicted an acentric cell although the HPR-plot was best interpreted as centric. The hexagonal lattice constants are: $\underline{a}$ = 3.6730(5) Å and $\underline{c}$ = 10.867(3) Å. The data were absorption corrected, reduced, and averaged in both $P\bar{3}m1$ (R=0.081) and centric P321 (R=0.082).

The broad peak profiles, large background counts and R of averaging led to a second data collection using a 2θ-ω scan. In the 2θ-ω scan, the peak was maximized in ω then stepped off in 2θ with the 2θ scan width increased from 0.5^{o} to 1.0^{o}. This resulted in much improved peak profiles and the background counts for larger peaks were generally less than 10% of the total counts. One hemisphere of data (644 reflections) was collected on the same cell, $\underline{a}$ = 3.6730(5) Å and $\underline{c}$ = 10.867(3) Å. The data were absorption corrected using a second Φ-scan, reduced, and averaged in $P\bar{3}m1$ (R=0.040) and P3 (R=0.038). The second data set was used for least squares refinement of the structure.

The yttrium and chlorine positions for a hcp, AbaB, stacking were obtained from geometrical and distance considerations. The isotropic refinement of Y and Cl in $P\bar{3}m1$ yielded an R=0.221. The electron density maps showed a peak at 0,0,0 which was assigned as potassium and a smaller peak at 0,0,1/2. The anisotropic refinement of the Y and Cl positions and the variation of the multiplier and isotropic B for K yielded an R=0.126 and R_w=0.150. The difference electron density map showed the extra peak of $\sim 4e^{-}$ at 0,0,1/2 and some residual electron density of $1\text{-}2e^{-}$ which was smeared out along the $\underline{c}$-axis but located near the Y and Cl positions.

It was noted at the time that an atom at 0,0,1/2 corresponded to a reasonable Y-C distance and based on the size of the interstices the trigonal antiprismatic site between the Y layers was a logical place to put a carbon. This was at first dismissed because it was hard to believe carbon was present in the system and the refinement of the carbon produced negative B's.

A short while later S.-J. Hwu found a crystal in the binary scandium-chloride system which had a similar cell.[46] Structural refinement using the Y and Cl positions from this structure yielded an R=0.126 and a difference electron density map which also had a peak of $4e^-$ at 0,0,1/2.

The most bothersome aspect of both these structures (besides the density at 0,0,1/2) was the metal-metal bond distances. The intralayer metal-metal bonds were similar to those in the respective metals while the interlayer metal-metal bonds were more than 0.15 Å shorter than the interlayer distances in the metal and ∿0.13 Å shorter than the interlayer distances in the respective monochlorides. This again led to the consideration of light atom interstitial derivatives and the carbide and nitride in particular. In the scandium chloride case, the carbide was chosen and the structure refined to a composition of $Sc_2Cl_2C_{1.1}$ and R=0.033.

In the present case, the refinement was not as easy. When the Y and Cl positions were refined with anisotropic parameters along with variation of the multipliers and isotropic B's on K and C, the potassium and carbon coupled producing a large B for K and a negative B for C. This problem was avoided by dropping the K from the refinement and fixing the B on C

while letting the multiplier vary. The B and multiplier on carbon were then fixed and the multiplier and B on potassium were varied together. This yielded a R=0.110 and R_w=0.133.

The structure is not without problems as indicated by the large R values and standard deviations. See Table 16 for the final atom parameters. The anisotropic thermal ellipsoids for Y and Cl are cigar shaped with B_{11} on Y less than 1σ negative. The problems with the coupling of the carbon and potassium along with the smeared residual electron density near the Y and Cl positions were discussed earlier. Most of these problems would appear to be associated with a streaking disorder along $\underline{c}^*$ which is the result of poor crystal quality. The poor crystal quality is also evident in the Weissenberg photo which shows some double spots and horizontal streaking, the reason for broad peaks in the ω-scan.

Because of the way the structure was refined the composition $K_{0.52}Y_2Cl_2C_{0.80}$ should only be regarded as approximate. The presence of the carbide is supported by the synthesis of 1T-$K_xY_2Cl_2C_z$, 1T-$Na_xY_2Cl_2C_z$, and 1T-$Y_2Cl_2C_z$ in high yields in reactions using powdered graphite.

In Table 17 the bond distances in $K_{0.52}Y_2Cl_2C_{0.8}$ are compared with the distances in YCl. A schematic representation of the (110) section is shown in Figure 10.

1T-$K_{0.52}Y_2Cl_2C_{0.80}$ is isostructural with Ta_2S_2C[45] and the recently found Sc_2Cl_2C[46] with the trigonal antiprismatic holes between the anion layers statistically occupied with potassium atoms. The basic unit in the structure is a Cl-Y-C-Y-Cl slab which consists of four

Table 16. Crystallographic data for 1T-$K_{0.52}Y_2Cl_2C_{0.80}$

Composition: $K_{0.52(8)}Y_2Cl_2C_{0.80}$

Cell: Trigonal, $P\bar{3}m1$

Lattice Constants: a = 3.6730(5) Å, c = 10.867(5) Å

Refinement: R = 0.110 R_w = 0.138

Atom Parameters:

	x	y	z	$B_{11}^a=B_{22}$	B_{33}
Y	2/3	1/3	0.3789(5)	-0.03(15)	3.46(27)
Cl	1/3	2/3	0.211(1)	0.32(27)	2.90(50)
C[b,c]	0.0	0.0	1/2	2.73	
O[d,c]	0.0	0.0	0.0	6.6(20)	

[a]The thermal parameter expression used is $\exp-(1/4(B_{11}a^{*2}(h^2+hk+k^2)+B_{33}l^2c^{*2}))$, $B_{12}=1/2B_{11}$, $B_{13}=-B_{23}=0$.

[b]Occupancy = 0.40.

[c]Isotropic B.

[d]Occupancy = 0.26(4).

Table 17. Comparison of distances in YCl and 1T-$K_{0.52}Y_2Cl_2C_{0.80}$

Intralayer Distances, (Å)		
	YCl	$K_{0.52}Y_2Cl_2C_{0.80}$
	3.7523(2)	3.6730(5)
Interlayer Distances, (Å)		
	YCl	$K_{0.52}Y_2Cl_2C_{0.80}$
Y-3Y	3.511(2)	3.380(8)
Y-3Cl	2.750(2)	2.796(9)
Cl-3Cl	3.722(5)	
K-6Cl		3.125(10)
C-6Y		2.496(3)
C-6Cl		3.787(11)

hexagonally-closed-packed layers of Cl-Y-Y-Cl with the carbon randomly disordered over the octahedral-like interstices between the yttrium layers. The layering geometry using only the chlorine (upper case letters) and yttrium layers is •••|AbaB|••• or for the complete cell including the potassium and carbide •••|cAbcaB|•••.

The carbon occupies the larger trigonal antiprismatic interstice between the yttrium layers because of its large size (crystal radius $\tilde{\sim}$1.45 Å). The binary yttrium carbides also show tap coordination of the carbide. If the chlorine and yttrium layers were to stack cubic-closed-

packed as in YCl and the $M_x^I YClO_z$ phases, then the chlorine layers would be directly above and below the carbide layer, •••|AbacA|•••. This would lead to a Cl-C distance of 3.14 Å. Instead the Cl-C distance is maximized by using hexagonally-close-packed layers, •••|AbcaB|•••

The bond distances are all very reasonable. The Y-C distance of 2.496(3) Å compares with 2.483(3) Å in Y_2C and 2.558(1) Å in $YC_{0.44}$. The Y-Y intra- and interlayer distances are shorter than those in YCl because the yttrium layers are strongly bonded by the carbon. The Y-Y interlayer distance of 3.388 Å can be compared with the shortest Y-Y interlayer distance in Y_2C of 3.402(7) Å.[48] The Y-Cl distance of 2.796(9) Å is a reasonable distance compared with the Y-Cl distances in YCl and $M_x^I YClO_z$. The K-Cl distance of 3.125(10) Å can be compared with the distance in $K_{0.08}YClO_{0.82}$ of 3.140(4) Å (trigonal prismatic coordination of potassium) and the sum of the crystal radii, 3.19 Å.

Other phases

1T-$Li_xY_2Cl_2C_z$ and 1T-$Cs_xY_2Cl_2C_z$ have also been found in "ternary" reactions. The "ternary" reaction conditions and lattice parameters for 1T-$Li_xY_2Cl_2C_z$ are reported in Table 15. The black plate crystals were found in 10-15% yield in the crimped end of the reaction tube. An oscillation and Weissenberg photograph of a nearly single crystal supported the 1-slab structure and $P\bar{3}m1$ as the space group. The structure of 1T-$Li_xY_2Cl_2C_z$ was confirmed to be isostructural with 1T-$K_xY_2Cl_2C_z$ by comparison of powder patterns. Reactions using powdered graphite were not run but based on the evidence from the NaCl and KCl systems with

powdered graphite it appears there would be no problem producing large yields of 1T-$Li_xY_2Cl_2C_z$ using powdered graphite.

Only a few lines which correspond to 1T-$Cs_xY_2Cl_2C_z$ have been observed in one powder pattern from a "ternary" reaction. Five lines were indexed, 101, 102, 110, 110, and 200, and these gave lattice constants of $\underline{a} = \underline{b}$ = 3.667(2) Å and $\underline{c}$ = 11.4(1) Å. The large standard deviations in the lattice constants are the result of only a few lines. These are characteristic lines for the 1T phases and this led to the assignment of 1T-$Cs_xY_2Cl_2C_z$. No reactions have been run in this system using powdered graphite.

DISCUSSION

Lattice Constants of YCl

As was alluded to in the introduction, there has been some disagreement over the lattice parameters of YCl. Mattausch et al. reported he hexagonal lattice constants of $\underline{a}$ = 3.748(1) Å and $\underline{c}$ = 27.318(9) Å for YCl from Guinier data.[3] A private communication from Professor Simon has assured us that $\underline{c}$ = 27.318(9) Å is the correct value from their investigations of the YCl_3/Y system based on remeasuring the 0,0,ℓ lines of YCl powder patterns. For comparison, the significantly larger $\underline{c}$ lattice constants for YCl repeatedly obtained in this investigation and by S.-J. Hwu[46] are reported in Table 18.

The only synthetic difference has been that our investigations have used Y powder while Professor Simon's group used Y metal which was melted in small lumps. Because the Y powder had been prepared by dehydrogenation of YH_2 it was postulated that the expansion in the $\underline{c}$ lattice constant may be explained by a solid solution of hydrogen in YCl. The occurrence of a new phase such as a hemihydride is unlikely because results with ZrCl and ZrBr have shown that the formation of the hemihydride is accompanied by a structural change.[19] The best way to prove the lattice constant expansion is not due to hydrogen is to prepare YCl using Y strips or filed Y. There have been many reactions involving Y strips in this work and in the investigation of the binary system by Jess Hendricks[1] but none has ever produced YCl. Recently S.-J. Hwu was able to prepare YCl using strips which had been reacted with YCl_3 and 10 mol % KCl at 550°C

Table 18. The lattice constants for YCl

Source	a	c	Δ/σ(Δ), Å: c vs 27.525(5)(a)	Δ/σ(Δ), Å: c vs 27.318(9)(f)
a	3.7523(2)	27.525(5)	-	20.1
b	3.7526(4)	27.50(3)	0.8	5.8
c	3.7520(3)	27.519(9)	0.6	15.8
c	3.7511(2)	27.511(8)	1.5	16.0
c	3.7515(4)	27.50(1)	2.2	13.5
d	3.7546(3)	27.468(9)	5.5	11.8
e	3.754(4)	27.455(8)	7.4	11.4
f	3.748(1)	27.318(9)	20.1	-
g	3.7478(9)	27.525(5)	0	20.1

a - diffractometer lattice constants from the single crystal study of YCl.

b - this investigation, prepared using 50 mol % LiCl as a flux.

c - this investigation, binary reactions.

d - this investigation, prepared using 20 mol % KCl as a flux.

e - diffractometer lattice constants by S.-J. Hwu, prepared using Y strips and 10 mol % KCl.[46]

f - Guinier lattice constants from Mattausch et al.[3]

g - Guinier lattice constants from the thesis of N. Holzer.[2]

for 17 days.[46] The lattice constants obtained from a single crystal which was indexed on the diffractometer are also reported in Table 18. These lattice constants fall in an intermediate range but are definitely closer to the lattice constants from the YCl structure determination. If the average value of $\underline{c}$ for YCl from this investigation is compared with that from the strip reaction then the difference is only 3σ. At any rate, there is still a large difference in $\underline{c}$ between what is observed in this group and reported by Professor Simon's group.

A plot of $r_{Cl^-}/r_{RE^{+3}}$ versus $\underline{c}/\underline{a}$, where r is the six coordinate crystal radii for Cl^- and rare earth metal ions, for various rare earth metal monochlorides according to Mattausch et al.[49] shows a nearly linear relationship (Figure 11). The values reported for YCl are from Mattausch et al.[3] and the YCl crystal structure. The plot shows that the value for YCl determined in this investigation give a more reasonable fit than that of Mattausch et al.[3]

The picture is further clouded by the observed powder pattern of YCl reported in the dissertation of Norbert Holzer (Max-Planck-Institute).[2] He reports the lattice parameters of YCl are: $\underline{a}$ = 3.7478(9) Å and $\underline{c}$ = 27.525(5) Å. These have also been confirmed by this investigator who used Holzer's indices and 2θ values and obtained the same lattice constants with LATT.[28] This means that Professor Simon's group has observed the same lattice constants as this investigation. This may be more of a communication than a scientific problem.

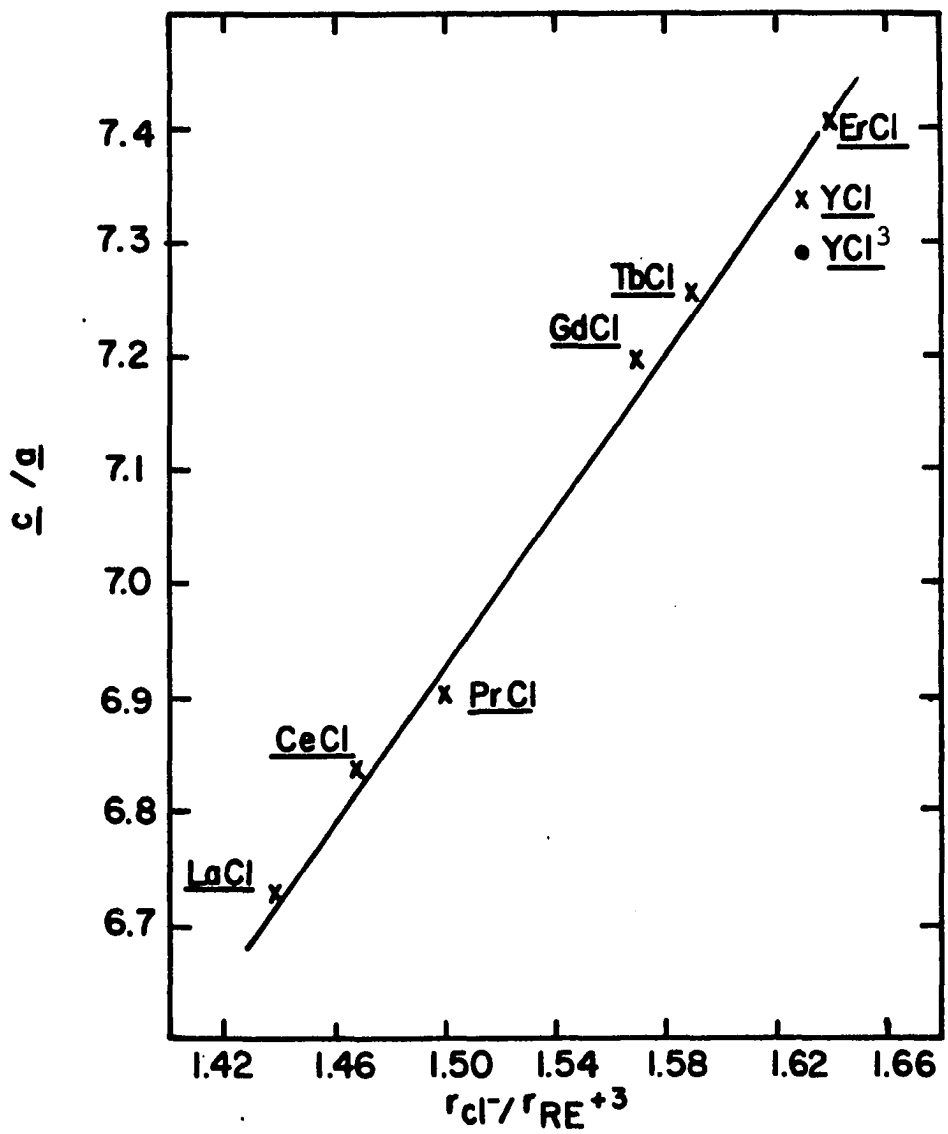

Figure 11. A plot of c/a versus $r_{Cl^-}/r_{RE^{+3}}$ (six coordinate Shannon crystal radii[41]) for the rare earth metal monochlorides[49]

Intercalation of YCl

The determination of lithium in compounds produced in small quantities is difficult. Because of the small scattering power of lithium the detection using X-ray crystallography when heavy elements are present is limited. This is especially true in the case of $Li_{0.09}YCl$ where the amount of lithium is about one-third of the maximum composition. Nonetheless the results section showed that lithium could be refined in the tap hole between the chlorine layers. This alone does not prove that lithium is present in the structure but other evidence based on the structure results, lattice parameters, and comparison with other systems helps support the assignment of this phase as $Li_{0.09}YCl$.

The bond distances obtained from the structure are very reasonable for such a phase. The interlayer Y-Y distance shows an 8σ decrease which can be explained by the reduction, $Li^{+}_{0.09}(YCl)^{0.09-}$. The $\underline{c}$-axis expansion is also indicative of intercalation in YCl. The expansion along $\underline{c}$ per slab in going from YCl to Li_xYCl, $YClO_z$ to Li_xYClO_z, and $Y_2Cl_2C_z$ to $Li_xY_2Cl_2C_z$ are 0.27 Å, 0.24 Å, and 0.22 Å, respectively. This shows the $\underline{c}$-axis expansion in Li_xYCl is typical for lithium intercalation.

Recent work by G. Meyer has yielded a second lithium intercalate of a monohalide, Li_xGdCl by the reaction:

$$Li + KGd_2Cl_7 \xrightarrow{500^{\circ}C} Li_xGdCl + K_2GdCl_5 + \text{other products.}^{50}$$

It is surprising that this low temperature reaction produced β-GdCl (high temperature form, ZrBr structure-type) with an expanded lattice. Meyer's structure results are reported in Table 19. The expansion along $\underline{c}$ in

Table 19. Crystallographic data for 3R-$Li_{0.3}GdCl$ (from Meyer[50])

Cell: Trigonal $R\bar{3}m$

Lattice Constants: a = 3.815 Å, c = 27.832 Å

β-GdCl Lattice Constants: a = 3.819(1) Å, c = 27.482(6) Å

Refinement: R = 0.087 R_w = 0.088

Atom Parameters:[a]

	z	$B_{11}^{b}=B_{22}$	B_{33}
Gd	0.21708(6)	0.24(6)	1.49(9)
Cl	0.3875(3)	0.76(21)	1.09(6)
Li[c,d]	0.0	1.6(18)	

Distances (Å):

Gd-Gd	3.567(3)
Gd-Cl	2.800(2)
Li-Cl	2.669(1)

[a] x = 0.0 and y = 0.0.

[b] The thermal parameter expression used in $\exp-(1/4(B_{11}a^{*2}(h^2+hk+k^2)+B_{33}\ell^2c^{*2}))$, $B_{12}=1/2B_{11}$, $B_{13}=-B_{23}=0$.

[c] Occupancy = 0.31(10).

[d] Isotropic B.

going from GdCl to Li_xGdCl of 0.35 Å is similar to the results in Li_xYCl (above). The Li-Cl bond distance of 2.668 Å agrees very well with 2.651 Å in Li_xYCl and is only slightly longer than the sum of the crystal radii for Li and Cl, 2.57 Å. The crystal structure of β-GdCl has not been determined so the intralayer Gd-Gd distances cannot be compared. The structural evidence suggests the phase is Li_xGdCl which is isostructural with Li_xYCl.

A Li-Cl distance which is longer than the crystal radius sum can be contrasted to the Na-Cl and K-Cl distances in $Na_{0.08}YClO_{1.0}$ and $K_{0.08}YClO_{0.82}$, respectively, which are shorter than the crystal radius sums. In fact the size of the tap site between the Cl layers in YCl is already large enough to accommodate a lithium atom. The question that arises is why does the host lattice expand at all to accommodate lithium? In the lithium intercalation of MCh_2, in particular TiS_2 and VSe_2, it was noted that the interlayer expansion was not associated with simple space filling and propping open by the intercalated Li^+ since Li^+ is smaller than the tap site in TiS_2 and much smaller than the site in VSe_2. It has been concluded based on the ideal packing of lithium intercalates and a diffusive model for the intercalation of lithium that the expansion of the layered compounds on insertion of lithium is <u>not</u> associated with the propping open of the layers by lithium but is rather associated with the change in charge density on the surrounding sulfur atoms caused by reduction of the slab.[51,52] The electrostatic charge separation of the host layers on reduction with lithium intercalation would also explain

the c-axis expansion and longer than expected Li-Cl bond distances in Li_xYCl and Li_xGdCl.

Unfortunately, other M^I_xYCl or M^I_xGdCl phases have not been synthesized. In this investigation the large yields of impurity phases make it very difficult to find or isolate a possible ternary phase. If the impurities are eliminated, then other M^I_xYCl phases may result. In the case of M^I_xGdCl, reactions with other alkali metals have not been tried. The possible advantage of this low temperature route would be the avoidance of impurity phases.

Coordination of Intercalated Alkali Metals

Rouxel et al. has concluded that the coordination of the alkali metal in intercalated transition metal disulfides (MS_2) and Ta_2S_2C is determined by three factors.[53] The two most important are the size and amount of the intercalated atoms. The third factor uses the nature of the M-S bond to compare the results in systems with different transition metals and different chalcogen and does not apply to this investigation where the metal and halide remain the same. (The first two factors apply to this investigation and each will be discussed in detail for the $M^I_xYClO_z$ phases.)

The first factor involves the size of the alkali metal atom and is that smaller intercalated alkali metal atoms exhibit trigonal antiprismatic (tap) coordination while larger atoms exhibit trigonal prismatic (tp) coordination. This can be understood by noting that with smaller alkali metal atoms the anion layers are closer together (as in the

unintercalated case) and trigonal antiprismatic coordination (tap) is retained. In the $M^I_xYClO_z$ phases the influence of the M^I size can be correlated to the structure. For example, when M^I=Li the only phase observed is the 3R-Li_xYClO_z where the Li^+ has tap coordination. On the other hand, the 2H- and 1T-Cs_xYClO_z phases where Cs^+ is tp are the more prevalent. It should be noted that the 3R-Cs_xYClO_z phase exists where Cs^+ is tap but when the 3R phase is annealed at temperatures greater than 900°C the product is the 1T phase. A possible reason for the change from tap to tp coordination of the Cs^+ on annealing is the stability offered by the tp coordination. For the cases where M^I=Na-Rb both the tp and tap coordination of M^I have been observed (the 2H- and 3R-$M^I_xYClO_z$, respectively) and other factors influence the coordination of M^I.

The second factor is that as the alkali metal concentration of the intercalated species increases the tap coordination is favored. This can be understood because an octahedron (tap) can accommodate higher charges on the nonmetal than a trigonal prism since the atoms in adjacent layers are further apart. The higher charge on the nonmetal at higher M^I concentrations is consistent with the formulation of $M^{I+}_x(MS_2)^{-x}$ or $M^{I+}_x(YClO_z)^-$. In this investigation for reaction (1)

$$(1)\quad dY\ \text{powder} + dM^ICl + YCl_3 + Y_2O_3 \xrightarrow{>925^oC} M^I_dY_{3+d}Cl_{3+d}O_{3+e}$$

where M^I=Na-Rb it became apparent that as d was increased the yield of 3R-$M^I_xYClO_z$ (tap coordination of M^I) was also increased. Looking at the case for M^I=K, when d=0.45 the only product was 2H-K_xYClO_z (tp

coordination of K), when d=0.68 both the 2H and 3R phases were obtained in equal amounts, and when d=1.5 and 2.4 the only product was the 3R phase.

When reaction (2) is used the concentration of the $M^{I}Cl$, d,

$$(2)\ dY\ \text{powder} + dM^{I}Cl + 3YOCl \xrightarrow{>925^{o}C} M^{I}_{d}Y_{3+d}Cl_{3+d}O_{3+e}$$

has no effect on the products obtained. For all reactions where M^{I}=Li-K, the only phase obtained from reaction (2) is 3R-$M^{I}_{x}YClO_{z}$ where M^{I} is tap. In the case where M^{I}=K the 3R phase was obtained when d = 0.19, 0.36, 0.51, 1.0, 1.3 and 1.6. It was expected that reactions (1) and (2) would yield the same product for a given d. Since the reactions where M^{I}=K have demonstrated that this is not the case then there must be a different reaction mechanism in the two reactions. For reaction (2) the structure is influenced by the method of the reaction and not the concentration of $M^{I}Cl$.

Although the factors stated by Rouxel for the intercalation of M^{I} in MS_2 do apply for the $M^{I}_{x}YClO_{z}$ phases there are also some differences. In the intercalation of M^{I} in MS_2 for a given M there is only one M^{I} which may appear in both tp and tap coordination.[15,16] For example, in the $M^{I}_{x}TiS_2$ system when M^{I}=Li only the tap coordination is observed, if M^{I}=Na then both tap and tp coordination results with the tap at higher Na concentrations, and finally for M^{I}=K-Cs the coordination of M^{I} is tp. This can be compared with the $M^{I}_{x}YClO_{z}$ phases where when M^{I}=Na-Rb both the tp and tap coordination of M^{I} is observed.

A second difference is the lack of staged compounds in the $M^I_xYClO_z$ phases. Here, the $M^I_xYClO_z$ compounds resemble the $M^I_xTa_2S_2C$[54] phases which also show no staged compounds. In the intercalated sulfide carbides, it is thought that the larger screening effect due to five layers (-S-Ta-C-Ta-S-) is responsible for the lack of staged compounds.[16,54] The same argument can be used to explain the lack of staged compounds for the five layer slabs of $M^I_xY_2Cl_2C_z$ (-Cl-Y-C-Y-Cl-) and the six layer slabs in $M^I_xYClO_z$ (-Cl-Y-O-O-Y-Cl-).

Intercalation of $Y_2Cl_2C_z$

The 1T forms of $Y_2Cl_2C_z$ and Ta_2S_2C[45] are isostructural and represent a direct comparison between the intercalation of metal-halide-carbides with metal-sulfide-carbides. There is also a 3R-Ta_2S_2C (space group $R\bar{3}m$) which is formed at high temperatures and involves the rhombohedral stacking of the same 1T-type slabs.[45] There have been two independent investigations of M^I intercalation in Ta_2S_2C by Brec et al.[54] and Schöllhorn et al.[55] The results from these investigations are quite different so each will be discussed independently and compared with the intercalation of 1T-$Y_2Cl_2C_z$.

In the work of Schöllhorn et al., the 1T-Ta_2S_2C was intercalated either chemically or electrochemically in aqueous electrolyte solutions at room temperature.[55] The chemical intercalation was accomplished using sodium dithionite, $Na_2S_2O_4$, in aqueous solutions at pH>7. The $Na^+_{0.2}(H_2O)_a(Ta_2S_2C)^{0.2-}$ obtained by this method can undergo cation exchange with 1M aqueous solutions of M^I to form $M^I_{0.2}(H_2O)_a(Ta_2S_2C)^{0.2-}$.

Structurally, the hydrated cation causes a large expansion in the c-axis (∿3.25 Å for M^I=K-Cs and ∿6.0 Å for M^I=Li or Na where a water bilayer is formed) but the 1T structure is retained. This results in the tap coordination of all hydrated cations in this structure. This is analogous to the 1T-$M^I_xY_2Cl_2C_z$ phases where M^I=Li-K the 1T structure is retained and the M^I has tap coordination.

In the work by Brec et al., the intercalate, $M^I_xTa_2S_2C$, was prepared by reacting Ta_2S_2C with M^I in liquid NH_3.[54] The ammonia was removed by heating to 250°C for 12 hrs. under vacuum. The structure types, based on X-ray diffraction, are a 3R-type with tap coordination of Li, two different 2H modifications with tap and tp Na, a 3R-type with tp coordination for K, and a 2H-type with tp coordination of Rb or Cs. This is quite different from $M^I_xY_2Cl_2C_z$ where only the 1T structure with tap coordination of M^I is observed for phases prepared at high temperature.

The difference in structures between the work of Brec et al.[54] and this investigation may be due to the synthetic methods. The paper by Brec et al. does not indicate whether the 1T- or 3R-Ta_2S_2C is used in these reactions but the reaction conditions used to prepare Ta_2S_2C suggest the phase is the 3R-type.[54] If only the 3R-Ta_2S_2C was used in their intercalation reactions then the different structure types may be due to a difference in reactivity between the 1T and 3R types. It may be possible to make the 3R-Y_2Cl_2C and the 3R- and 2H-$M^I_xY_2Cl_2C_z$ phases by reactions at higher temperatures.

Unsuccessful Intercalation Reactions

Unless there had been some degradation of 3R-$YClO_z$ during the oxidation of $M^I_xYClO_z$ with I_2 then this material should have reintercalated. The reactions of 3R-$YClO_z$ at room temperature with either n-butyllithium or sodium dithionite were unsuccessful. It may be possible to intercalate the 3R phase at room temperature using a stronger reducing agent, e.g., M^I in liquid ammonia. A second possibility may be the use of high temperature reactions of 3R-$YClO_z$ with M^ICl and Y.

The lack of success in intercalating REOCl (PbFCl structure) may be explained by the absence of a true van der Waals gap in REOCL.[15] Using YOCl as an example, the Y^{3+} is located in a distorted square antiprismatic site with four oxygen atoms in a plane at 2.28 Å and four chlorine atoms in a plane at 3.00 Å. There is also a fifth chlorine in an adjacent slab at 3.03 Å which caps the four-chlorine face of the square antiprism, making the yttrium nine-coordinate. Thus, there is no true van der Waals gap and to intercalate REOCl the interslab RE-Cl bond must be ruptured. It might be possible to intercalate REOCl with a Lewis base which would occupy the ninth coordination site of the RE^{+3} ion. It might also be possible to intercalate REOBr or REOI (PbFCl structures) where the RE^{+3} ion is eight-coordinate and there exists a van der Waals gap between the halogens.

Light Atom Interstitial Compounds

One of the most interesting aspects of the $M^I_xYClO_z$ and $M^I_xY_2Cl_2C_z$ phases was finding light atom interstitials between the Y layers. This

was especially surprising considering the initial "ternary" reactions which produced these phases were thought to be free of these "impurities". It was not until the reactions were repeated with Y_2O_3, YOCl or powdered graphite and the yields were nearly quantitative that the presence of the interstitial atoms was believed.

When this investigation was started and up until a couple of years ago hydrogen was the only known interstitial atom in reduced metal halides. On reaction of H_2 with ZrCl, ZrBr, Nb_6I_{11}, and $CsNb_6I_{11}$ the phases $ZrXH_{0.5}$, $ZrXH_{1.0}$, $Nb_6I_{11}H$, and $CsNb_6I_{11}H$ could be formed.[19,56,57] These are interesting compounds which contain hydrogen that is considered hydridic within the metal-metal bonding framework. For $Nb_6I_{11}H$ and $CsNb_6I_{11}H$ the hydride is in the center of Nb_6 octahedron while in the monohalides the hydride is in the tetrahedral-like interstices between the Zr layers. There is a structural rearrangement that occurs in the ZrX structures but the basic layered nature of the structure is retained.

Recently oxygen was found to be an interstitial atom in $ZrXO_x$ which is formed by reacting ZrX, X = Cl, Br, with ZrO_2.[17] It was originally expected that oxygen would replace the halide atoms in the halide layers but structural studies have shown that oxygen is in the tetrahedral-like interstices between the Zr layers. In this case, the ZrX structure is retained with some expansion of the Zr-Zr inter- and intralayer distances needed to accommodate the oxygen.

Now, this investigation has shown a second example of compounds which form with oxygen atoms in the tetrahedral-like interstices between the

yttrium layers. In particular, 3R-$M^{I}_{x}YClO_{z}$ and 3R-$YClO_{z}$ are isostructural with $ZrBrO_{x}$ if the alkali metal in 3R-$M^{I}_{x}YClO_{z}$ is ignored.

The other structures, 1T-$M^{I}_{x}YClO_{z}$ and 2H-$M^{I}_{x}YClO_{z}$, show different ways of generating and packing slabs that are determined primarily by the size and concentration of the alkali metal and second nearest neighbor considerations. Even though the way the slabs are stacked has changed, the structure within a slab has remained the same and in particular the tetrahedral-like interstices between the yttrium layers again accommodate the oxygen atoms.

There are some examples of ionic compounds that are layered with light nonmetal interstitial derivatives between metal layers. The SmSI structure[14] where sulfur is in the tetrahedral-like holes is isostructural with $ZrClO_{x}$ for x=1. The YOF structure [43,14] where both the oxygen and fluorine atoms can be considered filling the tetrahedral-like interstices between the yttrium layers in an ordered trigonally distorted CaF_2 structure is isostructural with $ZrBrO_{x}$, 3R-$YClO_{z}$, and with 3R-$M^{I}_{x}YClO_{z}$ ignoring the alkali metal.

At this time, there are no proven examples of oxygen atoms in the center of metal octahedra. There are a number of chain compounds and isolated clusters that have residual electron density within the metal octahedra. The cause of the residual density may be a light nonmetal interstitial atom but this has not been confirmed.

Until recently, the only example of a compound containg a carbide between the metal layers (other than the metal carbides) was Ta_2S_2C.[45] In Ta_2S_2C, the carbide occupies the trigonal antiprismatic site between

the Ta layers. This investigation has now shown the compounds $Y_2Cl_2C_z$ and $M^I_xY_2Cl_2C_z$ exist and are isostructural with Ta_2S_2C and $M^I_xTa_2S_2C$, respectively. The list of carbides is now growing larger with the recent work of Professor Simon's group who have made $Gd_{10}Cl_{18}C_4$,[58] $Gd_{10}Cl_{17}C_4$,[58] $Gd_{12}I_{17}C_6$,[59] $Gd_6I_7C_2$,[60] $Gd_2Br_2C_2$,[60] and Gd_3CCl_3.[60] Only $Gd_6I_7C_2$ which has an infinite double chain of metal octahedra similar to Er_6I_7 with each octahedron containing a carbon and Gd_3CCl_3 which has isolated Gd octahedra containing carbon are examples of monocarbides. The other compounds contain C_2^{6-} or C_2^{4-} units within a metal octahedron.

Professor Simon's group has also made the first rare earth metal halide that contained a nitride, Gd_2Cl_3N.[60] Judging from the number of gadolinium halide carbides there are probably more nitrides still to be discovered.

The group III, IV, V, and rare earth metal halide compounds containing light nonmetal interstitials are summarized in Table 20.

Looking more closely at the layered compounds which contain light nonmetal atoms it becomes apparent that the size of the interstitial ions determines which site it will occupy. The $M^I_xYClO_z$ and $M^I_xY_2Cl_2C_z$ phases offer good examples of how the difference in size of the carbide and oxide ions influence the sites they adopt. The size of the unoccupied sites in YCl, Y, ZrX along with the size of the sites in interstitial derivatives are reported in Table 21. In YCl, the radius of the tetrahedral-like site is 2.23 Å while that of the tap site is 2.57 Å. For the case with a six-coordinate crystal radius sum of 2.28 Å for Y-O

Table 20. The known interstitial derivatives of layered compounds, metal chain compounds, and metal cluster compounds

	Layered compounds	Metal chain compounds	Metal cluster compounds
H	$ZrClH_{0.5}$[19] $ZrClH_{1.0}$[19]		$Nb_6I_{11}H$[56]
	$ZrBrH_{0.5}$[19] $ZrBrH_{1.0}$[19]		$CsNb_6I_{11}H$[57]
O	$ZrClO_x$[17], $ZrBrO_x$[17]		
	$3R\text{-}M^I_xYClO_z$, $2H\text{-}M^I_xYClO_z$		
	$1T\text{-}Cs_xYClO_z$, $3R\text{-}YClO_z$		
C	$1T\text{-}Y_2Cl_2C$, $1T\text{-}M^I_xY_2Cl_2C_z$	$Gd_{12}I_{17}C_6$[59a]	Gd_3Cl_3C[60]
	$1T\text{-}Sc_2Cl_2C$,[46] $1T\text{-}Zr_2Br_2C$[61]	$Gd_6I_7C_2$[60]	$Gd_{10}Cl_{18}C_4$[58b]
	$1T\text{-}Zr_2Cl_2C$[62]		$Gd_{10}Cl_{17}C_4$[58b]
N		Gd_2Cl_3N[60]	
?[c]		$\beta\text{-}Sc_2Cl_3$[46]	$CsZr_6I_{14}$[63]
		$Sc_7Cl_{10}O_2$[46]	Sc_7Cl_{12}[64]
			Zr_6Cl_{15}[64]

[a]Extended metal chain with C_2 units.

[b]Clusters formed by edge-sharing of two Gd_6 octahedra with C_2 units.

[c]Refined structures with residual electron density in the center of the cluster.

Table 21. The size of the interstitial sites in various compounds compared with the sum of the metal-interstitial atom crystal radii

Phase	Site Radius Tetrah.	ΣC.R.[a]	Site Radius Oct.	ΣC.R.[b,c]	Observed Occupancy
Y[40]	2.20		2.54		
YOCl[14]	2.27	2.28			T_d
YOF[43]	2.27	2.28	2.61		T_d
YCl	2.23		2.57		
$2H\text{-}K_{0.08}YClO_{0.82}$	2.26	2.28	2.60		T_d
$3R\text{-}Na_{0.08}YClO_{1.0}$	2.27	2.28	2.61		T_d
ZrCl[12]	2.01		2.31		
$ZrClO_{0.43}$[17]	2.06	2.10	2.37		T_d
ZrBr[13]	2.05		2.35		
$ZrBrO_{\sim 0.23}$[17]	2.08	2.10	2.38		T_d
Y[40]	2.20		2.54		
Y_2C[48]	2.16		2.48	2.50	O_h
Ta_2S_2C[45]	1.94		2.23	2.24	O_h
ScCl[42]	2.05		2.37		
Sc_2Cl_2C[46]	2.01		2.31	2.345	O_h
YCl	2.23		2.57		
$1T\text{-}K_{0.52}Y_2Cl_2C_{0.8}$	2.16		2.49	2.50	O_h

[a] ΣC.R.=four coordinate O^{-2} crystal radius + six coordinate metal radius.

[b] ΣC.R.=sum of the six coordinate metal and C^{-4} radii.

[c] The crystal radius of C^{-4} (1.46 Å) was determined from the lattice constants of several MC (rock-salt structure) compounds.

oxygen can occupy the tetrahedral-like site which would result in a slight expansion of the yttrium layers or occupy the much larger tap site where it would "rattle" or cause a large contraction of the metal layers. The result is that the oxide is found in the tetrahedral-like site with Y-O bond lengths of 2.284 Å and 2.251 Å. This is also the site which oxygen occupies in YOF, YOCl, $ZrClO_x$, and $ZrBrO_x$ which are also listed in Table 21. This is very similar to the insertion of oxygen in ZrCl and ZrBr and is discussed by Seaverson and Corbett.[17]

In the case of the carbide with a crystal radius sum of 2.50 Å, the choice is much easier. The tetrahedral-like site in YCl is much too small and the carbide occupies the tap site. Since the tap site is slightly larger than the carbide there is a contraction in the yttrium-yttrium distances from YCl. In Table 21, the sizes of the tap site occupied by C in Y_2C and 1T-$K_{0.52}Y_2Cl_2C_{0.8}$ are compared.

It is easy to compare the similarities of the $M^I_xYClO_z$ phases with the $ZrXO_x$ and $ZrXH_x$ phases but the differences should not be overlooked. The major difference is that $M^I_xYClO_z$ and $YClO_z$ are more ionic. In 2H-$K_{0.08}YClO_{0.82}$, the oxidation state of yttrium is +2.5, and this can probably be assumed to be the yttrium oxidation state in other $M^I_xYClO_z$ phases. This leaves only one-half of an electron for metal-metal bonding. The compositions in the $M^I_xY_2Cl_2C_z$ phases have not been determined very well but it can be assumed that these phases also have less than one electron per yttrium for metal-metal bonding. On the other hand, the maximum compositions of $ZrXO_{0.4}$ and $ZrXH_{1.0}$ leave at least two electrons per zirconium for metal-metal bonding.

Hydrates of $M^I_xYClO_z$

The hydrates, $M^I_x(H_2O)_aYClO_z$, may be compared with the well-documented hydrates of alkali-metal-intercalated transition metal disulfides, $M^I_x(H_2O)_aMS_2$.[15] Studies by Schöllhorn and Weiss on the hydration properties of $M^I_xTiS_2$ and $M^I_xMoS_2$ have established the ion and solvent exchange reactions, the ionic structure $M^{I+}_x(H_2O)_a(MS_2)^{x-}$, and the existence of two defined hydration stages dependent on cation hydration energy and water vapor pressure.[65,66] The phases can be prepared directly by hydration of $M^I_xMS_2$ or by chemical and electrochemical reduction of the binary sulfides in the corresponding aqueous electrolytes.

The structure and bonding of the hydrated phases $M^I_x(H_2O)_aMS_2$ are described by an ionic model: the $(MS_2)^{x-}$ layers represent quasi-two-dimensional macroanions with delocalized negative charges; the interlayer space is occupied by solvated cations which are highly mobile at room temperature.[15] As a consequence, these hydrates have typical poly-electrolyte character and undergo ion- and solvent-exchange reactions. Two structurally-defined hydrate stages are found with alkali metals that correspond with monolayers of H_2O, $\Delta c \sim 3$ Å and bilayers of H_2O, $\Delta c \sim 6$ Å, where Δc is the elongation of the c-axis on hydration. The formation of either structure depends on the charge to radius ratio (e/r) of the cation, i.e., on the cation hydration energy. Large cations, usually K-Cs, with $e/r<1$ exhibit monolayers of H_2O while smaller cations, usually Li and Na, with $e/r>1$ have the capacity to form bilayers of H_2O. The stability of the phase with H_2O bilayers also is dependent on the water vapor pressure: with decreasing p_{H_2O} a bilayer to monolayer transition

takes place. The X-ray single crystal structures of two monolayer hydrates, $K_x(H_2O)_yTaS_2$ and $K_x(H_2O)_yNbS_2$ where only the Nb or Ta and S were refined, showed tp sites for the K-hydrate.[67] An X-ray and neutron diffraction study of powdered bilayer hydrates indicated a tap site for the M^I hydrate.[68] The orientation of H_2O based on neutron diffraction and ^1H NMR places the oxygen in the plane of the alkali metal layer and the hydrogens directed towards the sulfur layers for the monohydrates and one H atom of each H_2O in the plane of the oxygen atoms (the oxygen atoms are above and below the plane of the alkali metal) and the other H atom directed towards the sulfur layers in the bilayer.[15]

The most striking similarity between $M^I_x(H_2O)_aMS_2$ and $M^I_x(H_2O)_aYClO_z$, M^I=K or Rb, formed on exposure to air is the Δc of $\sim$2.6 Å and the trigonal prismatic coordination of M^I and presumably H_2O. Based on the results from the $M^I_x(H_2O)_aMS_2$ system, this can probably be considered a monolayer of H_2O with the H_2O in trigonal prismatic sites and the oxygen in the M^I plane and the hydrogens near the Cl layers. Like the hydrated dichalcogenides the hydration-dehydration reactions of the chorides are reversible with the original alkali metal oxide phase obtained on dehydration.

In the case of 3R-Li_xYClO_z, there is no hydration reaction in air and this can be contrasted with Li_xMS_2 which forms bilayer hydrates. The chlorines are probably more polar than the sulfurs, thus the Li-Cl lattice energy is higher than the Li^+ hydration energy. It is possible that the 3R phase will hydrate on exposure to higher water vapor pressures but this

has not been investigated. The hydration of Na_xYClO_z, another phase expected to form bilayer hydrates, has not been studied.

When 3R-$M^I_xYClO_z$, M=Li-Cs, phases are placed in H_2O they react in a very different manner from the $M^I_xMS_2$ phases. In H_2O, the $M^I_xYClO_z$ phases are oxidized, evidenced by the evolution of H_2, and the crystals exfoliate as described in the results section. The $M^I_xMS_2$ phases do not oxidize or exfoliate in H_2O and only form crystalline hydrates, $M^I_x(H_2O)_aMS_2$.[15] When hydrogen was intercalated electrolytically into single crystals of 2H-TaS_2 in dilute acid electrolytes there was a large degree of exfoliation with no gas evolved.[69] The exfoliation in both cases is similar in appearance to the swelling observed in smectites or vermiculites and in particular the alkali metal montmorillonites, $\sim M^I_xAl_4Si_8O_{16}(OH)_{12}\cdot nH_2O$.[70] There may also be some structural similarities but the hydration in these sheet silicates is dominated by hydrogen bonding to the oxygen layers.

A "mechanism" may be postulated for the exfoliation of 3R-$M^I_xYClO_z$ based on visual evidence and the results from other exfoliated systems. The first step is the hydration of M^I to form 1-$M^I_x(H_2O)_aYClO_z$. This is followed by the oxidation of the slabs with loss of M^I to give neutral slabs, probably with some decomposition of the slabs. The water then enters the interlayer region between the slabs and hydrogen bonds with the Cl layers. It is the hydrogen-bonded water within the interlayer region that causes the swelling or exfoliation. When these exfoliated "crystals" are removed from the water and mildly heated (by the microscope light), most of the water evaporates and the "crystal" collapses back to a plate. The plate must retain some water which allows the process to

reverse when the plate is placed in water. When the exfoliated "crystals" are heated to ∿110°C then the plate crystals cannot be exfoliated a second time. This can be explained by the loss of the cation during the exfoliation and the evaporation of all water during heating. Powder patterns of the plates after heating show only very broad lines indicative of disorder which occurred during exfoliation.

The 2H-$M^{I}_{x}YClO_{z}$ phase where M =K or Rb have been observed to form apparent monolayer hydrates, 2H-$M^{I}_{x}(H_2O)_aYClO_z$, on exposure to air. There is no structural change as there are already tp sites available for H_2O and $\Delta c \sim 2.6$ Å. When placed in water the 2H phases do not exfoliate or evolve H_2. It is believed that they only form the monolayer hydrates in water.

Sources of Impurities

Oxygen impurities have always been a problem in most rare earth metal-halide systems as evidenced by the ubiquitous REOCl. In this investigation, YOCl was observed at temperature lower than 875°C but at temperatures greater than 875°C with $M^{I}Cl$, $M^{I}_{x}YClO_{z}$ is formed. There are a number of possible oxygen sources including the reactants, dry box, atmosphere, the transfer to the welder, fused silica jackets, and possibly the Nb tube and the manner in which it was cleaned (see below). One likely suspect for oxygen contamination was a 10-12 g batch of powdered yttrium which gave large yields (40-60%) of $M^{I}_{x}YClO_{z}$. There was no oxygen analysis of the powdered yttrium but the yields of $M^{I}_{x}YClO_{z}$ were less than 20% with other yttrium samples.

The amount of oxygen in these reactions can be reduced by careful distillations of the reactants and handling only small amounts of the reactants in the dry box at one time. The amount of oxygen in the dry box has already been reduced by the use of Ridox as an oxygen scavenger. The oxygen from the tube and jacket can be reduced by only cleaning the Nb tube once, before it is welded, with Ta cleaning solution and flaming the fused silica jacket under vacuum before the seal off. When preparing powdered metal, care has to be taken to ensure that there are no leaks in the vacuum system during hydrogenation and dehydrogenation.

The source of carbon is not as obvious and has led to much speculation. The reactants are unlikely sources because the YCl_3 and M^ICl were distilled and the analysis of the yttrium showed less than 300 atomic ppm carbon. The analysis of the Nb tubing showed only 0.06 mg of carbon per 10 cm of tubing. The most likely source is a white precipitate formed when acetone is added to Ta and Nb tubes which have not been thoroughly washed with distilled water and contain Ta cleaning solution in the crimp. Acetone is known to react with H_2SO_4 and undergo an aldol condensation to form mesitylene, $1,3,5\text{-}C_6H_3(CH_3)_3$.[71] The white precipitate may be a polymer, also formed by an aldol condensation of acetone, which would pyrolize at higher temperatures. One or two milligrams would be enough carbon to produce $1T\text{-}M^I_xY_2Cl_2C_z$ in a 10-15% yield. Some experimental evidence which supports the precipitate theory is that not all reactions produce the 1T phase while not all tubes were rinsed with acetone. Also, many of the 1T products were found in the crimped ends of the reaction tubes. This cannot be used as a confirmation of the

precipitate because it was not recorded which tubes were or were not rinsed with acetone and which crimp was washed with cleaning solution and acetone. If the white precipitate is the carbon source then only an initial cleaning of the tube with Ta cleaning solution before it is crimped should avoid the carbon impurity and the 1T-phase.

FUTURE WORK

Synthesis of M^I_xREX

This investigation has shown that lithium can be intercalated in YCl to form $Li_{0.09}YCl$. Studies of other ternary reactions were complicated by the presence of impurity phases which made the detection of possible M^I_xYCl phases difficult. In order to isolate M^I_xYCl, where M^I=Na-Cs, the impurities need to be eliminated as described earlier. The contact between the metal and the melt should be maximized by the use of Y powder or the use of pressed tube reactions with Y strips. Results from the lithium system suggests that the product will be found on the metal.

A second method for the intercalation of monohalides is the reduction of ternary alkali metal-rare earth metal halides by alkali metals at low temperatures, <600°C. This method was used by G. Meyer to produce Li_xGdCl. The advantage of a low temperature route is that impurity phases can be avoided. A disadvantage may be the number of phases formed, as in the reaction that produced Li_xGdCl. There is also the possibility that the salt may be reduced all the way to the metal.

In this investigation, the work has been limited to the yttrium chlorides but other systems should also be tried. A likely candidate in the yttrium system is YBr which forms both the ZrBr- and ZrCl-type structures between 800° and 850°C. Other systems which have not been investigated include ScCl, LaCl, and GdCl using M^ICl at high temperatures.

Synthesis of other $M^{I}_{x}REXO_{z}$ Phases

This investigation showed that a number of $M^{I}_{x}YClO_{z}$ phases are formed with M^{I}=Li-Cs. It would be of interest to see if $M^{I}_{x}REClO_{z}$ can be formed as the size of the rare earth metal is increased. The smaller rare earth oxychlorides (REOCl, RE=Er-Lu) have the SmSI structure type which is isostructural with $ZrClO_{x}$. A slab in REOCl (SmSI-type) is the same as that in 3R-$YClO_{z}$ or 3R-$M^{I}_{x}YClO_{z}$ and only the slab stacking sequence is different, e.g., ZrCl vs. ZrBr. The site available for intercalation in REOCl (SmSI) has tap coordination with rare earth metals as second nearest neighbors. A general observation from this investigation is that on intercalation a structure is adopted where the alkali metal to yttrium distance is maximized. If this is true then the intercalation of REOCl (SmSI) would involve an interslab rearrangement which would probably result in a product that is isostructural with 3R-$M^{I}_{x}YClO_{z}$. Thus, reactions of REOCl (SmSI) with $M^{I}Cl$ and RE at high temperatures could have interesting results.

The remaining larger rare earth metal oxyhalides, RE=La-Ho, Y have the PbFCl structure with erbium forming the PbFCl and SmSI structure-types. In previous sections, it was shown that REOCl (PbFCl-structure) would not intercalate but YOCl (PbFCl) will react with Y and $M^{I}Cl$ to produce $M^{I}_{x}YClO_{z}$. The size of Y is comparable to Ho which means it is one of the smaller rare earth metals to form REOCl (PbFCl). Reactions of larger REOCl (PbFCl) with $M^{I}Cl$ and RE would show whether the increased stability of REOCl limits the reaction to form $M^{I}_{x}REClO_{z}$.

Synthesis of $M^{I}_{x}RE_2X_2C$

The ternary carbide, 1T-Y_2Cl_2C and its intercalation compounds 1T-$M^{I}_{x}Y_2Cl_2C_z$ where M^{I}=Li-K, and possibly Cs, are very recent discoveries. The larger alkali metals, Rb and Cs, should be more thoroughly investigated to see if the 1T structure and tap coordination is retained. A second study would be to see if the 3R phases, similar to 3R-Ta_2S_2C, can be formed by varying the reaction temperatures or compositions.

The intercalation of 1T-Y_2Cl_2C could also be tried via room temperature methods using n-butyllithium and M^{I} in liquid ammonia. The reversibility of the intercalation could also be checked by deintercalation using I_2 in CH_3CN.

The results of this work could also be extended to form other possible ternary and quaternary layered carbides of the rare earth metal halides, group IV metal halides, and group V metal halides by similar reactions.

Other Interstitial Compounds

It may be possible to prepare intercalated nitride and fluoride derivatives of YCl by reactions of Y, YCl_3, $M^{I}Cl$ and, as appropriate, YN or YF_3. The predicted structure for $M^{I}_{x}YClN_z$, based on the size of the interstitial sites in YCl versus the sum of the YN and YF crystal radii, would be the 1T-$M^{I}_{x}YClC_{1/2}$ structure where the nitride is tap between the Y layers and for $M^{I}_{x}YClF_z$ it would be similar to $M^{I}_{x}YClO_z$ with the fluoride in the tetrahedral-like interstices between the Y layers.

The interstitial derivatives would not have to be limited to the 1st row nonmetal atoms and could include the sulfides. YSCl is known and it

forms in the FeOCl structure type which is a distorted PbFCl structure. FeOCl is known to undergo intercalation reactions with alkali metals and thus it may be possible to intercalate YSCl in the FeOCl structure-type or it could intercalate at higher temperatures to form a compound similar to $M_x^I YClC_z$. YSI is not known but the compounds PrSI, NdSI, and SmSI are known (SmSI type). As described previously for REOCl, RE=Er-Lu, the structure can be thought of as a ZrCl-structure with all tetrahedral-like interstices between the metal layers filled with sulfur. This is again a layered structure which may intercalate, although as alluded to earlier the expected product may be similar to $3R\text{-}M_x^I YClO_z$.

Physical Properties

Most of this investigation has dealt with the synthesis and characterization of these new phases. It would be of interest to look at the XPS and UPS spectra, determine conductivities, and look at the ^7Li NMR of $1T\text{-}Li_xY_2Cl_2C_z$.

LITERATURE CITED

1. Hendricks, J. B. M.S. Dissertation, Iowa State University, Ames, IA, 1980.

2. Holzer, N. Ph.D. Dissertation, Universität Stuttgart, Stuttgart, West Germany, 1978.

3. Mattausch, Hj; Hendricks, J. B.; Eger, R.; Corbett, J. D.; Simon, A. Inorg. Chem. 1980, 19, 2128.

4. Poeppelmeier, K. Ph.D. Dissertation, Iowa State University, Ames, IA, 1978.

5. Polyachenok, O. G.; Novikov, G. I. Russ. J. Inorg. 1963, 8, 1478.

6. Corbett, J. D.; Pollard, D. L.; Mee, J. E. Inorg. Chem. 1966, 5, 762.

7. Mellors, C. W.; Senderoff, S. J. Phys. Chem. 1959, 63, 111.

8. Ford, J. E., unpublished research.

9. Bullet, D. W. Inorg. Chem. 1980, 19, 1780.

10. Ebbinghaus, G.; Simon, A.; Griffith, A. Z. Naturforsch. 1982, 37A, 564.

11. Simon, A. Angew. Chem. Intl. Eng. Ed. 1981, 20, 1.

12. Adolphson, D. G.; Corbett, J. D. Inorg. Chem. 1976, 15, 1820.

13. Daake, R. L.; Corbett, J. D. Inorg. Chem. 1977, 16, 2029.

14. Hulliger, F. "Structural Chemistry of Layer-Type Phases" (Lévy, F., Ed.), D. Reidel Publishing Company: Boston, 1976.

15. Whittingham, M. S.; Jacobson, A. J. "Intercalation Chemistry"; Academic Press: New York, 1982.

16. Lévy, F. (Ed.) "Intercalated Layered Materials"; D. Reidel Publishing Company: Boston, 1979.

17. Seaverson, L. M.; Corbett, J. D. Inorg. Chem. 1983, accepted for publication.

18. Marchiando, J. F.; Harmon, B. N.; Liu, S. H. Physica 1980, 99B, 259.

19. Marek, H. S.; Corbett, J. D.; Daake, R. L. J. Less Common Met. 1983, 89, 243.

20. Corbett, J. D. Inorg. Syn. 1983, 22, in press.

21. Gmelin Handbuch der Anorganischen Chemie, 8th ed.; Springer-Verlag: Berlin, 1974; No. 39, Teil C1, p. 22.

22. Corbett, J. D. Inorg. Syn. 1983, 22, in press.

23. Gmelin Handbuch der Anorganischen Chemie, 8th ed.; Springer-Verlag; Berlin, 1974; No. 39, Teil C5, p. 17.

24. Daake, R. L. Ph.D. Dissertation, Iowa State University, Ames, IA, 1976.

25. Cisar, A. Ph.D. Dissertation, Iowa State University, Ames, IA, 1978.

26. Araujo, R. E. M. S. Thesis, Iowa State University, Ames, IA, 1981.

27. Clark, C. M.; Smith, D. K.; Johnson, G. J. "A Fortran IV Program for Calculating X-Ray Powder Diffraction Patterns--Version 5", Department of Geosciences, Pennsylvania State University, University Park, PA, 1973.

28. Takusagawa, F. Ames Laboratory, Iowa State University, unpublished research, 1976.

29. Schroeder, D. R.; Jacobson, R. A. Inorg. Chem. 1973, 12. 210.

30. Jacobson, R. A. J. Appl. Crystallogr. 1976, 9, 115.

31. Karcher, B. Ph.D. Dissertation, Iowa State University, Ames, IA, 1981.

32. Rodgers, J.; Jacobson, R. A. AEC Report IS-2155, Ames, IA, 1967.

33. Lawton, S. A.; Jacobson, R. A. Inorg. Chem. 1968, 7, 2124.

34. Helland, B. Ames Laboratory, Iowa State University, unpublished research, 1981.

35. Lapp, R. L.; Jacobson, R. A. Department of Chemistry, Iowa State University, unpublished research, 1979.

36. Powell, D. R.; Jacobson, R. A. Department of Chemistry, Iowa State University, unpublished research, 1979.

37. Johnson, C. K. "ORTEP: A Fortran Thermal-Ellipsoid Plot Program for Crystal Structure Illustrations", ORNL Report 3794, Oak Ridge National Laboratory, Oak Ridge, TN, 1970.

38. Gmelin Handbuch der Anorganischen Chemie, 8th ed.; Springer-Verlag: Berlin, 1974; No. 39, Teil C5, p. 125.

39. Poeppelmeier, K. R.; Corbett, J. D. Inorg. Chem. 1977, 16, 294.

40. Spedding, F. H.; Daane, A. H.; Herrman, K. W. Acta Cryst. 1956, 9, 559.

41. Shannon, R. D. Acta Cryst., Sect. A 1976, A32, 751.

42. O'Connor, B. H.; Valentine, T. M. Acta Cryst., Sect. A 1969, 2140.

43. Mann, A. W.; Bevan, D. J. M. Acta Cryst., Sect. B 1970, B26, 2129.

44. Röder, U.; Müller-Warmuth, W.; Schöllhorn, R. J. Chem. Phys. 1979, 70, 2864.

45. Beckman, O.; Boller, H.; Nowotny, H. Monatsh. Chem. 1970, 101, 955.

46. Hwu, S.-J. Department of Chemistry, Iowa State University, personal communication, 1983.

47. Smith, J. D. Department of Chemistry, Iowa State University, personal communication, 1983.

48. Atoji, M.; Kikuchi, M. J. Chem. Phys. 1969, 51, 3863.

49. Mattausch, Hj.; Simon, A.; Holzer, N.; Eger, R. Z. Anorg. Allg. Chem. 1980, 466, 7.

50. Meyer, G. Justus Liebig Institut für Anorganische and Analystische Chemie, Giessen, West Germany, personal communication, 1983.

51. Thompson, A. H.; Scanlon, J. C.; Symon, C. R. Solid State Ionics 1980, 1, 47.

52. Thompson, A. H.; Symon, C. R. Solid State Ionics 1981, 3, 175.

53. Rouxel, J.; Trichet, P.; Chevalier, P.; Colombet, P.; Ghaloun, O. A. J. Solid State Chem. 1979, 29, 311.

54. Brec, R.; Ritsma, J.; Ouvard, G.; Rouxel, J. Inorg. Chem. 1977, 16, 660.

55. Schöllhorn, R.; Schmucker, W. Z. Naturforsch 1975, 306, 975.

56. Simon, A. Z. Anorg. Allg. Chem. 1967, 335, 311.

57. Imoto, H.; Corbett, J. D. Inorg. Chem. 1980, 19, 1241.

58. Warkentin, E.; Masse, R.; Simon, A. Z. Anorg. Allg. Chem. 1983, 491, 323.

59. Simon, A.; Warkentin, E. Z. Anorg. Allg. Chem. 1983, in press.

60. Simon, A. Max-Planck-Institute, Stuttgart, West Germany, personal communication, 1983.

61. Ziebarth, R. Department of Chemistry, Iowa State University, personal communication, 1983.

62. Seaverson, L. M. Department of Chemistry, Iowa State University, personal communication, 1983.

63. Guthrie, D. H.; Corbett, J. D. Inorg. Chem. 1982, 21, 3290.

64. Corbett, J. D.; Poeppelmeier, K. R.; Daake, R. L. Z. Anorg. Allg. Chem. 1982, 491, 51.

65. Schöllhorn, R.; Weiss, A. Z. Naturforsch, 1973, B28, 711.

66. Schöllhorn, R.; Weiss, A. J. Less-Common Met. 1974, 36, 229.

67. Graf, H. A.; Lerf, A.; Schöllhorn, R. J. Less-Common Met. 1977, 55, 213.

68. Bos-Alberink, A. J. A.; Haange, R. J.; Wiegers, G. A. J. Less-Common Met. 1979, 63, 69.

69. Murphy, D. W.; Hull, C. W. J. Chem. Phys. 1975, 62, 973.

70. Grim, R. F. "Clay Mineralogy"; McGraw-Hill: New York, 1968.

71. Royals, E. E. "Advanced Organic Chemistry", 2nd ed.; Prentice-Hall: Englewood Cliffs, NJ, 1956; p. 759.

ACKNOWLEDGEMENTS

The author would especially like to thank Professor John D. Corbett for his guidance and constructive criticism throughout this investigation.

He is particularly thankful to J. Benson, J. Richardson, B. Helland, Dr. R. A. Jacobson and other members of his group for their support in the use of the diffractometer and assistance with the crystallographic programs.

B. Beaudry and P. Palmer kindly provided the yttrium for this work. F. Laabs is thanked for the microprobe analyses.

D. Torgeson and Dr. R. G. Barnes are thanked for the NMR study.

The help, cooperation, and friendship from past and present members of Physical and Inorganic Chemistry Group IX of the Ames Laboratory will always be remembered.

The author would like to especially note the love, understanding, and sacrifices of his parents and family during his educational years.

Last and most important he thanks his wife LuAnn for her patience, encouragement, understanding, and love.

APPENDIX A: OBSERVED AND CALCULATED STRUCTURE FACTORS (x10)

FOR YC1

H = 0

K	L	FO	FC
0	3	721	743
0	6	1125	1045
0	9	1064	909
0	12	1867	1631
0	15	272	237
0	18	1752	1510
0	21	878	778
0	24	92	115
0	27	156	179
0	30	966	896
1	2	1488	1510
1	5	2073	2182
1	8	410	381
1	11	1163	1187
1	14	801	814
1	17	876	847
1	20	502	507
1	23	1291	1266
1	26	283	262
1	29	171	186
2	1	109	125
2	4	388	408
2	7	1346	1333
2	10	923	908
2	13	837	855
2	16	885	891
2	19	395	414
2	22	200	211
2	25	741	715
2	28	719	756
3	3	373	371
3	6	448	442
3	9	522	513
3	12	811	824
3	15	101	118
3	18	854	851

H = 1

K	L	FO	FC
0	1	232	242
0	4	412	466
0	7	1701	1783
0	10	1184	1213
0	13	1080	1111
0	16	1105	1100
0	19	485	495
0	22	253	257
0	25	804	844
0	28	884	886
0	31	100	157
1	0	1998	2016
1	3	534	550
1	6	682	692
1	9	737	740
1	12	1206	1218
1	15	158	175
1	18	1270	1205
1	21	613	647
1	27	93	157
2	2	897	898
2	5	1260	1246
2	8	206	198
2	11	731	753
2	14	555	558
2	17	559	568
2	20	370	357
2	23	885	904
3	1	67	62
3	4	258	252
3	7	766	767
3	10	522	524

H = 2

K	L	FO	FC
0	2	1116	1119
0	5	1491	1564
0	8	263	253
0	11	876	918
0	14	642	665
0	17	648	680
0	20	420	421
0	23	1066	1062
0	26	220	227
1	1	84	91
1	4	330	342
1	7	1074	1076
1	10	750	736
1	13	727	701
1	16	748	746
1	19	357	353
1	22	132	177
2	0	1147	1071
2	3	327	316
2	6	379	373
2	9	434	441
2	12	695	702

H = 3

K	L	FO	FC
0	0	1285	1272
0	3	367	371
0	6	468	442
0	9	514	513
0	12	847	824
0	15	87	118
0	18	848	851
1	2	645	637
1	5	934	878
1	8	113	137
1	11	551	542

APPENDIX B: OBSERVED AND CALCULATED STRUCTURE FACTORS (x10)

FOR 3R-$Li_{0.09}YCl$

H = -5		
K	L	FO	FC
2	-1	88	46
H = -4		
K	L	FO	FC
0	-1	54	53
H= -3		
K	L	FO	FC
1	-31	94	49
H = -2		
K	L	FO	FC
0	-2	1123	1092
1	-27	91	79
H = 0		
K	L	FO	FC
0	3	815	762
0	6	1175	963
0	9	1104	891
0	12	2127	1688
0	15	498	379
0	18	1701	1446
0	21	972	838
0	24	316	259
0	27	124	88
0	30	1019	928
0	33	623	587
0	36	313	317
0	39	285	300
1	2	1433	1478
1	5	2042	2198
1	8	350	303
1	11	1079	1112
1	14	742	852
1	17	896	960
1	20	395	389
1	23	1218	1285
1	26	410	370
1	32	318	313
1	35	772	739
1	38	163	159
2	1	103	110
2	4	366	387
2	7	1308	1318
2	10	952	974
2	13	778	779
2	16	806	871
2	19	433	492
2	22	300	324
2	25	670	668
2	28	799	834
2	34	193	210
3	3	389	372
3	6	421	405
3	9	500	491
3	12	858	853
3	15	202	198
3	18	791	815
3	21	453	501
3	24	136	161
3	27	66	65
4	2	562	530
4	5	786	758
4	8	102	95
4	11	456	434
4	14	375	363
4	17	381	405
H = 1		
K	L	FO	FC
0	1	208	218
0	4	369	444
0	7	1599	1768
0	10	1205	1297
0	13	942	1014
0	16	1001	1079
0	19	598	595
0	22	468	388
0	25	886	790
0	28	1049	979
0	31	76	62
0	34	243	242
0	37	384	374
1	0	2045	1999
1	3	586	561
1	6	620	630
1	9	702	722
1	12	1211	1259
1	15	280	288
1	18	1123	1154
1	21	694	691
1	24	220	217
1	30	710	792
1	33	502	504
1	36	257	271
2	2	899	874
2	5	1237	1256
2	8	179	158
2	11	711	702
2	14	578	572
2	17	637	647
2	20	269	273
2	23	883	916
2	26	284	274
3	1	52	61
3	4	240	230
3	7	778	756
3	10	558	565
3	13	455	460
3	16	527	531
3	19	305	309
3	22	185	200
H = 2		
K	L	FO	FC
0	5	1537	1574
0	8	216	198
0	11	846	858
0	14	647	688
0	17	724	774
0	20	307	322
0	23	1019	1077
0	26	316	316
0	32	264	272
0	35	650	636
1	1	81	84
1	4	311	320
1	7	1049	1063
1	10	766	792
1	13	638	641
1	16	722	727
1	19	397	416
1	22	279	275
1	25	598	571
1	28	717	716
2	0	1115	1065
2	3	344	315
2	6	351	342
2	9	434	418
2	12	713	726
2	15	163	168
2	18	696	697
2	21	435	433
2	24	124	140
3	2	481	457
3	5	661	652
3	8	76	81
3	11	388	375
H = 3		
K	L	FO	FC
0	0	1319	1265
0	3	390	372
0	6	412	405
0	9	490	490
0	12	828	853
0	15	204	198
0	18	778	815
0	21	475	508
0	24	142	161
1	2	652	617
1	5	910	886
1	8	123	112
1	11	515	504
1	14	417	418
1	17	464	471
1	20	206	202
1	23	653	676
2	4	178	175
2	7	565	559
2	10	412	416
H = 4		
K	L	FO	FC
0	4	206	200
0	7	668	648
0	10	465	484
0	13	374	394
0	16	453	459

APPENDIX C: OBSERVED AND CALCULATED STRUCTURE FACTORS (x10)

FOR $2H\text{-}K_{0.08}YClO_{0.82}$

H = -4		
K	L	FO	FC
1	0	137	104

H = -2		
K	L	FO	FC
1	-20	73	74
3	-12	46	7

H = -1		
K	L	FO	FC
4	-7	104	83

H = 0		
K	L	FO	FC
-2	12	60	8
-2	-10	59	31
0	2	917	972
0	4	467	414
0	6	699	550
0	8	1022	897
0	10	1263	1126
0	12	58	47
0	14	743	728
0	16	442	431
0	18	113	121
0	20	80	91
0	22	298	274
0	24	382	355
1	0	197	201
1	1	306	327
1	2	623	610
1	3	859	857
1	4	487	454
1	5	638	666
1	6	727	731
1	7	143	153
1	8	670	672
1	9	470	503
1	10	70	34
1	11	642	693
1	14	66	51
1	15	53	44
1	16	387	392
1	17	302	310
1	18	224	237
1	19	422	459
1	20	178	185
1	21	299	292
1	22	169	158
1	25	155	159
2	0	140	180
2	1	233	248
2	2	413	423
2	3	642	643
2	4	304	293
2	5	525	522
2	6	527	527
2	7	123	132
2	8	501	504
2	9	363	376
2	11	531	547
2	13	403	427
2	16	324	324
2	17	257	255
2	18	205	198
2	20	146	156
2	21	248	248
2	22	143	135
3	0	1027	914
3	2	439	400
3	4	168	164
3	6	292	290
3	8	457	452
3	10	539	539
3	14	417	419
3	16	263	259
3	-12	48	39

H = 1		
K	L	FO	FC
0	12	50	11
0	13	520	530
0	23	63	57
1	0	1606	1494
1	2	675	640
1	4	245	250
1	6	437	433
1	8	654	677
1	10	794	818
1	14	542	590
1	16	354	358
1	18	81	104
1	22	231	234
2	0	77	146
2	1	189	202
2	2	296	330
2	3	497	519
2	4	166	225
2	5	422	430
2	6	412	420
2	7	104	113
2	8	399	407
2	9	298	301
2	11	444	451
2	13	347	356
2	15	69	36
2	16	275	273
2	17	207	215
2	18	152	167
2	19	321	326
3	1	101	145
3	2	180	228
3	3	333	367
3	4	137	153
3	5	314	310
3	6	306	294
3	7	69	83
3	8	289	288
3	9	208	212

H = 2		
K	L	FO	FC
-1	-12	40	48
0	14	51	41
0	15	52	41
0	19	378	383
1	0	150	146
1	1	188	202
1	2	340	330
1	3	551	519
1	4	232	225
1	5	457	430
1	6	442	420
1	7	99	113
1	8	433	407
1	9	321	301
1	11	456	451
1	13	358	356
1	16	277	273
1	17	218	215
1	18	176	167
1	19	324	326
2	0	887	763
2	2	385	336
2	4	100	139
2	6	253	246
2	8	395	384
2	10	446	455

H = 3		
K	L	FO	FC
1	0	88	104
1	1	112	145
1	2	231	228
1	3	382	367
1	4	135	153
1	5	349	309
1	6	334	294
1	8	319	288
1	9	221	212

APPENDIX D: OBSERVED AND CALCULATED STRUCTURE FACTORS (x10)

FOR 3R-$Na_{0.08}YClO_{1.0}$

H = -3			H = -2			H = -1			H = 0			H = 1			H = 2			H = 3		
K	L	FO	FC	K	L	FO	FC	K	L	FO	FC	K	L	FO	FC	K	L	FO	FC	K	L	FO	FC
-1	4	225	229	0	1	92	101	-2	4	190	246	0	3	901	1162	0	7	1209	1363	0	2	1035	1141	0	0	1848	1592
1	-1	132	84	0	4	236	239	0-31		159	68	0	6	716	845	0	10	1255	1366	0	5	1456	1591	0	3	681	581
2	-8	239	225									0	9	931	1014	0	13	805	782	0	8	285	308	0	6	410	402
												0	12	2024	1815	0	16	927	894	0	11	995	1068	0	9	643	636
												0	15	1141	931	0	19	420	321	0	14	780	765	0	12	1081	1001
												0	18	1326	1115	0	22	325	281	0	17	740	713	0	15	539	483
												0	21	992	837	0	25	504	412	0	23	925	1108	0	18	740	707
												0	24	224	274	0	28	816	826	0	26	415	464	0	21	539	585
												0	27	136	229	1	0	3245	2383	1	7	958	975	1	2	705	763
												0	30	555	391	1	3	1116	825	1	10	904	904	1	5	1023	1025
												0	33	617	950	1	6	675	569	1	13	949	927	1	8	145	146
												1	2	1228	1458	1	9	912	844	1	16	706	694	1	11	635	697
												1	5	2006	2104	1	12	1464	1380	1	19	302	293				
												1	8	492	505	1	15	722	693	1	22	186	218				
												1	11	1270	1377	1	18	963	927	1	25	332	335				
												1	14	766	905	1	21	769	726	2	0	1772	1389				
												1	17	900	845	1	24	173	240	2	3	594	518				
												1	23	1053	1292	1	30	228	356	2	6	371	354				
												1	26	515	520	2	2	873	966	2	9	570	575				
												2	7	1064	1121	2	5	1282	1332	2	12	945	889				
												2	10	992	1069	2	11	870	897	2	15	454	420				
												2	13	639	621	2	14	648	670								
												2	16	788	778	2	17	671	623								
												2	19	279	309	2	23	837	972								
												2	22	228	247	3	7	708	784								
												2	25	357	369	3	10	614	697								
												2	28	725	729	3	13	357	401								
												3	3	655	581												
												3	6	399	402												
												3	9	632	635												
												3	12	1088	1000												
												3	15	529	482												
												3	18	770	706												
												3	21	544	584												

APPENDIX E: OBSERVED AND CALCULATED STRUCTURE FACTORS (x10)

FOR 1T-$K_{0.52}Y_2Cl_2C_{0.80}$

H = -2

K	L	FO	FC
-1	9	76	80

H = -1

K	L	FO	FC
-2	7	48	67
-1	11	47	40
0	-8	43	54

H = 0

K	L	FO	FC
0	1	275	387
0	2	100	112
0	3	167	245
0	4	280	304
0	5	532	564
0	7	339	313
0	8	269	259
0	9	118	108
0	10	142	127
0	12	219	161
0	-11	45	44
1	0	484	340
1	1	74	84
1	2	829	775
1	3	546	559
1	4	131	148
1	6	112	111
1	7	317	400
1	8	198	216
1	9	76	92
1	10	175	160
1	11	99	80
1	12	162	111
2	0	368	287
2	1	351	297
2	2	384	360
2	3	300	313
2	4	258	262
2	5	416	431
2	6	222	218
2	7	74	70
2	9	179	185
2	10	204	217
2	-9	60	86
3	0	701	544
3	1	280	241
3	2	68	87
3	3	133	145
3	4	205	244
3	5	316	344
3	7	221	231

H = 1

K	L	FO	FC
0	1	394	361
0	2	449	411
0	3	392	420
0	4	327	347
0	5	495	504
0	6	263	263
0	7	62	73
0	9	212	207
0	10	255	233
0	12	92	74
1	0	1053	766
1	1	380	300
1	2	96	93
1	3	179	196
1	4	261	285
1	5	443	443
1	7	282	275
1	8	234	221
1	9	102	102
1	10	102	110
2	0	301	260
2	2	546	481
2	3	403	410
2	4	94	93
2	6	98	109
2	7	308	311
2	8	158	187
3	0	231	224
3	1	223	210
3	2	254	280
3	3	194	215

H = 2

K	L	FO	FC
-2	-1	36	37
0	2	675	571
0	3	485	462
0	4	127	113
0	6	110	113
0	7	362	346
0	8	194	200
0	10	151	142
1	1	288	255
1	2	331	326
1	3	258	266
1	4	224	221
1	5	377	388
1	6	201	191
1	9	175	169
2	0	593	491
2	1	251	223
2	2	62	83
2	3	111	133
2	4	185	229
2	5	277	315

H = 3

K	L	FO	FC
0	1	296	241
0	2	76	87
0	3	134	145
0	4	212	244
0	5	327	344
0	7	230	231
1	1	70	18
1	2	409	388
1	3	325	346

APPENDIX F: CALCULATED AND OBSERVED GUINIER POWDER PATTERNS FOR 1T-Cs_xYClO_z

h k ℓ	$2\theta^{a}_{calc.}$	$I_{obs.}$	$I^{b}_{calc.}$
0 0 1	7.44	9	10
0 0 3	22.44	1	1
1 0 0	27.13	2	0.5
1 0 1	28.17	6	3
0 0 4	30.07		0.2
1 0 2	31.10	8	6
1 0 3	35.49	3	3
0 0 5	37.84	1	1
1 0 4	40.94	1	0.8
1 0 5	47.18		0.5
1 1 0	47.95	10	3
1 1 1	48.59	2	0.6
1 1 3	53.55	1	0.8
1 0 6	54.04		0.5
2 0 1	56.54	1	0.2
1 1 4	57.64	0.5	0.2
2 0 2	58.26	1	0.5
2 0 3	61.05	0.5	0.3
1 0 7	61.46		0.2
0 0 8	62.50		0.3
1 1 5	62.64	2	2
2 0 4	64.84	1	0.2
2 0 5	69.54		0.2
2 0 6	75.11	0.5	0.3
2 1 1	77.22	0.5	0.2
2 1 2	78.70	1	0.5
2 1 3	81.15	0.5	0.4
1 1 8	82.44		1
2 1 4	84.55	0.5	0.4
1 0 10	87.20		0.3
2 1 5	88.89		0.2
3 0 0	89.46	1	0.4

[a] $2\theta_{obs.} = 2\theta_{calc.} \pm 0.03^{o}$.

[b] All lines with $I_{calc.} \geq 0.2$ are reported.

APPENDIX G: CALCULATED AND OBSERVED GUINIER POWDER PATTERNS FOR 1T-$K_x(H_2O)_aYClO_z$

h k ℓ	$2\theta^{a}_{calc.}$	$I_{obs.}$	$I^{b}_{calc.}$
0 0 1	7.45	7	10
0 0 3	22.48		0.8
1 0 0	27.20	0.5	0.2
1 0 1	28.24	6	2
0 0 4	30.13		0.3
1 0 2	31.17	10	3
1 0 3	35.57	2	1
0 0 5	37.92		0.4
1 0 4	41.03	0.5	0.6
1 0 5	47.29		0.2
1 1 0	48.07	8	2
1 1 1	48.71	3	0.6
1 1 3	53.68	0.5	0.4
1 0 6	54.17		0.2
2 0 1	56.68	1	0.3
2 0 2	58.40	2	0.4
2 0 3	61.20	0.5	0.2
0 0 8	62.64		0.2
1 1 5	62.80	0.5	0.6
2 0 4	65.00	0.5	0.2
1 1 6	68.64		0.2
2 1 1	77.44	1	0.2
2 1 2	78.92	1.5	0.3
2 1 3	81.37	0.5	0.2
1 1 8	82.65		0.6
2 1 4	84.79	0.5	0.2
3 0 0	89.72	1	0.4

[a] $2\theta_{obs.} = 2\theta_{calc.} \pm 0.03^{o}$.

[b] All lines with $I_{calc.} \geq 0.2$ are reported.

APPENDIX H: CALCULATED AND OBSERVED GUINIER POWDER PATTERNS FOR 1T-Y_2Cl_2C

h k ℓ	$2\theta^{a}_{calc.}$	$I_{obs.}$	$I^{b}_{calc.}$
0 0 1	9.62	8	10
0 0 2	19.31	1	0.5
1 0 0	27.78	5	2
0 0 3	29.14	0.5	0.2
1 0 1	29.46	1	1
1 0 2	34.05	5b	6
0 0 4	39.19	2	0.5
1 0 3	40.69	0.5	1
1 1 0	49.14	10	2
0 0 5	49.57		0.4
1 1 1	50.19	2	1
1 1 2	53.27	1	0.1
2 0 0	57.38	2	0.3
1 1 3	58.15	2	0.2
2 0 2	61.13	1	0.6
1 1 4	64.58	3	0.6
2 0 3	65.64		0.3
1 1 5	72.37		1
2 1 0	78.86	1	0.3
2 0 5	79.19	0.5	0.2
1 1 6	81.48	2	0.1
2 1 2	82.42	1	1

[a] $2\theta_{obs.} = 2\theta_{calc.} \pm 0.04^{o}$.

[b] All lines with $I_{calc.} \geq 0.2$ are reported.

APPENDIX I: CALCULATED AND OBSERVED GUINIER POWDER PATTERNS FOR 1T-$K_{0.52}YClC_{0.80}$

h k ℓ	$2\theta^{a}_{calc.}$	$I_{obs.}$	$I^{b}_{calc.}$
0 0 1	8.13	8	10
0 0 3	24.55		0.4
1 0 0	28.03	3	1.5
1 0 1	29.23	4	2
1 0 2	32.59	7	6
0 0 4	32.94		0.4
1 0 3	37.60	3	2.5
0 0 5	41.51	1	0.8
1 0 4	43.78	1	0.5
1 1 0	49.59	10	2
1 1 1	50.35	2	0.7
1 0 5	50.84	0.5	1
1 1 3	56.10		0.2
2 0 0	57.93	0.5	0.2
1 0 6	58.60	0.5	0.2
2 0 1	58.61		0.2
0 0 7	59.49		0.2
2 0 2	60.61	1.5b	0.6
1 1 4	60.83		0.6
2 0 3	63.87	vvw	0.4
1 1 5	66.61	1	1
1 0 7	67.02		0.3
2 0 5	73.76	0.5	0.3
2 1 0	79.68	0.5	0.3
2 1 1	80.27	0.5	0.2
1 1 7	81.03	0.5	0.6
2 1 2	82.02	1b	1
2 1 3	84.91	0.5	0.6
2 0 7	87.79		0.2
2 1 4	88.95		0.2
1 1 8	89.71	0.5	0.5

[a] $2\theta_{obs.} = 2\theta_{calc.} \pm 0.04^{o}$.

[b] All lines with $I_{calc.} \geq 0.2$ are reported.